EUROPEAN COMMISSION
5th EURATOM FRAMEWORK PROGRAMME 1998-2002
KEY ACTION : NUCLEAR FISSION

HTR-F

High-Temperature Reactor Fuel Technology

CONTRACT N°
FIKI-CT-2000-00099

Extraction of the current knowledge for HTR coated particle

HTR-F WP3

1st Deliverable

A collaboration of work performed by

BNFL, CEA, FRAMATOME/ANP and FZJ

December 2002

Dissemination level : RE
Document Number: HTR-F-0212-D-3.1.1
First Version
Deliverable Number: 11

Summary

The following Report represents the First Deliverable of the Work Package 3 (Fuel modelling) in the HTR-F created by the European Community.

It concerns the extraction of the current knowledge on properties and models for the materials, kernel and coatings which constitute the gas reactor coated particle fuel.

This review and this evaluation of the existing data was performed by the four organisations involved in the WP3 : BNFL, CEA, FRAMATOME/ANP and FZJ.

This report is a compilation of three documents relating to the following items:

Fuel properties and models,

Diffusion data,

Coatings properties.

List of documents

1. **Fuel properties and models (CEA)**

   "HTR-F PROJECT : Collect of the current knowledge on existing properties and models for the coated particle (CEA contribution)"

   by M. Pelletier

   Report SESC/LSC 02-036 ind.0 November 2002

2. **Diffusion data (FRAMATOME/ANP)**

   "Data List for HTR Fission Products Behaviour : FRA-ANP Contribution of HTR-F WP3"

   by P. Guillermier

   Report HTRF0110D312 ind.A 10/10/2001

3. **Coatings properties (FZJ, BNFL and CEA)**

   "HTR-F PROJECT : Collect of the current knowledge on existing properties and models for the coated particle – PyC and SiC"

   by M. Pelletier, H. Nabielek and T. Abram

   Report SESC/LSC 02-037 ind.A November 2002

DIRECTION DE L'ENERGIE NUCLÉAIRE

DIRECTION DU CEA/CADARACHE

DÉPARTEMENT D'ETUDES DES COMBUSTIBLES

SERVICE D'ETUDES ET DE SIMULATION DU COMPORTEMENT DES COMBUSTIBLES

LABORATOIRE D'ÉTUDES ET DE SIMULATION DU COMPORTEMENT DES COMBUSTIBLES

HTR-F PROJECT : COLLECT OF THE CURRENT KNOWLEDGE ON EXISTING PROPERTIES AND MODELS FOR THE COATED PARTICLE (CEA CONTRIBUTION)

M. PELLETIER

Report SESC/LSC 02-036 | **First Issue 0** | **November 2002**

CEA/CADARACHE - BÂTIMENT N°315 - DEN/CAD/DEC/SESC/LSC – 13108 – SAINT PAUL LEZ DURANCE CEDEX

04 42 25 38 62 - 04 42 25 29 49 - sesclsc@drncad.cea.fr

DIRECTION DE L'ENERGIE NUCLÉAIRE

DIRECTION DU CEA/CADARACHE
DÉPARTEMENT D'ETUDES DES COMBUSTIBLES
SERVICE D'ETUDES ET DE SIMULATION DU COMPORTEMENT DES COMBUSTIBLES
LABORATOIRE D'ÉTUDES ET DE SIMULATION DU COMPORTEMENT DES COMBUSTIBLES

Title : HTR-F PROJECT : COLLECT OF THE CURRENT KNOWLEDGE ON EXISTING PROPERTIES AND MODELS FOR THE COATED PARTICLE (CEA CONTRIBUTION)

Author(s) : M. PELLETIER

Summary :

In order to develop HTR reactor in Europe, a program devoted to fuel technology development (HTR-F) was launched in 2000 in the framework of the European network HTR-TN. Around the world, the HTR fuel is based on spherical coated particles inserted in graphite blocks or pebble type elements. Their kernel generally consists of enriched uranium dioxide and the coatings are made of ceramic layers ensuring leak tightness to the fission products during normal and accidental situations.

One of the four Work Package of the HTR-F program (WP3) is dedicated to the modelling of the different phenomena which occur into the fuel particle during irradiation and to develop at the European level a common code. This tool has to main mission to predict the time-to-failure taking into account several mechanisms such pressure vessel, SiC layer corrosion, coating debonding or kernel migration.

Among the tasks of the WP3, the first one consists to gather the knowledge on particle component properties and fundamental models for describing the behaviour of the coated particle under irradiation in order to reach the best accuracy. This collection of the current knowledge on physical processes and relevant existing models is the first "Deliverable" of the HTR-F WP3 and must be supplied by the end of October 2002.

The present document builds up the CEA contribution for this task which is mainly focused on the kernel properties and models.

Key Word	HTR, FUEL, KERNEL, UO2, (U, PU)O2, PHYSICAL PROPERTIES, MODELS, MODELLING

EOTP	A-FIHTR-03-01

	Name	Signature	Date	Classification				
Quality Assurance	***G. ARÈNE***			Open	DR	CC	CD	SD
Head of Unit	***P. OBRY***			✘				
Checked by	***M. PHELIP***			Framework				
Written by	***M. PELLETIER***			*DDIN/SYST. DU FUTUR : FILIÈRE HTR*				

REVISIONS

DATE	PURPOSE OF THE REVISIONS	ISSUE
déc. 2002	Initial distribution.	0

CONTENTS

1. INTRODUCTION

In order to develop HTR reactor in Europe, a program devoted to fuel technology development (HTR-F) was launched in 2000 in the framework of the European network HTR-TN. Around the world, the HTR fuel is based on spherical coated particles inserted in graphite blocks or pebble type elements. Their kernel generally consists of enriched uranium dioxide and the coatings are made of ceramic layers ensuring leak tightness to the fission products during normal and accidental situations.

One of the four Work Package of the HTR-F program (WP3) is dedicated to the modelling of the different phenomena which occur into the fuel particle during irradiation and to develop at the European level a common code. This tool has to main mission to predict the time-to-failure taking into account several mechanisms such pressure vessel, SiC layer corrosion, coating debonding or kernel migration.

Among the tasks of the WP3, the first one consists to gather the knowledge on particle component properties and fundamental models for describing the behaviour of the coated particle under irradiation in order to reach the best accuracy. This collection of the current knowledge on physical processes and relevant existing models is the first “Deliverable” of the HTR-F WP3 and must be supplied by the end of October 2002.

The present document builds up the CEA contribution for this task which is mainly focused on the kernel properties and models. The chapter 2 is devoted to physical and mechanical properties of UO_2 fuel and the chapter 3 to the (U, Pu)O_2 ones. In the chapter 4, some model, more or less mechanistic, relatives in the behaviour of the fuel under irradiation such as pile densification, fuel swelling, fission gas release and CO production for oxide fuels are described. To finish, we propose in the chapter 5 models on one hand, in relation with the neutronics: fission rate, burn-up and fission product production and on the other hand, for the calculation of the free volume and the internal pressure of the particle.

2. PHYSICAL AND MECHANICAL PROPERTIES

Most of the properties of UO_2 and $(UPu)O_2$ fuels proposed below result from recommendations for sintered fuels fabrication of the fields PWR and FBR. In our knowledge, there are no laws so complete for oxide fuels made according to the Solgel process. In the future, for the new kernel fabrications, measurements of certain properties would be necessary to verify the merits of the present recommendations.

2.1. UO_2 FUEL

2.1.1. Density

The theoretical density of UO_2 at 293 K is ***[1]***:

$$\rho = 10950\ (1 - P),$$

with:

ρ	:	density	kg/m^3,
P	:	pore fraction	(/).

2.1.2. Linear thermal Expansion

The linear thermal expansion of the UO_2 fuel is given by ***[2]***:

For $T_K < 923$ K:

$$\frac{l_{T_K}}{l_{273}} = 9.9734\ 10^{-1} + 9.802\ 10^{-6} T_K - 2.705\ 10^{-10} T_K^2 + 4.391\ 10^{-13} T_K^3$$

For $T_K \geq 923$ K:

$$\frac{l_{T_K}}{l_{273}} = 9.9672\ 10^{-1} + 1.179\ 10^{-5} T_K - 2.429\ 10^{-9} T_K^2 + 1.219\ 10^{-12} T_K^3$$

with:

T_K	:	temperature	(K).

The averaged linear thermal expansion coefficient (alpha) between 273 and T_K is given by (Figure 1):

$$\alpha_{(273-T_K)} = \frac{1}{(T_K - 273)} \left(\frac{l_{T_K}}{l_{273}} - 1 \right)$$

2.1.3. Heat Capacity

The heat capacity is given by ***[3]*** (Figure 2):

$$C_P = 12.54 + 0.017\ T_K - 0.117\ 10^{-4}\ T_K^2 + 0.307\ 10^{-8}\ T_K^3$$

Where:

C_P	:	heat capacity	(cal/(mole.K))
T_K	:	temperature	(K)

NB: 1 cal/(mole.K) = 4.1868 J/(mole.K)

2.1.4. Thermal Conductivity

1st law:

For unirradiated fuel, the law is that found in D. MARTIN's recommendation ***[4]***. Variation, as a function of burn-up, comes from the LUCUTA recommendations ***[5]*** (Figure 3):

$$\lambda(T_K,\tau) = \frac{1}{0.0375 + (2.165 - 0.005\tau)10^{-4}T_K + 1.5510^{-2}\tau} + \frac{4.71510^9}{T_K^2}\exp\left(-\frac{16{,}361}{T_K}\right)$$

The correction relating to porosity is obtained from the following equation:

$$\lambda(T_K, P) = (1 - P)^{2.5}\ \lambda(T_K, 0)$$

where:

λ	:	thermal conductivity	(W/(m.K))
T_K	:	temperature	(K)
P	:	pore fraction	(/)
τ	:	burn-up	(at% FIMA)

2nd law (recent recommendation):

A study on the laws of UO_2 thermal conductivity, available in the opened literature was recently driven. This study allows to propose a new recommendation, inspired by the "LUCUTA's law" of 1996 and validated on instrumented experiences with a thermocouple until 1900K ***[6]*** (Figure 4).

This law is henceforth used by default for UO_2 in the last version of the PWR rod code METEOR.

$$\lambda = K_{1d}\ K_{1p}\ K_{2p}\ K_{3x}\ K_{4r}\ \lambda_0$$

With:

$$\lambda_0(T_K) = \frac{1}{0.0375 + 2.165\ 10^{-4} T_K} + \frac{4.715\ 10^9}{T_K^2} \exp\left(-\frac{16{,}361}{T_K}\right)$$

$$K_{1d} = \left(\frac{1.09}{\tau^{3.265}} + \frac{0.0643}{\sqrt{\tau}}\sqrt{T_K}\right) \arctan\left[\frac{1}{\left(\frac{1.09}{\tau^{3.265}} + \frac{0.0643}{\sqrt{\tau}}\sqrt{T_K}\right)}\right]$$

$$K_{1p} = 1 + \frac{0.019\,\tau}{3 - 0.019\,\tau} \frac{1}{\left(1 + \exp\left(-\frac{(T_K - 1200}{100}\right)\right)}$$

$$K_{2p} = \frac{1 - P}{1 + 2\,P}$$

$$K_{3x} = 1$$

$$K_{4r} = 1 - \frac{0.2}{\left(1 + \exp\left(\frac{(T_K - 900}{80}\right)\right)} (1 - \exp(-\tau))$$

where:

λ, λ_0	:	thermal conductivity	(W/(m.K))
T_K	:	temperature	(K)
τ	:	burn-up	(at% FIMA)
P	:	pore fraction	(/)
x	:	2 - O/M	(/)

2.1.5. Emissivity

The recommended value for the emissivity of oxide fuels is as follow ***[7]***:

$\varepsilon = 0.87$

With:

ε	:	emissivity	(/)

2.1.6. Young's Modulus

The evolution of the Young's modulus with both temperature and porosity is given by the following equations ***[2]*** (Figure 5):

For $273 \leq T_K \leq 2{,}610$ K:

$E_0 = 2.2693\ 10^2 - 1.5399\ 10^{-2}\ T_K - 9.597\ 10^{-6}\ T_K^2$

For T_K > 2,610 K:

$$E_0 = -1.33445\ 10^3 + 1.18106\ T_K - 2.38803\ 10^{-4}\ T_K^2$$

The correction due to porosity is as follows:

If P ≤ 0.3:

$$E = (1 - 2.5\ P)\ E_0$$

If P > 0.3:

$$E = \frac{1-P}{1+6P} E_0$$

where:

E, E_0	:	Young's modulus	(GPa)
T_K	:	temperature	(K)
P	:	fuel pore fraction	(/)

2.1.7. Poisson's Ratio

The Poisson's ratio is given by the following equation (Figure 6):

$$\upsilon = \frac{E}{2G} - 1$$

where E is the Young's modulus and G the shear modulus.

The equations for the shear modulus are the following ***[2]*** :

For 273 ≤ T_K ≤ 2,610 K:

$$G_0 = 85.83 - 5.157\ 10^{-3}\ T_K - 3.747\ 10^{-6}\ T_K^2$$

For T_K > 2,610 K:

$$G_0 = -5.7625\ 10^2 + 5.02189\ 10^{-1}\ T_K - 1.00939\ 10^{-4}\ T_K^2$$

The correction due to porosity is as follows:

If P ≤ 0.3:

$$G = (1 - 2.25\ P)\ G_0$$

If P > 0.3:

$$G = \frac{1-P}{1+3.85P} G_0$$

where:

G :		shear modulus	(GPa)
T_K :		temperature	(K)
P :		fuel pore fraction	(/)

E : Young's modulus (GPa)

2.1.8. Yield stress

The yield stress is given by the following equation ***[8]***:

$$\sigma_y = -0.1153 T_C + 261$$

with:

σ_y :	yield stress	(MPa)
T_C	temperature	(°C)

2.1.9. Irradiation induced thermal creep

The equation of the stationary creep law is as follow ***[9]*** (Figure 7):

$$\dot{\varepsilon}_{st} = k_\phi \min\left[\max\left(\dot{\varepsilon}_{st1};\dot{\varepsilon}_{st2}\right);\dot{\varepsilon}_{st\,lim}\right] + \dot{\varepsilon}_{irr}$$

with:

$\dot{\varepsilon}_{st}$	:	equivalent creep rate	(%/h)
$\dot{\varepsilon}_{st1}$	:	equivalent creep rate (1st mechanism)	(%/h)
$\dot{\varepsilon}_{st2}$	:	equivalent creep rate (2nd mechanism)	(%/h)
$\dot{\varepsilon}_{st\,lim}$	:	equivalent creep rate (limit law)	(%/h)
$\dot{\varepsilon}_{irr}$	:	irradiation induced equivalent creep rate	(%/h)
k_ϕ	:	multiplicative factor of the thermal creep under irradiation	

The 5 terms of the stationary creep law spell in the following way:

$$\dot{\varepsilon}_{st1} = 3.16\,10^{7} \exp\left(0.32\,P\right) D^{-1.87}\ \sigma^{3.06}\ \exp\left(-\frac{401{,}700}{R\,T}\right)$$

$$\dot{\varepsilon}_{st2} = 5.33\,10^{-2} \exp\left(0.37\,P\right) D^{2.01}\ \sigma^{8.4}\ \exp\left(-\frac{534{,}700}{R\,T}\right)$$

$$\dot{\varepsilon}_{st\,lim} = 7.13\,10^{6}\,\exp(0.15\,P_m)\,\sigma^{4.03}\,\exp\left(-\frac{461{,}300}{R\,T}\right)$$

$$\dot{\varepsilon}_{irr} = 1.87\,10^{-18}\,\sigma\;\Phi\exp\left(-\frac{8{,}100}{R\,T}\right)$$

$$k_{\Phi} = 1 + 2.44\,10^{-13}\,\Phi$$

with:

σ	:	equivalent stress	(MPa)
Φ	:	fission rate	(fiss/(cm^3.s))
P	:	porosity	(%)
P_m	:	maximum of porosity for the limit law (P_m = 7%)	
D	:	grain diameter	(µm)
T	:	temperature	(K)
R	:	8.314	(J/(mole.K))

2.2. $(U, Pu)O_2$ FUEL

2.2.1. Density

For a fuel: $(U_{1-y}\ Pu_y)\ O_{2-x}$ at 293 K, the density is given by ***[2] [10]*** (Figure 8):

$$\rho = \frac{4}{N_A}\left(\frac{M_{UPu} + 16(2-x)}{a^3}\right)(1-P)$$

where:

ρ : (kg / m^3)

N_A : Avogadro's number : $6.0221\ 10^{23}$

$$M_{UPu} = (1-y)\left[235\,U_5 + 236\,U_6 + 238\,U_8\right] + y\left[238\,Pu_8 + 239\,Pu_9 + 240\,Pu_0 + 241\,Pu_1 + 242\,Pu_2\right]$$

U_n : isotopic composition in terms of ^{235}U, ^{236}U, ^{238}U. $\left[\frac{U_n}{U_{total}}\right]$

Pu_n : isotopic composition in terms of $^{238}Pu \rightarrow {}^{242}Pu$. $\left[\frac{Pu_n}{Pu_{total}}\right]$

a : lattice parameter (m)

= $[5.47 - 0.074\ y + (0.301 + 0.11\ y)\ x - 0.00039\ \tau]10^{-10}$

τ : burn-up (at% FIMA)

P : pore fraction (/)

2.2.2. Linear thermal Expansion

The UO_2' law is used.

The correction for substoichiometric mixed oxide fuels (O / M < 2) is as follows ***[2]*** (Figure 9):

$$\left(\frac{l_{T_K} - l_{273}}{l_{273}}\right)_{2-x} = \left(\frac{l_{T_K} - l_{273}}{l_{273}}\right)_2 (1 + 3{,}9\ x) \quad \text{avec : } x = 2 - (O/M)$$

2.2.3. Heat Capacity

The heat capacity for a mixed oxide is given by ***[11]*** (Figure 10):

$$c_p\left[(U_{1-y}\ Pu_y)O_{2+x}\right] = c_p\left[(U_{1-y}\ Pu_y)O_2\right] + \frac{x}{2}c_p(O_2)$$

$$c_p\left[(U_{1-y}\ Pu_y)O_2\right] = (1-y)\ c_p(UO_2) + y\ c_p(PuO_2)$$

with:

$$C_p\,(UO_{2.00}) = 46.776 + 10.015\,10^{-2}\,T_K - 10.045\,10^{-5}\,T_K^{\,2} + 4.2386\,10^{-8}\,T_K^{\,3} - 5.0145\,10^{-12}\,T_K^{\,4}$$

$$C_p\,(PuO_{2.00}) = 91.526 + 3.184\,10^{-6}\,T_K^{\,2} - 2.269\,10^{6}\,T_K^{\,-2}$$

$$C_p\,(O_2) = 27.849 + 8.530\,10^{-3}\,T_K - 2.0454\,10^{-6}\,T_K^{\,2} + 1.932\,10^{-10}\,T_K^{\,3}$$

where:

T_K	:	temperature	(K)
C_p	:	heat capacity	(J/(mole.K))

2.2.4. Thermal Conductivity

This recommendation is based on the review of mixed oxide fuel ***[2]***. The general equation for the thermal conductivity is modelled by (Figure 11):

$$\lambda_0 = \frac{1}{A + B\,T_K} + C\,T_K^3$$

with:

$$A = 1.32\,\sqrt{x_s + 0.00931} - 0.0911 + 0.38\,\tau$$

The correction relating to porosity is as follows:

$$\lambda = \left(\frac{1-P}{1+2P}\right)\lambda_0$$

where:

λ	:		(W/(m.K))
B	:	$2.493\,10^{-4}$	(m/W)
C	:	$88.4\,10^{-12}$	(W/(m.K⁴))
x_s	:	2 - O/M (as a function of burn-up)	restricted to 2
τ	:	fractional burn-up	(/)
T_K	:	temperature	(K)
P	:	pore fraction	(/)

As a first approximation, the thermal conductivity may be considered independent from the plutonium content up to 30%.

The degradation in conductivity included in the term "A" is due to:

- the impact of solid fission products ($0.38\,\tau$),
- the variation in the oxide of $\frac{O}{U+Pu}$ ratio (Figure 12):

$$\frac{O}{U+Pu}(\tau)=\left(\frac{O}{U+Pu}\right)_0+\frac{\tau}{1-\tau}\left[\left(\frac{O}{U+Pu}\right)_0-1.5\right]$$

where:

$\left(\frac{O}{U+Pu}\right)_0$: fabrication value,

1.5 : mean half-value of fission product valence

2.2.5. Emissivity

The UO_2 law is used ***[7]***.

2.2.6. Irradiation induced thermal creep

The equation of the stationary creep law is as follow ***[2] [12]*** (Figure 13):

$$\dot{\varepsilon}_{éq}=\exp(25P)\left[A\sigma_{éq}\exp\left(-\frac{48{,}000}{T_K}\right)+B\sigma_{éq}^{4,5}\exp\left(-\frac{75{,}000}{T_K}\right)+C\sigma_{éq}\right]$$

in which:

$A = \frac{3.84\ 10^{-7}}{D^2}$

$B = 3.13\ 10^4$

$C = 2.69\ 10^{-30}\ \dot{F}$

where:

$\dot{\varepsilon}_{eq}$	:	equivalent creep rate	(1/s)
D	:	grain diameter	(m)
T_K	:	temperature	(K)
σ_{eq}	:	equivalent stress (MPa)	limited to 100 MPa
P	:	pore fraction	(/)
$\dot{F}$	:	fission rate	(fission/(m^3.s))

2.2.7. Young's Modulus, Poisson Ratio and Yield stress

The laws for mixed oxide are taken identical to the UO_2 respective laws ***[2] [8]***.

3. OXIDE FUEL MODELS

The main models of behaviour under irradiation to be considered for the kernel are:

- In pile densification,
- Fuel swelling due to fission products,
- Fission gas release
- CO / CO_2's production

For the three ones, the proposed models come from the CEA experience on PWR and FBR oxide fuels. Most are used in our CEA codes for several years and were validated on numerous experiences.

Concerning CO's production, we chose in the open literature empirical models built on experimental data and which were already used in the past in other applications.

3.1. DENSIFICATION

The fuel densification, at the beginning of the irradiation, results from a sintering under both the temperature and the fission spikes. It is the fine porosity population ($\Phi < 1.5\ \mu m$), which is the natural residue of the sintering, which is mainly removed.

Densification models are generally more or less empirical.

In the case of present HTR fuels, the manufactured kernel density is required to be ≥ 95%TD. Consequently, we recommend to apply the following semi-empirical CEA model newly developed for PWR UO_2 and MOX fuels in 2001 ***[13]***.

Nevertheless, the different mode of manufacture from both types of fuels: sintering for the PWR pellets, Sol gel process for the HTR kernels can lead to a size and a distribution in size of the porosity which could probably be different.

1- The volume variation due to the reduction of the porosity is expressed by:

$$\frac{\Delta V}{V} = A\left[1 - \exp\left[-\frac{3\,q\,t}{86{,}400\ \rho\,\tau_0}\left(1+\exp\left(-\frac{Q}{T}\right)\right)\right]\right] \quad (/)$$

with:

A:	function of maximum amplitude densification,	
q :	power density	(W/mm^3)
t :	irradiation time	(s)
ρ :	initial fuel density	(g/mm^3)
τ_0:	end of densification burn up	(MWd/t_{HM})

Q : activation thermal constant (K)
T : fuel temperature (K)

The equation takes into account the key roles of the fission spikes and local temperature to the removal of the small porosity.

Q and τ_0 are empirical constants which depend of the initial microstructure of the fabricated fuel and are set up from experimental data: Q = 750 K and τ_0 = 10,000 MWd / t_{HM}.

The function "A" was also determined from the experience. We provide the subsequent equation of which the coefficients are fitted from the characteristics of the French PWR fuel.

$$A = \alpha \max (5\ 10^{-3} ; 1.8\ 10^{-5}\ T - 1.26\ 10^{-2})$$

with:

α : ajustment parameter: 1 for the French PWR UO2 fuel

2- Evolution of the porosity:

The initial porosity is given by:

$$P_0 = 100\frac{\rho_{th} - \rho}{\rho_{th}} \quad (\%)$$

with:

ρ_{th} : theoretical fuel density (kg / m^3)
ρ : fabricated fuel density (kg / m^3)

The variation of porosity by in pile densification during a time increment Δt is given by:

$$\Delta P = -\left(\frac{\Delta V}{V}(t) - \frac{\Delta V}{V}(t - \Delta t) \right)$$

3- Example of application:

We present in Figure 14 the kinetic of densification (volume variation and reduction of the initial porosity) of a UO_2 fuel of which are the following parameters:

- fabricated fuel density: 95 % TD,
- mean power density: 2.4 W / mm^3,
- fuel temperatures: 900 and 1200 °C

3.2. SWELLING

3.2.1. Solid FP swelling

The fuel is considered as an isotropic material. The swelling rate which is determined in UO_2 and (U, Pu)O_2 fuels from density measurements reflects the "solid swelling". The density measurements carried out on post-irradiated PWR and FR fuels clearly display a linear behaviour in relation with the burn up.

This solid swelling includes not only the contribution of solid FP, but also that of the fission gas in super saturation in the fuel or partly precipitated as nanometric bubbles.

For both UO_2 and (U, Pu)O_2 fuels the solid swelling rate, $\dot{S}_S$ is given by the equation ***[14]***:

$$\dot{S}_s = \frac{dS_s}{d\tau} = \frac{d\left(\frac{\Delta V}{V_0}\right)}{d\tau} = 0.06$$

with:

$\dot{S}_s$: solid swelling rate (% / GWd / t_{HM})

The volume variation from solid swelling during a burn-up increment $\Delta\tau$ is given by:

$$\Delta S_s = \dot{S}_s \, \Delta\tau$$

Input data : $S_s (t - \Delta t)$

Output data : $S_s(t) = S_s(t - \Delta t) + \Delta S_s$

Validity domain : $0 < \tau < 150$ GWd / t_M

3.2.2. Gaseous swelling

The fuel swelling due to gaseous fission products (Xe, Kr) mainly results to the increase of the bubble population and the bubble size in the matrix and in the grain boundaries. The mechanisms which lead to this swelling are generally complex. It is the reason for which gaseous swelling models are often empirical correlations which depend only from some parameters of which the principals are temperature and burn-up.

Some models are available in open literature, and for the HTR application, we propose to use one of the two selected models :

- The "MATPRO" model ***[15]***,
- The "COMETHE" model ***[16]***.

3.2.2.1. The MATPRO model

This empirical model simulates the gaseous steady state free swelling between 1000 and 2000 K. It was correlated on the volumic variations related from CHUBB ***[17]*** and TURNBULL ***[18]***.

The gaseous swelling rate in relation with local temperature is as follow (Figure 15):

$$\dot{S}_g = \frac{dS_g}{d\tau} = 2.19912\ 10^{-28}\ (2800 - T_K)^{11.73}\ \exp\left[-0.0162(2800 - T_K)\right]$$

with:

$\dot{S}_g$: gaseous swelling rate (% / GWd / t_{HM})

T_K : temperature (K)

Taking into account the gas production, the volume variation from gaseous swelling during a burn-up increment is given by :

$$\Delta S_g = \dot{S}_g \exp(-0.19992\,\tau)\,\Delta\tau$$

with:

$\dot{S}g$: gaseous swelling rate (% / GWd / t_{HM})

τ : burn-up at time t (GWd / t_{HM})

$\Delta\tau$: burn – up increment (GWd / t_{HM})

Input data : S_g (t - Δt)

$\Delta\tau$

τ

T_K

Output data : $S_g(t) = S_g(t - \Delta t) + \Delta S_g$

Validity domain : $0 < \tau < 150$ GWd / t_{HM}

3.2.2.2. The COMETHE model

The COMETHE model, developed by BELGONUCLEAIRE, takes into account the effect of the hydrostatic pressure into the fuel on the amplitude of gaseous swelling.

The gaseous swelling rate is given by the following differential equation:

$$S'_g = \frac{dS_g}{dt} = k_0 \left(\frac{\Phi_0}{\Phi}\right) \frac{D_{eff}}{S_g}$$

with:

k_0 : 1.63 10^8

Φ_0 : grain size reference 4 µm

Φ : fuel mean grain size (µm)

D_{eff} : fission gas equivalent diffusion coefficient (m^2/s)

The fission gas equivalent diffusion coefficient is obtained from the fission gas release model (§ 2.3). It depends of the fission gas diffusion coefficient, of the redissolving coefficient of intragranular bubble atoms under the effect of the fission density and of the probability of gas trapping in these bubbles by:

$$D_{eff} = \frac{b_0 \dot{F}}{b_0 \dot{F} + P_{trap}} D$$

with:

D : fission gas diffusion coefficient (m^2/s)

b_0 : probability of resolution of intragranular bubbles (m^3/fiss)

$\dot{F}$ fission rate (fiss/(m^3 s))

P_{trap} : probability of trapping (m^3/fiss)

The volume variation by gaseous swelling during a time increment is as follows:

$$\Delta S_g = \left(2 k_0 \left(\frac{\Phi_0}{\Phi} \right) D_{eff} \right)^{1/2} \Delta t^{1/2}$$

To take into account the effect of the hydrostatic pressure, the following correction is made:

$$S_g(t) = \frac{S_g(t - \Delta t) + \Delta S_g}{1 + \frac{238}{270} \frac{P_{hydro}\, \Delta\tau}{a} + \frac{\Delta S_g}{S_{max}}}$$

with:

P_{hydro} : hydrostatic pressure (MPa)

a : parameter 50

$\Delta\tau$: burn up increment (GWd/t_{HM})

S_{max} : maximum gaseous swelling given by:

$$S_{max} = 0.06 \left(1 + \frac{T - 1400}{300 + |T - 1400|} \right)$$

with:

T : temperature (°C)

Input data : S_g (t - Δt)

D_{eff}

Δt

$\Delta \tau$

P_{hydro}

S_{max}

T_C

Output data : $S_g(t)$

Validity domain : $0 < \tau < 150\ GWd/t_{HM}$

3.2.2.3. Calculation of the gaseous porosity

The gaseous swelling leads to an increase of the porosity (new gaseous porosity):

Input data : $P_g\ (t - \Delta t)$

ΔS_g

Output data : $P_g\ (t)$

3.3. FISSION GAS RELEASE

A certain number of fission gas release models are available for steady state conditions. The release process is relatively complex but it may be reduced as a two stages process : In the first stage, the gas atoms in the grain migrate by several mechanisms towards the grain boundaries. In the second stage, the gas migrates from these boundaries to the free surfaces of the fuel and then it is released in the free volume:

- For its simplicity, the "equivalent sphere" diffusion model (Booth model) is the first selected. This model assumes that the fission gas is released by a diffusion mechanism within the fuel grains and escapes when it reaches the boundary of an equivalent sphere.
- More sophisticated models are always based on the original Booth model but take into account other contributions such the trapping of gas atoms by defects and the resolution by fission spikes or in the case of high burn-up the principle of a saturation threshold which leads to an increase of the kinetic release in the range of low temperatures.

3.3.1. Equivalent sphere model

The fractional gas release (GR) is defined as follows:

$$GR = 1 - \frac{6}{D't} \sum_{n=1}^{\infty} \frac{1 - \exp\left(-n^2 \pi^2 D' t\right)}{n^4 \pi^4}$$

with:

t :	irradiation time	(s)
D':	reduced gas diffusion coefficient	(s^{-1})

The reduced gas diffusion coefficient is related to the diffusion coefficient as $D' = D / a^2$

where "a" is the radius of the "equivalent sphere".

Figure 16 shows the variation of the fractional fission gas release as a function of the dimensionless parameter D' t.

This effective diffusion distance towards the free surfaces of the fuel (open porosity, micro cracks, interconnected bubbles, etc…) expressed by the reduced fission gas coefficient is the key parameter of the Booth model ; its choice have to be made from calibrations to experimental measurements.

HORSLEY ***[19]*** directly gives the relation of the reduced fission gas coefficient suitable for UO_2 and UCO fuel:

$\log_{10} D' = -2.3 + [-8116/T]$ (s^{-1})

with:

T :	fuel temperature	(K)

KOVACKS ***[20]*** proposes the following expression for the apparent fission gas diffusion coefficient*:

$$D = 7.4\ 10^{-12} \exp[-10067/T] \qquad (cm^2.s^{-1})$$

with:

T : fuel temperature (K)

and a value for the equivalent sphere radius for oxide fuels equal to 10 μm.

$$D' = D/a^2 = 7.4\ 10^{-6} \exp[-10067/T] \qquad (s^{-1})$$

Figure 17 shows the comparison between the two formulations and fission gas release calculated with the two propositions are plotted in Figure 18. This example illustrates the great influence of the choice of the reduced diffusion coefficient D' on the result of FGR.

Input data : GR (t - Δt)

T

Δt

Output data : GR (t)

3.3.2. CEA model 1

This semi-empirical model of gas release (model using several adjustable parameters) is well adapted for the calculation of gas release for the thermal conditions encountered in PWR fuels which are not far removed from those of the HTR particles ***[21]***.

We consider that this model is validated on this fuel until 7 % FIMA ; however, its application for higher burn-ups is for us not guaranteed because a new phenomenon such as the fission gas saturation of the matrix which is not taken into account in this model amplifies the release.

Description of the model.

This model is defined as a "two stages" model:

First, it calculates in every point of the fuel the evolution of the balance of the flux of fission gases put back by resolution in the fuel matrix and its diffusion towards the grain boundary:

$$\Phi = \Phi_d - \Phi_r$$

---

* *The effect of fuel defects such porosity, dislocations, grain boundaries etc… is taken account in this apparent diffusion coefficient D*

with:

Φ : gas flux	(at / m².s)
Φ_d : diffusion flux	(at / m².s)
Φ_r : resolution flux	(at / m².s)

$$\Phi_d = 2\frac{D}{d}(\beta t - N_a)$$

and

$$\Phi_r = b_1 \dot{F} \frac{a}{3} N_a$$

with:

D :	fission gas diffusion coefficient	(m² / s)
d :	resolution distance	(m)
β :	fission gas production	(at / m³ s)
t :	time	(s)
N_a :	fission gas retention at the grain boundary *	(at / m³)
b_1 :	probability of resolution of intergranular bubbles	(m³ / fiss)
$\dot{F}$:	fission density	(fiss / m³ s)
a :	mean grain radius *	(m)

* the fuel grain is likened to a sphere.

This gas diffusion, slowed down by the trapping of gas atoms in intragranular bubbles, is modelled by the use of a modified diffusion coefficient taking into account these phenomena:

$$D_{eff} = \frac{b_0 \dot{F}}{b_0 \dot{F} + P_{trap}} D$$

with

D :	fission gas diffusion coefficient #	(m² / s)
b_0 :	probability of resolution of intragranular bubbles	(m³ / fiss)
P_{trap} :	probability of trapping	(m³ / fiss)

the fission gas diffusion coefficient is from TURNBULL and WHITE:

$$D = 7.6\ 10^{-10} \exp\left(-\frac{35{,}225}{T}\right) + 1.2\ 10^{-39}\ \dot{F} + 6.9510^{-25} \sqrt{\dot{F}} \exp\left(-\frac{13{,}870}{T}\right)$$

After saturation in gas trapped at the grain boundaries: interconnection of intergranular bubbles, the quantity of fission gases which is released by percolation towards free volume is a function of the difference of pressure between the intergranular bubbles and the plenum, the medium permeability and the gas viscosity (Darcy's equation):

$$\frac{dN}{dt} = -\frac{k_0}{\mu(1+\xi\sigma_h)}(\Delta p)$$

with:

N	quantity of gas
k_0	permeability of the medium
μ	viscosity
ξ	Constante
σ_h	hydrostatic stress
Δp	pressure drop between intergranular bubbles and plenum

The two main adjustable parameters of the model are the coefficients of resolution of intra and intergranular gas bubbles. Other parameters of the model: diffusion coefficient, size and number of gas bubbles, medium permeability were fixed in a reasonable order of size.

The numerical values of the coefficients of resolution were defined from calculations made on a set of PWR fuel rods within the framework of the validation of the version 1.5 of the METEOR code; they were revised recently on a widened database (100 fuel elements) for the current version (V1.9).

The fission gas release rate for various imposed irradiation temperature is given in Figure 19.

3.3.3. CEA model 2

This second CEA model was developed for the FBR mixed oxide fuel ; it takes into account the fact that the fission gas release evolves with the burn-up increase ***[22]***. If a "booth" model is suitable for low burn-up, it does not allow to correctly assess the FGR when the fuel structure changes at high burn-up particularly in the temperature range : 600 – 1200°C. Consequently, this model seems rather adapted for fuel burn-up larger than 10% FIMA.

The model takes into account an athermal diffusion of the fission gas atoms which is prevailing below 1000°C and a gas saturation threshold function of the temperature. For the calculation of the saturation threshold, the model adopts the SPEIGHT theory ***[23]*** which considers that the phenomena is controlled by the resolution into the matrix of the gas atoms from the bubbles as a result of fission spikes. The main consequence is the formation of an intra and inter granular gaseous porosity which interconnects and favours the fission gas release.

We provide hereafter the outlines of the modelling.

A Saturation threshold model

The saturation threshold is reached when the value of the output flux of fission gas atoms from the fuel is equal to the value of the resolution flux from the bubbles in the fuel grain.

From the equality of the two fluxes, we can estimate the fission gas concentration in the fuel at the saturation threshold:

$$Q_{sat} = \frac{b d \dot{F} N_S}{2D} \qquad (at./m^3)$$

with:

b :	probability of resolution	(m^3 / fiss.)
d :	resolution distance	(m)
$\dot{F}$:	fission density	(fiss. / m^3.s)
N_S :	surface density of gas in the bubbles	(at. / m^2)
D :	fission gas diffusion coefficient	(m^2 / s)

- the coefficients “b” and “d” are adjustable ; their respective values are get from the open literature ***[24] [25] [26]***:

  $b = 5\ 10^{-24}$ m^3 / fiss.

  $d = 10^{-8}$ m

- the fission gas diffusion coefficient is from the LAWRENCE review ***[27]***:

$$D = 7.6\ 10^{-10} \exp[-35{,}225/T] + 1.2\ 10^{-39} F$$

- the surface density of gas in the bubbles is given by the following established equation for the lenticular bubbles :

$$N_S = 0.3839 \frac{r_b}{kT}\left(\frac{1.6}{r_b} + P_{ext.}\right) \qquad (at./m^2)$$

with:

r_b :	bubble radius	(m)
k :	Boltzmann’s constant	$1.38066\ 10^{-23}$ J / K
$P_{ext.}$:	plenum pressure	(Pa)

Experimental results on various PHENIX fuel allowed to determine a rough estimate for the bubble radius ***[22]***:

$r_b = 5\ 10^{-8}$ m

Figure 20 presents the temperature of the saturation threshold of fission gas in the oxide fuel Q_{sat} converted in cm^3 NTP / g_{oxide}. At low temperature (< 1100 °C), the figure shows that an athermal resolution takes place and consequently decreases the fission gas saturation level.

B Limit of gas retention

Experimental measurements (EPMA and fuel sublimations) indicate a limit of gas retention in the oxide fuel at high burn up independent from the fuel temperature below 1000 °C. This value is assessed to ***[22]*** :

$N_l = 0.8$ cm^3 NTP/g_{oxide}

At high burn up and in this range of fuel temperature, the kinetic of fission gas release tends towards a regime characterized by the following equation:

$$\frac{dN}{dt} = \beta - h'N$$

with:

N :	fission gas retention in the fuel	(cm^3 / g)
β :	fission gas production	(cm^3 / (g.s))
$h' = \frac{15\,D}{a'^2}$	time diffusion constant	(s^{-1})
D :	fission gas diffusion coefficient	(m^2 / s)
a'² :	radius of the equivalent sphere	(m)

For a limit of fission gas retention of 0.8 cm^3 NTP / g_{oxide}, the value of the radius of the equivalent sphere is equal to: 4 µm ***[22]***.

C Transition towards the high burn up regime

The transition towards the equilibrium regime for high burn up supposes that we accurately describe the development of the gas porosity and the kinetic of gas release. This type of description is very complex and we have preferred to adopt a advantageous simplification which consists to add at the diffusion equation a transient term indicating that the gas release is proportional to the excess of fission gas retained versus the equilibrium state:

$$\frac{dN}{dt} = \beta - h'N - k(N - N_l)$$

with:

k :	time constant	(s^{-1})
N_l :	limit of fission gas retention at high BU	(cm^3 / g_{oxide})

The time constant "k" compatible with the fission gas retention measurements performed on irradiated fuels is taken to: 2 10^{-7} s^{-1} ***[22]***.

3.4. CO PRODUCTION

Among the different gas which contribute to the inner pressure build-up, the CO production from the reaction between the free oxygen liberated by fissions and the carbon of the inner coatings may become a significant part.

In a large measure, the production of free oxygen depends on the nature of the fuel. It is proved that fuels containing carbon do not produce free oxygen unlike UO_2 and $(U, Pu)O_2$. A lot of data exists for UO_2 fuels but it is not the case for mixed oxide or pure PuO_2 fuels.

3.4.1. HOMAN model

The moles of CO produced are considered as equivalent to the moles of oxygen released by the UO_2 fuel during fissioning with the following reaction:

$C + ½ O_2 \rightarrow CO$

It is assumed that negligible CO_2 is formed under normal operating conditions.

The formulation proposed by HOMAN for low-enriched uranium fuels (^5U < 20wt%) takes into account the dependability of plutonium fissions on the oxygen production ***[28]***.

The following equations have been proposed :

$$O / f = 1.64 \exp[-3311/T]$$

and

$$O / f_{max} = 0.61$$

with:

O / f :	atomic oxygen release per fission	(/)
T :	temperature	(K)

The CO production rate may be set in cm^3 NTP per g oxide:

$$\frac{d[CO]}{dt} = \frac{22{,}414\ \dot{F}\ (O/f)}{N_A\ \rho}$$

with:

$\dot{F}$:	fission rate	fission / (cm^3.s)
22,414 :	molar volume	cm^3 NTP / mol
N_A	(Avogadro number)	$6.0221\ 10^{23}$
ρ :	fuel density	g / cm^3

For a given temperature, the CO production is proportional to the fuel burn-up.

Input data : $[CO]\ (t - \Delta t)$

Δt

T

$\dot{F}$

Output data : $[CO]\ (t)$

3.4.2. PROKSCH model

The formulation proposed by PROKSCH and coll. also takes into account the role of plutonium fissions on the oxygen production but in addition an increase of the oxygen release with the irradiation time ***[29]***.

He proposes the following equations:

$$\log_{10}\left[(O/f)/t^2\right] = -0.21 + (-8500/T)$$

and

$$O/f_{max} = 0.4\, f_U + 0.85\, f_{Pu} \text{ with a upper limit of } 0.625$$

with:

O/f :	atomic oxygen release per fission	(/)
t :	irradiation time	(d)
T :	temperature	(K)
f_U :	U fission rate	(/)
f_{Pu} :	Pu fission rate	(/)

The CO production rate may be set in cm^3 NTP per g oxide:

$$\frac{d[CO]}{dt} = \frac{22{,}414\, \dot{F}\, (O/f)}{N_A\, \rho}$$

Input data : $[CO]\ (t - \Delta t)$

t

Δt

T

$\dot{F}$

Output data : [CO] (t)

The comparison of Fig 2.9 (Holman model) and 2.10 (Proksch model) shows a great difference between the two formulations. The second one is more sensitive with the temperature.

To estimate better the kinetics of forming CO / CO_2 in the coated particle, DEC intends to launch a certain number of parametrical thermodynamic calculations for UO_2 then PuO_{2-x} fuel kernels with the "SAGE" software.

4. OTHER MODELS

4.1. NEUTRONICS

Numerous properties and models depend on irradiation parameters such the fission rate, the burn up … Therefore, it needs to accurately calculate these parameters all along the fuel irradiation.

4.1.1. Burn up

The burn up is the energy released during the life of fuel per unit of mass. Generally the burn up is expressed either by taking the oxide mass or the mass of heavy metal (HM).

The local increment of burn up is given by the following equation:

$$\Delta\tau = \frac{q\,\Delta t}{\rho} \qquad MWd/t_{HM}$$

with:

q :	power density	(W/cm^3)
Δt :	time increment	(d)
ρ :	HM fuel density	(g_{HM}/cm^3)

The total burn up at time t is:

$$\tau(t) = \tau(t-\Delta t) + \Delta\tau \qquad MWd/t_{HM}$$

4.1.2. Fission rate

Many properties of fuel are affected by the fission rate and by the cumulative number of fissions (fission density).

The fission rate per unit of volume is given by:

$$\dot{F} = N_{HM}\,\Phi \sum_i N_i \sigma_{fi} \qquad fissions/(cm^3.s)$$

with:

N_{HM} :	number of HM per unit volume	$(atoms/cm^3)$
Φ :	neutron flux	$(neutron/cm^2.s)$
N_i :	enrichment of the fissile actinide i	$(/)$
σ_{fi} :	effective fission cross section of the fissile actinide i in the appropriate neutron-energy spectrum	(cm^2)

To be solve, this equation needs to know, at each step of the irradiation, the evolution of the composition in fissile actinides : ^{235}U, ^{239}Pu ^{241}Pu etc..; for that, a more or less complex neutronics model have to be used.

However, if the power density is given as an input data by an external neutronics analysis, it is achievable to calculate the fission rate from the power density by the subsequent equation:

$$\dot{F} = \frac{q}{E_f} \qquad \text{fissions/(cm}^3\text{.s)}$$

with:

q :	power density	(W/cm^3)
E_f :	averaged fission energy	(J)

The recommended data for E_f is **200 MeV**, that is : **$3.204\ 10^{-11}$ J**

The fission density at time t is:

$$F(t) = F(t-\Delta t) + \dot{F}\Delta t \qquad \text{fissions/cm}^3$$

with:

Δt :	time increment	(s)

4.1.3. Fuel burn up

The fractional fuel burn up (% FIMA) may be deduced from the burn up or from the fission density with the following equation:

$$\tau = 100\frac{F}{HM_0} \qquad \text{\% FIMA}$$

with:

F :	fission density	$(fissions/cm^3)$
HM_0 :	initial density of heavy-metal atoms	$(atHM/cm^3)$

This initial density of heavy-metal atoms is obtained from:

$$HM_0 = N_A\frac{\rho_{HM}}{M_{HM}} \qquad \text{atHM/cm}^3$$

with:

NA :	Avogadro's number:	$6.0221\ 10^{23}$
ρ_{HM}:	HM fuel density	(gHM/cm^3)
M_{HM}:	HM molar mass	(g)

The HM fuel density and the HM molar mass depend on the nature of the fuel (UO_2, $(U,Pu_y)O_{2-x}$ or PuO_2). Refer to § 2.1.1 and 2.2.1.

4.1.4. Fission products production

Fission products (FPs) appear with a known probability following a curve with two bumps which depends both of the fissile nuclei (^{235}U, ^{239}Pu, ^{241}Pu ...) and also but less on the neutron spectrum.

Among the some hundred FPs isotopes produced of which the majority are very unstable short lived isotopes, the fission gas (xenon + krypton), caesium, silver, iodine, palladium and strontium isotopes have to be considered for the particle behaviour.

The quantities of each FP isotope produced are determined from the fission yield (FY) of this isotope :

FY(FPi) is the fraction of nuclei of the isotope FPi by one fission

with:

$$\sum_{FPi} FY(FPi) = 2$$

The main fission products isotopes to be considered would be:

Fission gas isotopes (xenon and krypton):

^{131}Xe (stable), ^{132}Xe (stable), ^{134}Xe (stable) and ^{136}Xe (> 10^{19} y)

^{83}Kr (stable), ^{84}Kr (stable), **^{85}Kr (10.7 y)** and ^{86}Kr (stable)

Cæsium isotopes:

^{133}Cs (stable), **^{134}Cs (2.07 y),** ^{135}Cs (2.3 10^6 y) and **^{137}Cs (30.07 y)**

Silver isotopes:

^{109}Ag (stable) and **^{110m}Ag (249.8 d)**

Iodine isotopes:

^{127}I (stable) and ^{129}I (1.57 10^7 y)

Strontium isotopes:

^{88}Sr (stable) and **^{90}Sr (28.78 y)**

Palladium isotopes:

^{104}Pd (stable), ^{105}Pd (stable), ^{106}Pd (stable), ^{107}Pd (6.5 10^6 y), ^{108}Pd (stable), and ^{110}Pd (stable)

The creation rate of each element (isotope) depends on:

- the fission yield of each isotope which changes with the fuel burnup (evolution of the concentration of the fissile nucleus)
- the capture cross section and the time constant of radioactive decay of these isotopes but also of their precursors.

We propose in the following table the creation rate data for the main FP and FP isotopes coming from a 4% ^5U enriched UO_2 fuel irradiated in a thermal spectrum:

Element or Isotope	FP production rate (Atom or isotope / fission)	FP decay period (year)
Xe	0.272	
Kr	0.029	
^{85}Kr	$2.15\ 10^{-3}$	10.71
^{134}Cs	$9.15\ 10^{-3}$	2.07
^{137}Cs	$6.20\ 10^{-2}$	30.07
^{90}Sr	$4.30\ 10^{-2}$	28.78
^{110m}Ag	$3.05\ 10^{-3}$	0.684 (249.8 d)

4.2. FREE VOLUME OF THE PARTICLE

The inner void volume available to released fission gas and CO production evolves during the life of the coated particle.

It may be assessed from the following assumptions:

- evolution of the open porosity in the fuel kernel and the buffer layer,
- expansion or/and reduction of the volumes of the fuel kernel (densification then swelling) and the buffer layer (densification).

$$F_V = V_{kop} + V_{bop} + V_{gap}$$

with:

F_V :	free volume in the coated particle	(mm^3)
V_{kop} :	volume from the kernel open porosity	(mm^3)
V_{bop} :	volume from the buffer open porosity	(mm^3)
V_{gap} :	volume of the kernel / buffer gap	(mm^3)

Calculation of these three contributions (spherical geometry):

1 - Volume from the kernel open porosity

$$V_{kop} = \frac{4}{3}\pi kop r_k^3$$

with:

kop :	kernel open porosity	(/)
r_k :	radius of the kernel	(mm)

2 - Volume from the buffer open porosity

$$V_{bop} = \frac{4}{3}\pi bop\left(r_{eb}^3 - r_{ib}^3\right)$$

with:

bop :	buffer open porosity	(/)
r_{eb} :	outer radius of the buffer	(mm)
r_{ib} :	inner radius of the buffer	(mm)

3 - Volume of the kernel / buffer gap

It is realistic that a slight open gap between kernel and buffer could be created after fabrication during the cooling down following the last thermal treatment of the compact. Furthermore, this gap tends to

increase during the strong densification of the buffer at the beginning of life, but later, it is going to decrease when the kernel is going to swell.

We have made an estimation of this possible gap opening after fabrication from the differential thermal expansion of the kernel and buffer materials:

$$g = r_k \, (\alpha_{kernel} - \alpha_{buffer}) \, \Delta\theta$$

with:

g :	gap opening	(mm)
r_k :	radius of the kernel	(mm)
α_{kernel} :	CTE of the kernel material ($10\ 10^{-6}$)	(K^{-1})
α_{buffer} :	CTE of the buffer material ($5\ 10^{-6}$)	(K^{-1})
$\Delta\theta$:	gap of temperature between the last thermal treatment of the compact and the currently temperature (K)	

The calculations for various ranges of variation of temperature ($\Delta\theta$ = 200 to 800 °C) always lead to very small values for this gap opening : < 1 µm. As a consequence, one can admit that the existence or not of this gap between the kernel and the buffer at the beginning of life does not contribute to the initial free volume of the coated particle.

4- Evolution of the free volume during irradiation

Under irradiation, several simultaneous phenomena, which are going to modify the free volume, take place with different kinetics:

- the strong buffer densification which is very fast at the beginning of life but ends at medium burn up and can be possibly substituted at high burn up by an anisotropic swelling of the material,
- the kernel swelling (§ 3.2),
- possibly changes in the buffer and kernel open porosities.

Both first phenomena directly play on the evolution of the gap. If one admits that buffer and IPyC stay mechanically bonded during irradiation, the densification of the buffer is going to lead to mainly an increase of the internal radius of the buffer. Let's note that this approach is voluntarily simplified because, in the reality, the strong densification of the buffer is going to initiate numerous cracks in the buffer ring.

The equation which gives the volume increment of the gap due to the densification of the buffer and to the swelling of the kernel during time step Δt, is given by:

$$\Delta V_{gap} = 4\pi (r_{ib}^2 \, \Delta r_{ib} - r_k^2 \, \Delta r_k) \qquad (mm^3)$$

with:

Δr_{ib} :	inner buffer radius variation	(mm)
Δr_k :	kernel radius variation	(mm)

$$V_{gap}(t) = V_{gap}(t - \Delta t) + \Delta V_{gap}$$

Concerning the third contribution, one may consider that a decrease of the initial open porosity of the buffer is mechanically equalled by an identical increase of the free volume ; as a consequence, there is not time variation of the volume from the buffer open porosity. The reduction of the kernel open porosity for a fuel with an high density of fabrication (> 95 %TD) which classically stand for less than 10% of the total porosity remains completely marginal.

The two next figures give an example of the probable extent of the free volume during irradiation [1]:

- initial fuel kernel radius : 250 µm
- buffer thickness : 100 µm
- kernel open porosity 0.5%
- buffer open porosity 25%

From these data, the calculated initial free volume of the particle is equal to 0.029 mm^3.

If we assume a complete reduction of the open porosity of the buffer and a fuel solid fission product swelling given by the equation § 3.2.1, the evolutions of the kernel and inner buffer radius are given by Fig. 24 and the evolutions of kernel / buffer gap volume and total free volume by Fig. 25.

4.3. INTERNAL PRESSURE

The internal particle pressure is a function of:

- the quantity of gas present in the free volume,
- the value of this free volume,
- the temperature.

$$P_{int} = \frac{R\sum_{i=1} n_i}{\frac{V_{kop}}{T_k} + \frac{V_{bop}}{T_b} + \frac{V_{gap}}{T_{gap}}} \qquad \text{(MPa)}$$

with:

R:	gas constant (8.31441 10^{-3})	(kJ/K.mol)
n_i :	mole quantity of gas i	(mol)
T_k, T_b, T_{gap} :	mean temperature in kernel (k), buffer (b) and gap	(K)

The considered gas are xenon, Krypton and carbon monoxide.

---

[1] *In this example, we do not take into account deformations such as the thermal expansion or the shrickage of the dense PyC layer.*

REFERENCES

[1] Propriétés physiques et mécaniques du dioxyde d'uranium - Aide mémoire
AIEA, Technical report series n°39
M. BRUET NT CEA DMG / SER référence : M22-B

[2] Catalogue européen des propriétés de l'oxyde mixte (U, Pu)O_2 AGT 010101
NT CEA SPU / LPCA n°2 11 / 1990

[3] K. LASSMANN , A.MORENO (System MAPLIB) ATKEBO 30 (1977) 207-215

[4] JH. HARDING, DC. MARTIN JNM 166 (1989) 223-226

[5] Modelling of UO_2 based SIMFUEL thermal conductivity : the effect of burn-up
LUCUTA - MATZKE – VERALL JNM 217 (1994) 279-286

[6] METEOR V2.0 : Conductivité thermique de l'UO_2
V. MARELLE NT CEA SESC / LSC 99-2026 (DR) de septembre 1999 (this document is classified)

[7] Thermophysical properties of uranium dioxide
JK. FINK , MG. CHASANOV , L. LEIBOWITZ JNM 102 (1981) 17-25

[8] Étude en compression de UO2 non dopé : évolution des grandeurs élasto-plastiques
V. BASINI A. MOCELLIN NT CEA SPUA / LACA N°19 de février. 2001

[9] Recommandation pour la loi de fluage stationnaire de l'UO2 non dopé : mise à jour de fin 1998 intégrant les études de fluage sur les lots L209609 et L209619
M. SLADKOFF, F. HUET et A. MOCELLIN NT CEA SPUA / LACA n°007 d'octobre 1999

[10] Programme de calcul GERMINAL 1.4 – Notice de présentation
M. PELLETIER et L. ROCHE NT CEA SESC / LSC 00-027

[11] Catalogue des propriétés du combustible MOX pour les réacteurs à eau sous pression – teneur en Pu comprise entre 3 et 15%
Y. PHILIPPONNEAU, C. DURIEZ, R. VIALLARD NT CEA LPCA n°49 d'août 1996

[12] Catalogue européen des propriétés de l'oxyde mixte (U, Pu)O_2 AGT 010101. A proposed amendment to the creep data sheet from D. G. MARTIN (1992)

[13] Étude et modélisation de la densification en pile des oxydes nucléaires UO2 et MOX
A. BOULORE
Thèse de l'Institut National Polytechnique de Grenoble et de l'École Nationale Supérieure des Mines de Saint-Etienne soutenue le 15 mars 2001 N°249 TD

[14] Le combustible nucléaire et son état physico-chimique à la sortie des réacteurs (chapitre VII)
P. DEHAUDT et al. CR CEA / DRN / DEC 99007

[15] MATPRO version 11 – A handbook of materials properties for use in the analysis of LWR fuel rod behavior
DL HAGRMAN and GA REYMAN NUREG / CR 0497 Feb. 1979

[16] COMETHE 3L – General description
N. HOPPE, M. BILLAUX and J. VAN VLIET BN8201-04 (January 1982)

[17] Observations relating to the mechanisms of swelling and gas release in uranium dioxide of high temperatures
W.CHUBB and al JNM 44 (1972) p 136

[18] Swelling in UO2 under conditions of gas release
J.A. TURNBULL and M.O. TUCKER The philosophical magazine, 30 (1974) p 47

[19] The Mathematical Basis of the PANAMA-I Code for modelling pressure vessel failure of TRISO coated particles under accident conditions
K. VERFONDERN and H. NABIELEK HTA-Projekt HTA-IB-03 / 90

[20] High-temperature gas-cooled reactor fuel pressure vessel performance models
W.J. KOVACS,et al Nuclear Technology vol 68 p 344 (1985)

[21] Relâchement des gaz de fission ; modélisation niveau 1
C. STRUZIK, E. FEDERICI et J.P. PIRON NT CEA SDC / LEMC 94-2049 (DR) (this document is classified)

[22] Modèle de relâchement des gaz de fission en régime permanent dans les combustibles RNR
J.P. PIRON NT CEA SDC / LMC 92-2006 (DR) (this document is classified)

[23] A calculation on the migration of fission gas in material exhibiting precipitation and resolution of gas atoms under irradiation
M.V. SPEIGHT Nuclear Science eng. p180 (1969)

[24] A new fission gas release model
R.J. WHITE et al. JNM 118 p1 (1983)

[25] The stability of gas bubbles in an irradiation environment
R.S. NELSON JNM 31 p153 (1969)

[26] Fundamental aspects of nuclear reactor fuel elements
D.R. OLANDER TID 26711 P.1 (1976)

[27] A review of the diffusion coefficient of fission product rare gases in uranium dioxide
G.T. LAWRENCE JNM 71 p195 (1978)

[28] Low enriched fuel particle performance review
F. Homan et al GA-A14759 US DOE Aug. 1978

[29] Production of carbon monoxide during burn-up of UO2 kerneled HTR fuel particles
E. PROKSCH, A. STRIGL and H. NABIELEK JNM 107 p280 (1982)

LIST OF FIGURES

FIGURE 1 : LINEAR THERMAL EXPANSION COEFFICIENT FOR UO_2

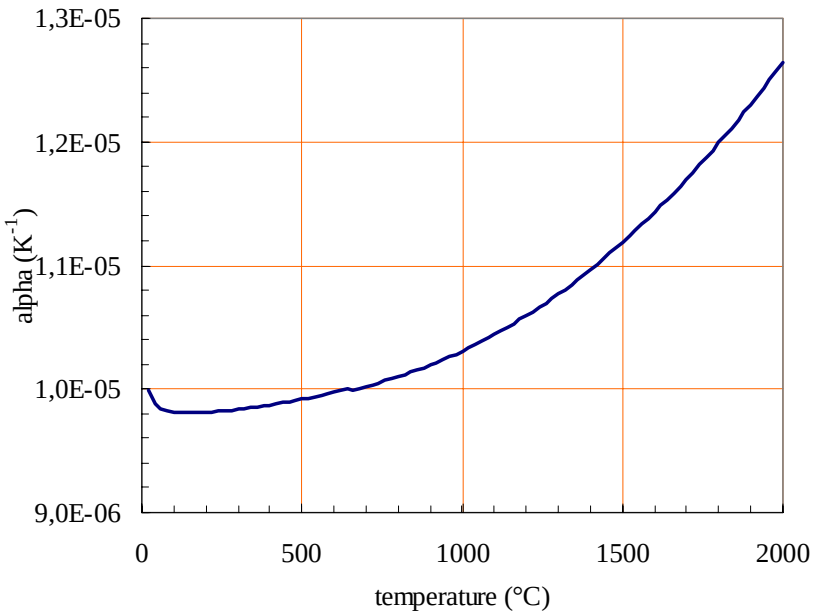

FIGURE 2 : HEAT CAPACITY FOR UO_2

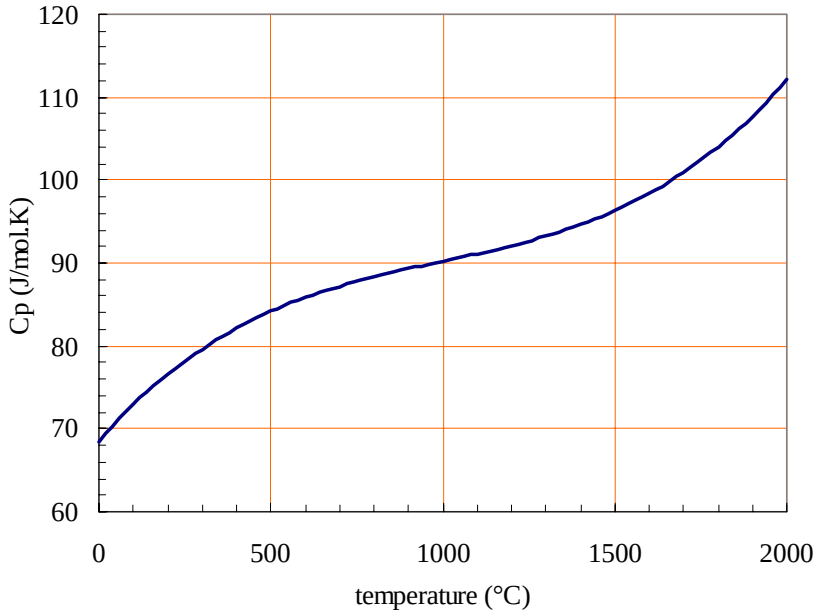

FIGURE 3 : THERMAL CONDUCTIVITY OF UO_2 FUEL

(Martin's recommendation)

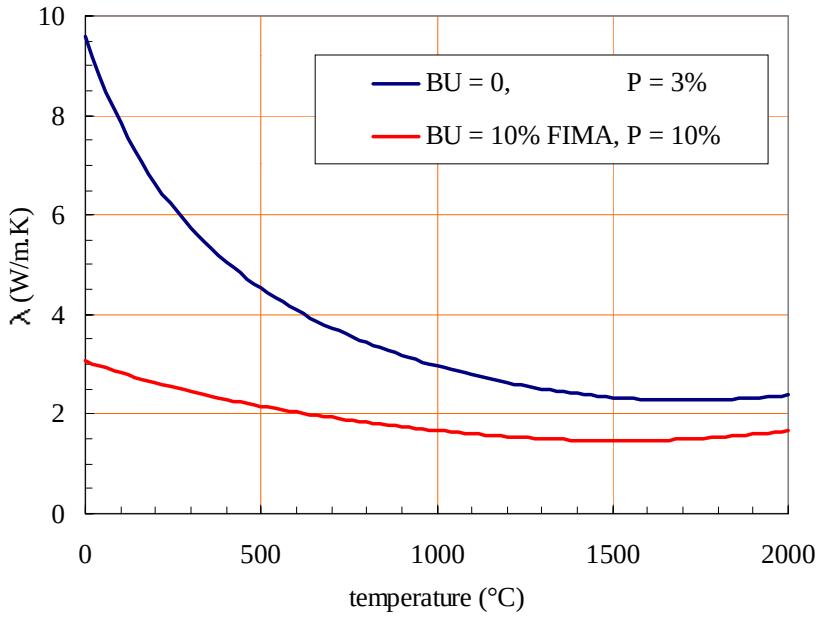

FIGURE 4 : THERMAL CONDUCTIVITY OF UO_2 FUEL

(CEA recommendation)

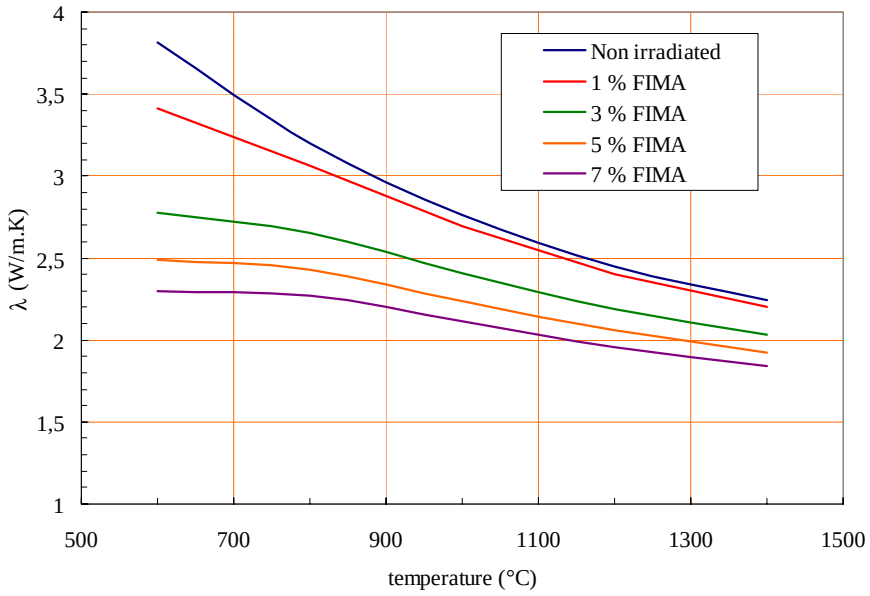

FIGURE 5 : YOUNG'S MODULUS FOR UO_2

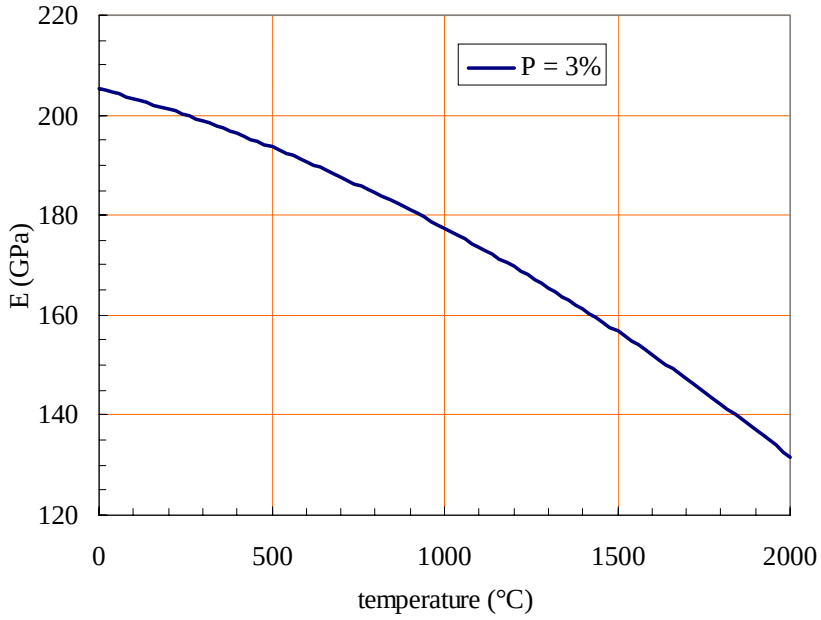

FIGURE 6 : POISSON'S RATIO FOR UO_2

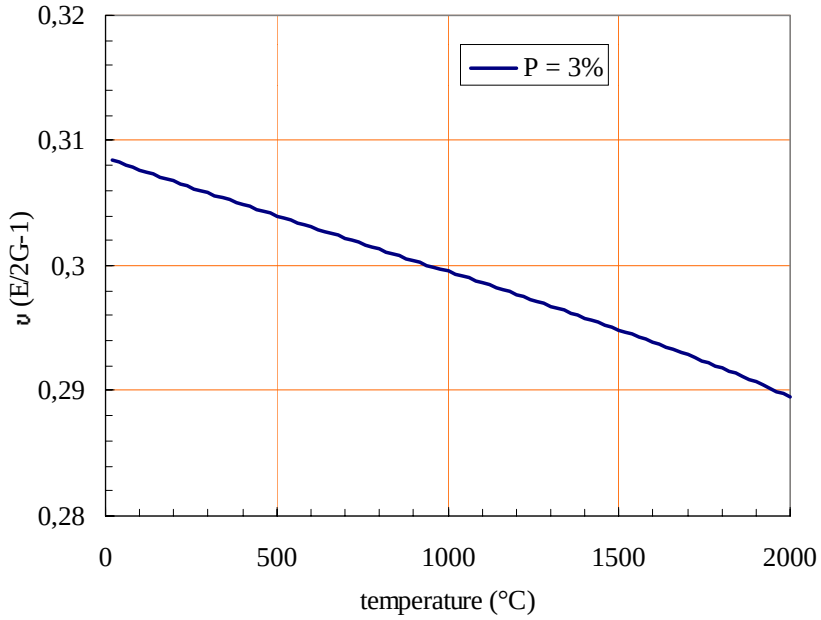

FIGURE 7 : IRRADIATION AND THERMAL CREEP RATE OF UO_2 FUEL

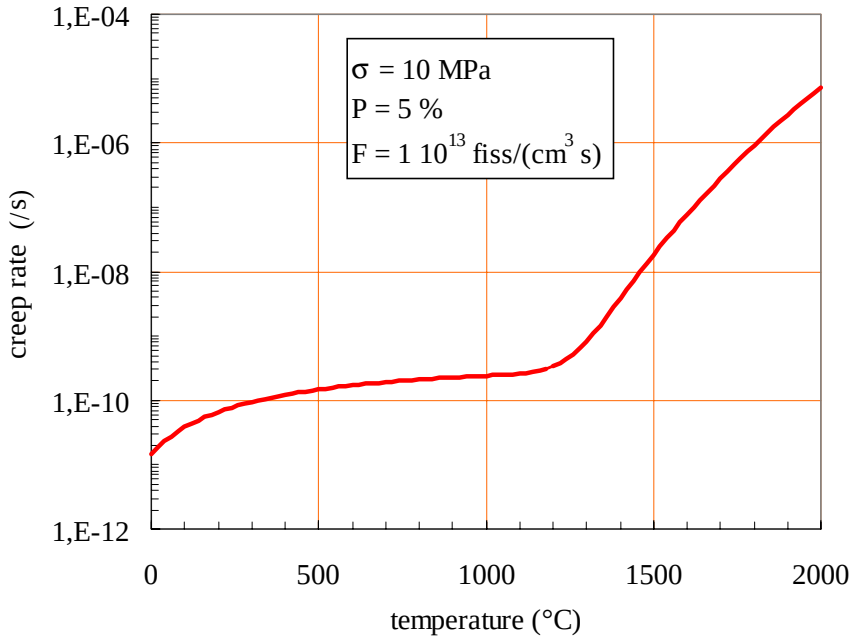

FIGURE 8 : DENSITY OF (U, PU)O_2 FUEL

Pu content = 20%

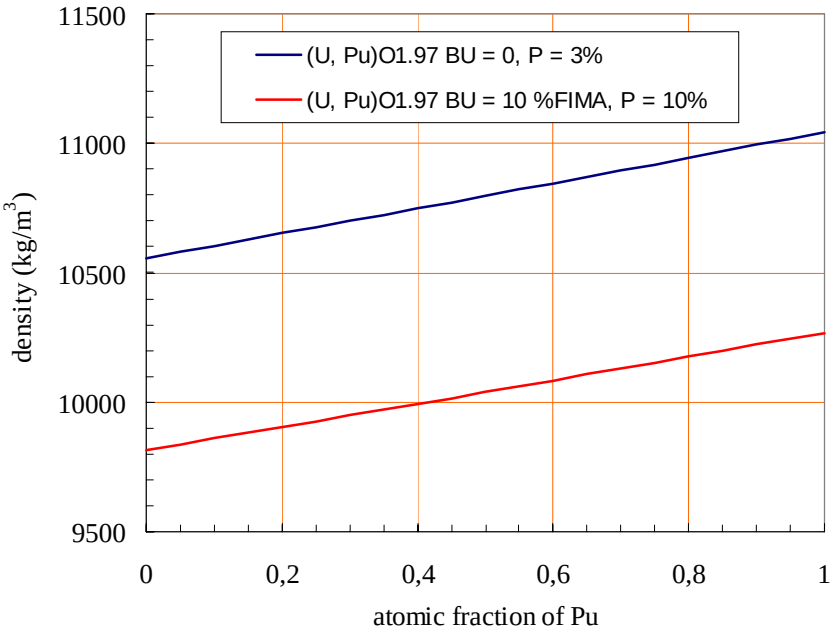

FIGURE 9 : LINEAR THERMAL EXPANSION COEFFICIENT FOR (U, PU)O_2

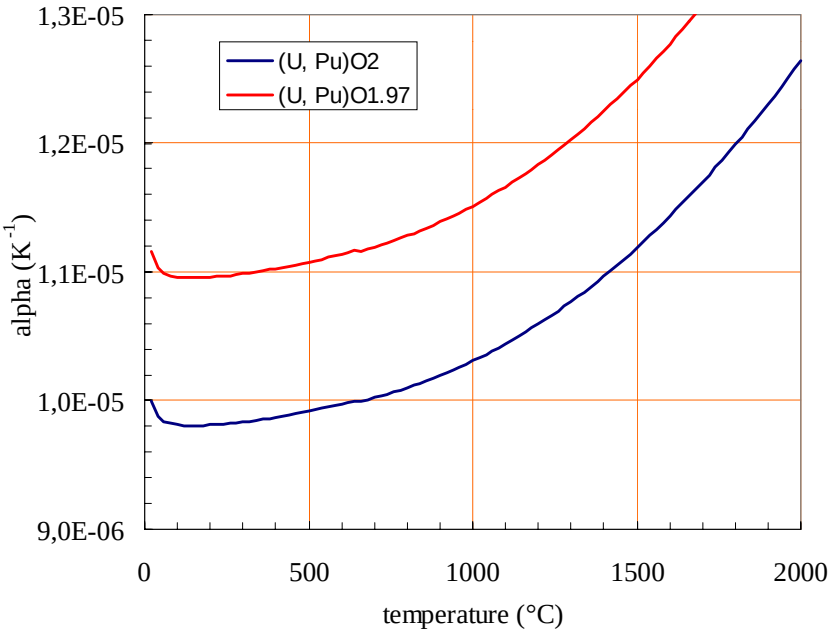

FIGURE 10 : MASS THERMAL CAPACITY FOR (U, PU)O_2

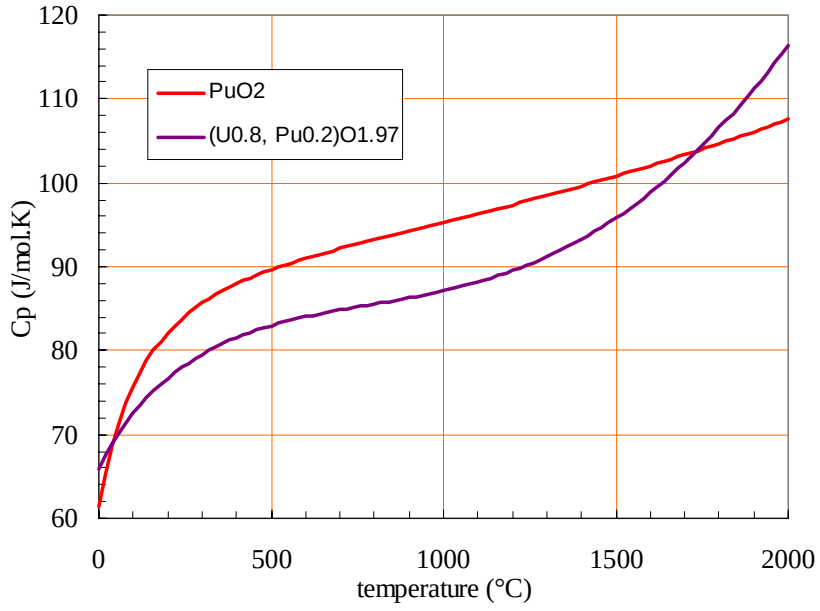

FIGURE 11 : THERMAL CONDUCTIVITY FOR $(U, Pu)O_2$

$(O/M)_0 = 1.97$, t = 10%FIMA, P = 10%

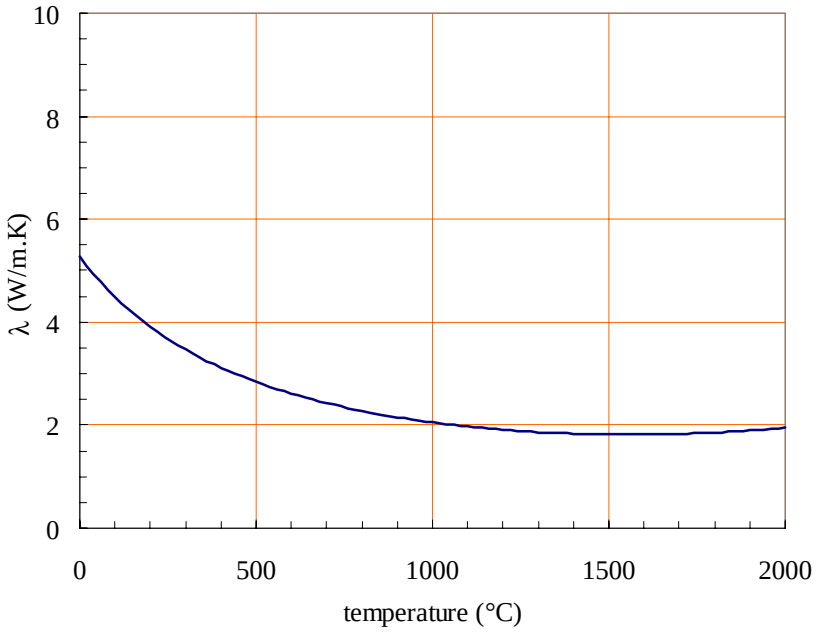

FIGURE 12 : EVOLUTION OF THE O/M RATIO

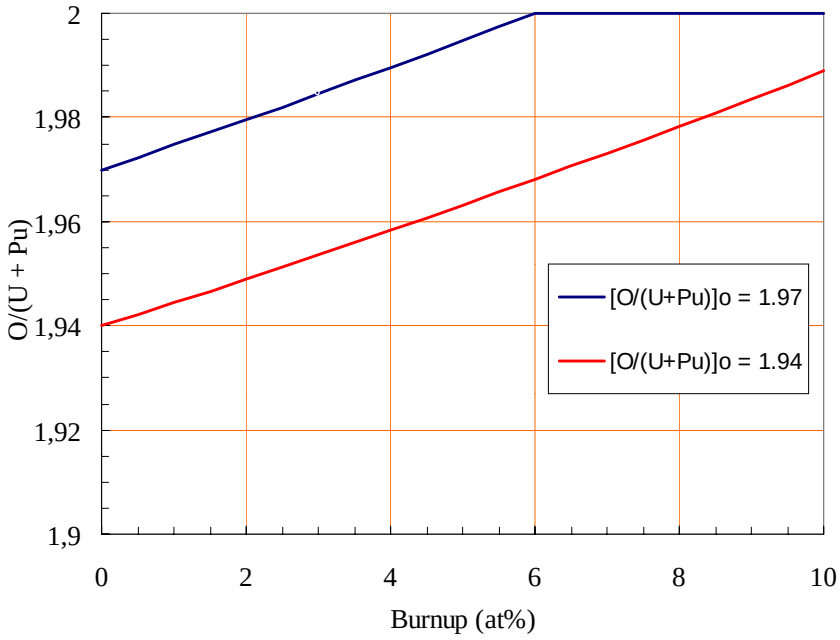

FIGURE 13 : : IRRADIATION AND THERMAL CREEP RATE OF (U, PU)O_2 FUEL

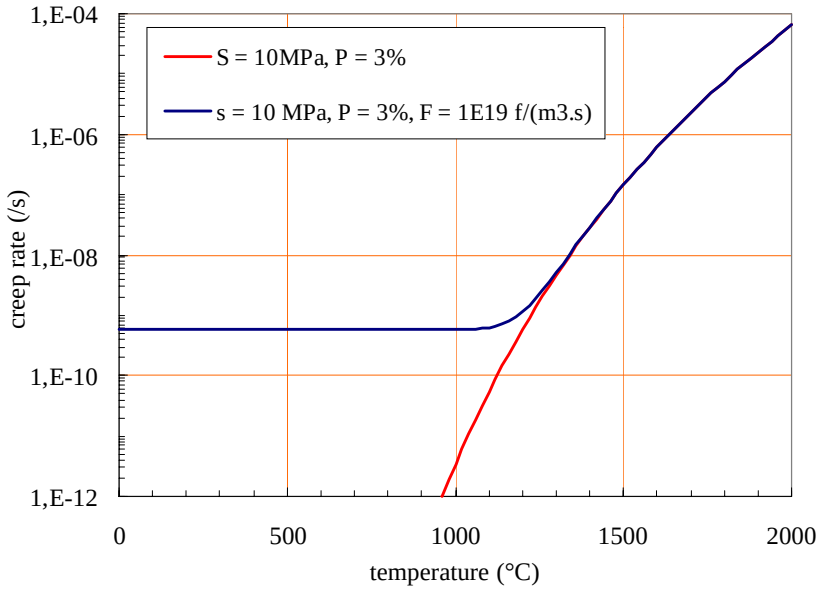

FIGURE 14 : IN PILE FUEL DENSIFICATION

Kinetic of pore densification of the GT_MHR fuel by means of the semi empirical CEA model

1 : Volume variation

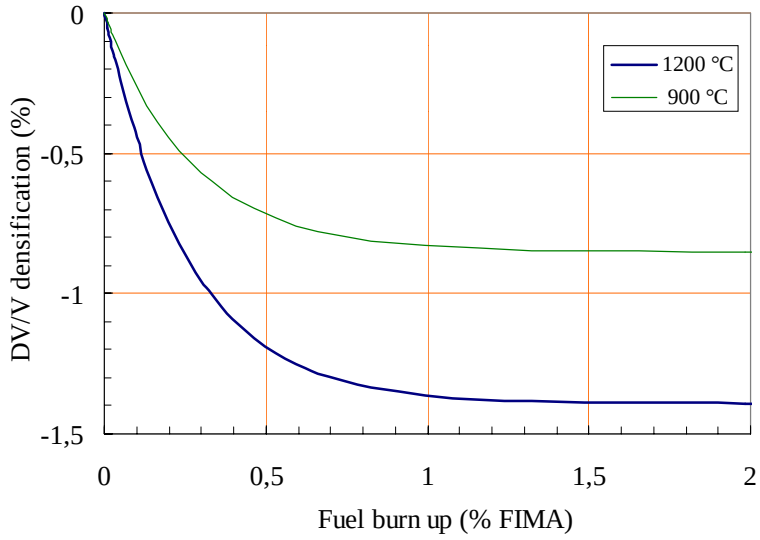

FIGURE 14: IN PILE FUEL DENSIFICATION

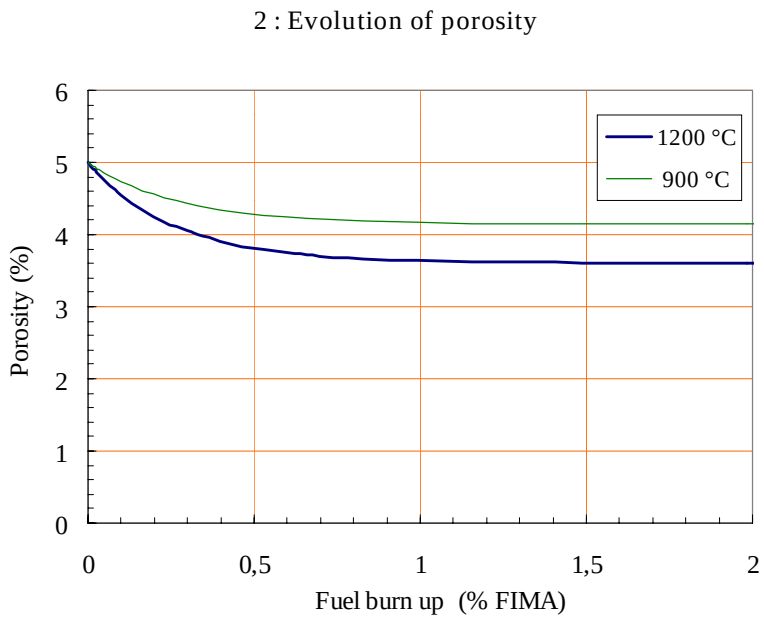

FIGURE 15 : GASEOUS SWELLING RATE FROM THE MATPRO MODEL

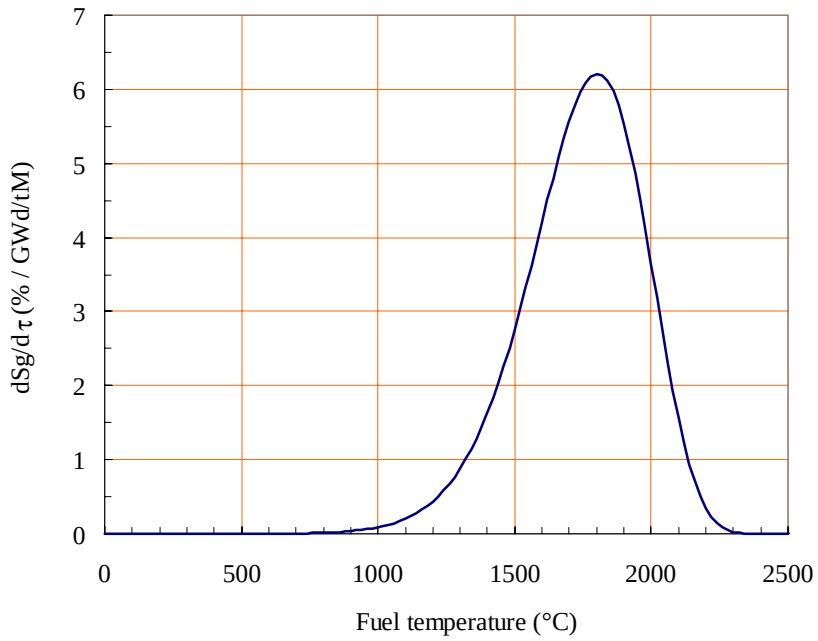

FIGURE 16 : EVOLUTION OF THE FRACTIONAL FISSION GAS RELEASE

(Equivalent sphere model)

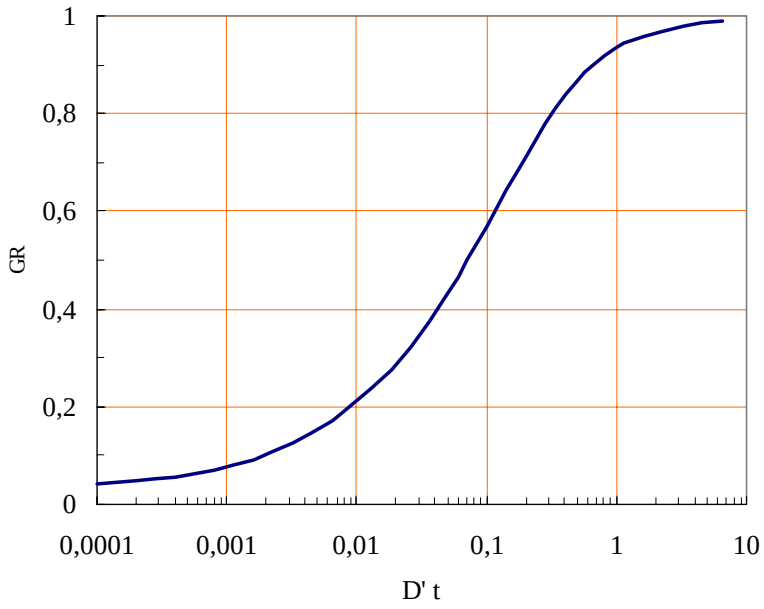

FIGURE 17 : REDUCED FISSION GAS DIFFUSION COEFFICIENT : D'

(Equivalent sphere model)

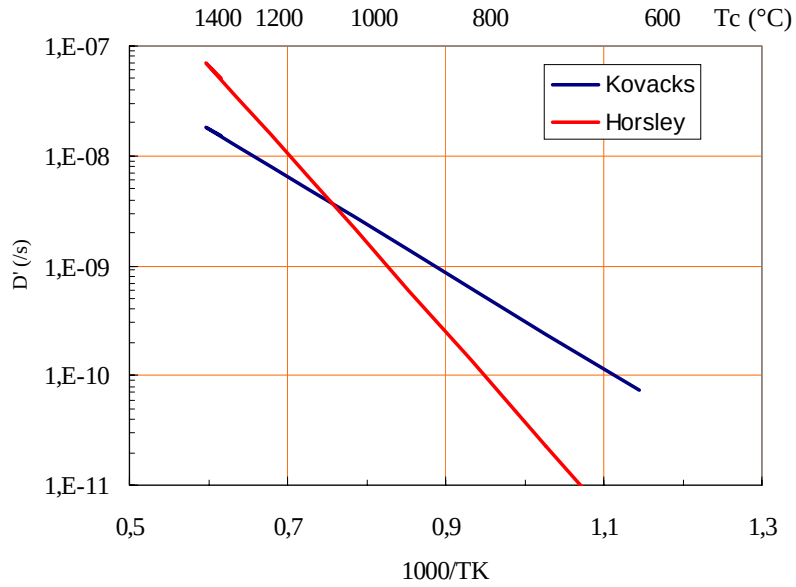

FIGURE 18 : CALCULATED FGR WITH EQUIVALENT SPHERE MODEL

Comparison of HORSLEY and KOVACKS relationships for 2 temperatures

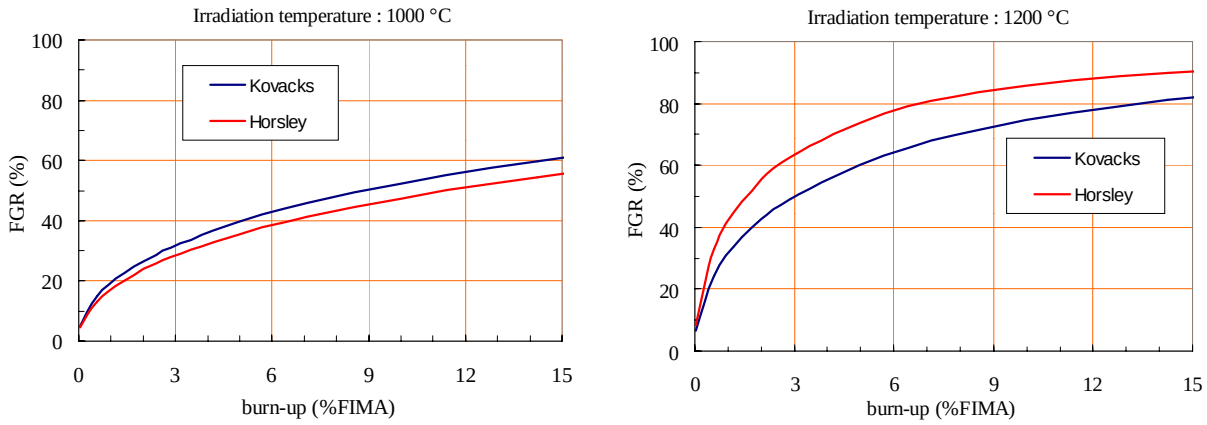

FIGURE 19 : FISSION GAS RELEASE CEA MODEL 1

Evolution of the Fission gas release rate with the fuel burn-up

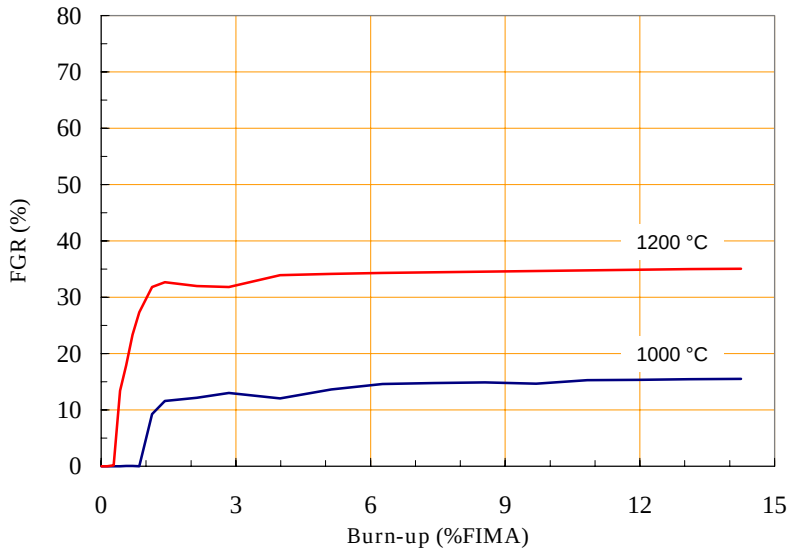

FIGURE 20 : FISSION GAS RELEASE CEA MODEL 2

limit of the gas saturation (super saturation in the matrix and in nanometre bubbles) in oxide fuel versus the fuel temperature

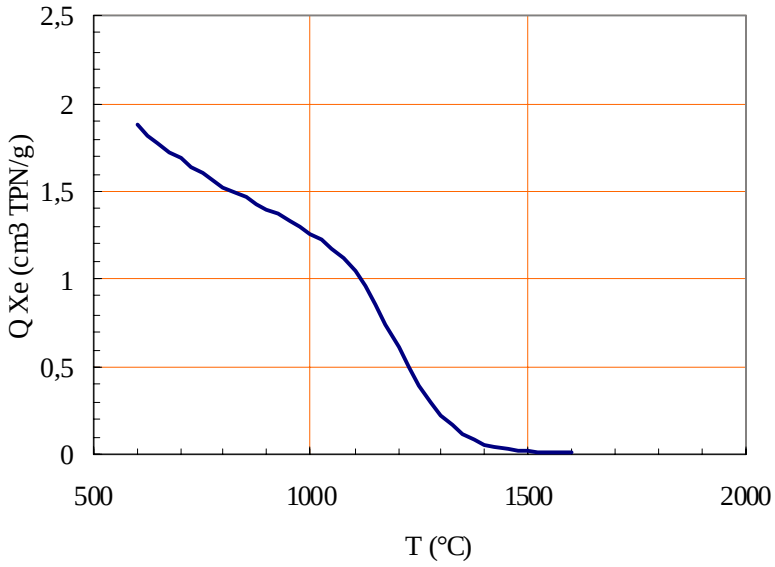

FIGURE 21 : FISSION GAS RELEASE CEA MODEL 2

Evolution of the Fission gas release rate with the fuel burn-up

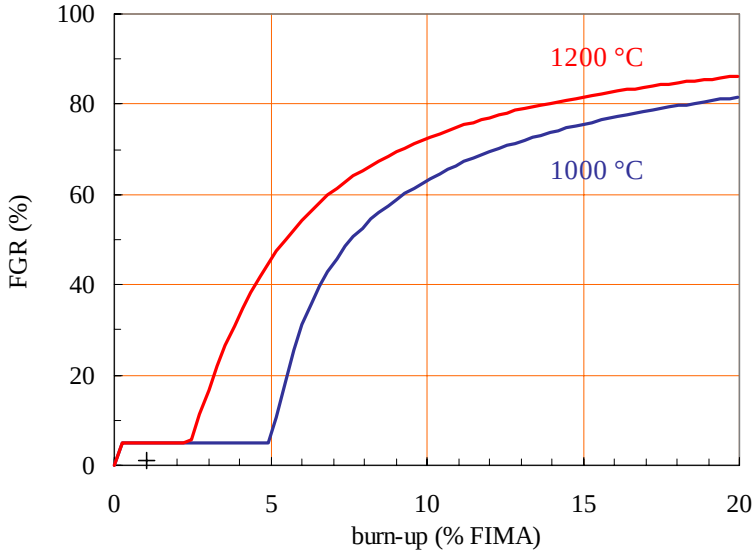

FIGURE 22 : CO PRODUCTION (HOLMAN)

HOLMAN's CO production as a function of BU and constant temperature for a fission density of 3,25 10^{13} f/cm^3.s

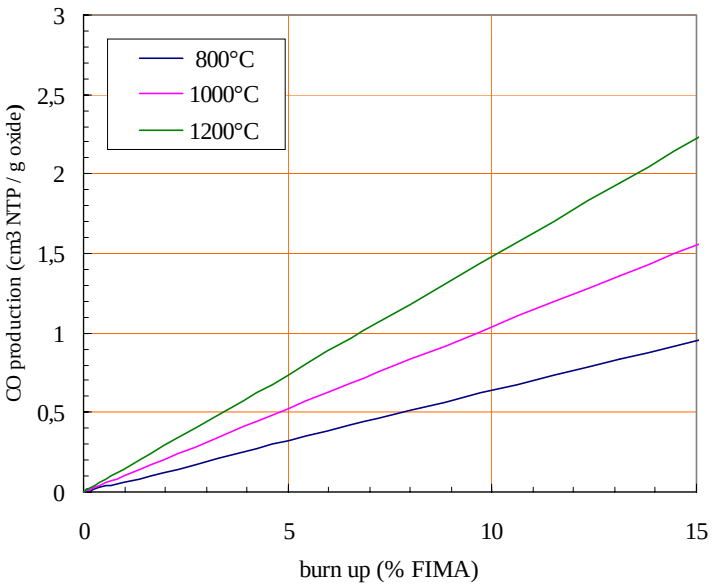

FIGURE 23 : CO PRODUCTION (PROKSCH)

PROKSCH's CO production as a function of BU and constant temperature for a fission density of 3,25 10^{13} f/cm^3.s

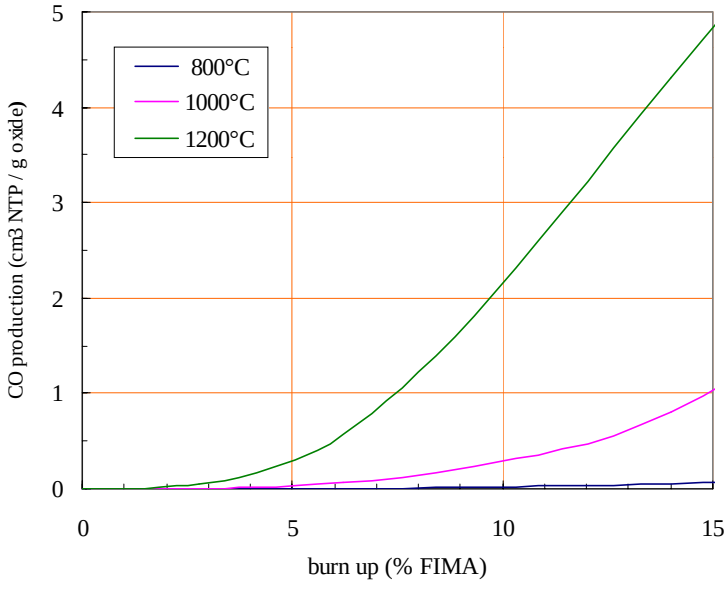

FIGURE 24 : EXAMPLES OF VARIATION OF KERNEL AND INNER BUFFER RADIUS

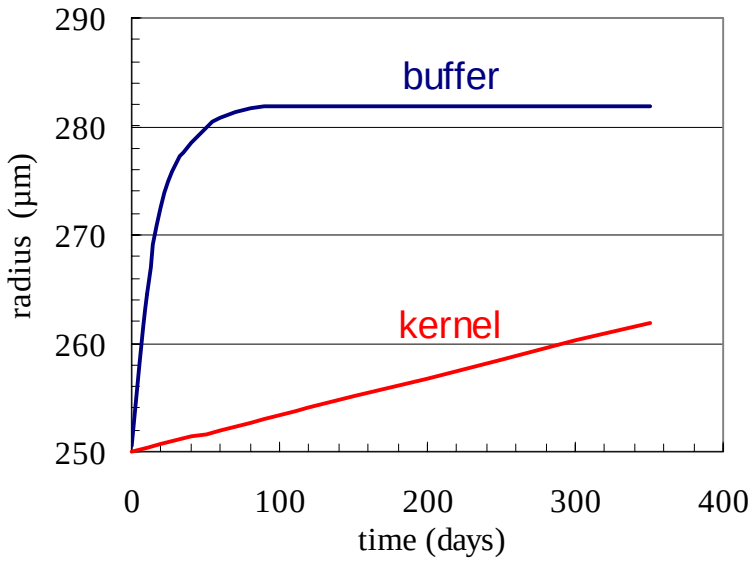

FIGURE 25 : EXAMPLES OF VARIATIONS OF KERNEL/BUFFER GAP VOLUME AND PARTICLE FREE VOLUME

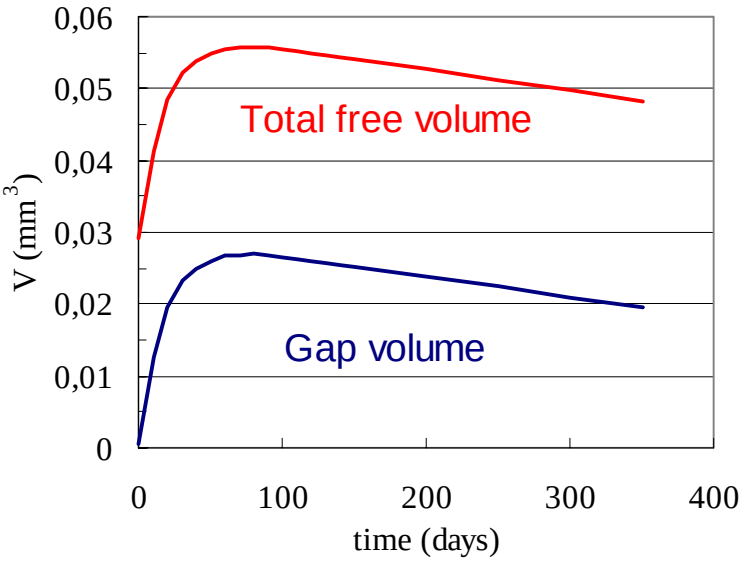

EUROPEAN COMMISSION
5th EURATOM FRAMEWORK PROGRAMME 1998-2002
KEY ACTION : NUCLEAR FISSION

HTR-F

High-Temperature Reactor Fuel Technology

CONTRACT N°
FIKI-CT-2000-00099

Guidelines for HTR Fuel Manufacture

P. GUILLERMIER

FRAMATOME-ANP

FRANCE

FRAMATOME ANP
NOVATOME

Dissemination level : DR
Document Number: HTR-F-0110-D-3.1.2
First Version
Deliverable Number:

FRAMATOME ANP

NOVATOME

NUMERO D'OTP OU EOTP	NOMBRE DE PAGES : 32	RAISON SOCIALE FOURNISSEUR :	
	NOMBRE D'ANNEXES : 0		
12T.DTHTRFWP3	CONFIDENTIALITE : N	NUMERO DE COMMANDE	IMMATRICULATION FOURNISSEUR

CODE		DESIGNATION
AFFAIRE	H T	**HTR**
NATURE	D T	**Note Technique**
THEME	E T	**Spécification Technique**
MATERIEL	3 2 0 0	**Assemblages Combustibles**

TITRE : **Data List for HTR Fission Products Behaviour**
FRA-ANP Contribution to HTR-F WP3

TITRE ABREGE : **F I S S I O N P R O D U C T S B E H A V I O U R**

IND	DATE	ETAT	REDACTEUR NOM-VISA	VERIFICATEUR NOM-VISA	APPROBATEUR NOM-VISA	MODIFICATIONS – OBSERVATIONS – ACCORDS REFERENCES ET DATES
A	10/10/2001	DES	P. GUILLERMIER	V. GRABON	J.M. HAMY	First issue

IMMATRICULATION CLIENT : **H T R - F - 0 1 1 0 - D - 3 . 1 . 2**

IMMATRICULATION INTERNE :	N V M K	D C	0 1	0 7 0 7	U R P / U R P
	UNITE	TYPE	ANNEE	CHRONO	TRIGRAMMES

10, rue Juliette Récamier 69456 LYON CEDEX 06 - Téléphone : 04.72.74.82.21 - Télécopie : 04.72.74.84.90

Modifications

Revision	Date	Modifications
A	10/10/2001	First issue

Summary

In the Work Package 3 (Modelling) in HTR-F (Fuel Technology) funded by the European Community, the participants intend, in order to understand and to predict the irradiation behaviour of HTR fuels, to model the different phenomenon occurring in the fuel in reactor.

This document is the contribution of FRAMATOME-ANP to the Work Package 3. It deals with fission products behaviour.

The fission products diffusion is described.

The diffusion coefficients data, used in different countries, are given, extracted from literature, especially from IAEA-TECDOC-978, Fuel performance and fission product behaviour in gas cooled reactors for :

1. Fuel kernel
2. Buffer layer
3. Pyrocarbon layer
4. Graphite

Conceptual models for particle failure are also described.

These data will be integrated in the common code taking into account relevant existing models that will be developed at the European level.

Contents

List of references

(1) Fuel performance and fission product behaviour in gas cooled reactors, IAEA-TECDOC-978, November 1997 – IAEA, Vienna, (1997).

(2) H. Ragoss, W Heit, H Nabielek and W Schenk, "Absicherung der brennelementspezifischen Quellterme fur die radiologische Auslegung HTR-Modul", Jahrestagung Kerntechnik, (May 1988).

(3) Limits of LEU TRISO Particle Performance, Werner Schenk, Karl Verfondern and H. Nabielek FZJ, and Enrique H Toscano ITU, JRC Karlsruhe, HTR Fuel Brussels Seminar, (Feb 2001).

(4) KFA-HBK, Projektbericht 1985, Internal Report KFA-HBK-IB-1/86, Research Center Jülich (1986).

(5) Kugelbrennelemente mit TRISO-Partikeln bei Störfalltemperaturen, W. Schenk and H. Nabielek, Report Jül-Spez-487, Research Center Jülich, (1989).

(6) Ein thermodynamisher Ansatz zur Spaltproduktrückhaltung - Entlastung von Barrieren, V. Dannert, (Proc. Jahresagung Kerntechnik 91 107-110, Bonn, 1991, Inforum GmbH, Bonn, (1991).

(7) Effect of Water Vapor on the Release of the Fission Gases from Uranium Oxicarbide in High Temperature, Gas Cooled Reactor Fuel Particles, B.F. Myers, J. Am. Ceram. Soc. p686-393, 75, (1992).

(8) Diffusion Coefficients of Fission Products in UO_2, PyC, SiC, Graphite Matrix and IG-110 Graphite, Unification of Coated Particle Performance Models and Fission Product Transport Data for the HTR, K. Minato, IAEA Technical Workshop, Jülich, (1991).

(9) The performance of HTR Fuel in Accidents, D.T. Goodin and H. Nabielek, Technical note KFA-HBK-TN-19/85, Research Center Jülich (1985).

(10) Diffusion of Metallic Fission Products in Pyrolytic Carbon, P.E. Gethard and L.R. Zumwalt, Nucl. Appl., p679-685, (1967).

(11) Results of Fission Product and Actinide Studies in Coated Fuel Particles and Matrix Graphite, Gas-Cooled Reactors Today, W. Amian and al., p153-160 (Proc. BNES Conference, Bristol, 1982), British Nuclear Energy Society, London (1982).

(12) Diffusion Coefficients of Fission Products in the UO_2 Kernel and Pyrocarbon Layer of BISO-Coated Fuel Particles at Extremely High Temperatures, K. Hayashi and K. Fukuda, J. Nucl. Mat., p35-44, 174 (1990).

(13) Diffusion Modeling of Fission Product Release during Depressurised Core Conduction Cooldown Conditions, Behaviour of GCR Fuel under Accident Conditions, R.C. Martin, (Proc. IAEA Specialists' Meeting, Oak Ridge, 1990), IAEA, IWGGCR/25, Vienna, p77-84 (1991).

(14) Capabilities of the Diffusion Model for Metallic Fission Products at Temperature Transients up to 1600°C - Case : Cs-137 Release from Spherical Fuel Element R2-K13,11, Unification of Coated Particle Performance Models and Fission Product Transport Data for the HTR, K. Rollig, (IAEA Technical Workshop, Jülich, 1991), (1991).

(15) The Determination of Diffusion Coefficients of Cesium and Silver by the Release Method in As-Received, Oxidized and Neutron Irradiated Graphitic Matrix, Transport of Fission Products in Matrix and Graphite, E. Hoinkis, (Proc. Colloquium, Berlin, 1981), Report HMI-B 372, Hahn-Meitner-Institut Berlin, 77-102 (1983).

(16) The Diffusion of Sr in the Graphitic Matrix A3-3 in Vacuum and in the Presence of Hydrogen, W. Hensel and E. Hoinkis, J. Nucl. Mat 184, p88-96 (1991).

(17) The Diffusion of Ag in the Graphitic Matrices A3-3 and A3-27, Report HNH-B 513, E. Hoinkis, Hahn-Meitner-Institut Berlin, (1994).

(18) Modeling of Fission Product Release Behavior from HTR Spherical Fuel Elements Under Accident Conditions, Behaviour of GCR Fuel under Accident Conditions, K. Verfondern and D. Müller, (Proc. IAEA Specialists' Meeting, Oak Ridge,1990), IAEA, IWGGCR/25, Vienna, 45-54 (1991).

(19) Diffusion of Fission Products in Matrix Graphite for VHTR Fuel Compacts, K. Fukuda, T. Sawai and K. Ikawa, J. Nucl. Sci. Tech. 21 p126-132 (1984).

(20) Iodine Retention in Spherical Fuel Elements under HTR MODUL Accident Conditions, W. Schenk and H. Nabielek, (Proc. Jahrestagung Kerntechnik '90, Nürnberg, 1990), Inforum GmbH, Bonn p363-366 (1991).

(21) Silver Transport in H-451 Graphite, R.A. Causey, Trans. Am. Nucl. Soc. 38 p316-317 (1981).

(22) Diffusion Coefficients of Cesium in Un-Irradiated Graphite and Comparison with Those Obtained from In-Pile Experiments, K. Hayashi and K. Fukuda, J. Nucl. Mat. 168 p328-336 (1989).

(23) In-Pile Release Behavior of Metallic Fission Products in Graphite Materials of an HTGR Fuel Assembly, K. Hayashi and al., J. Nucl. Mat. 149 p57-68 (1987).

(24) Laboratory Determinations of Strontium Diffusion Coefficients in Graphite, F.J. Sandalls and M.R. Walford, Report AERE-R 6911, Harwell (1972).

(25) FRESCO-I, Programm zur Berechnung, der Spaltproduktfreisetzung aus dem Core eines Kugelhaufenreaktors bei Kernaufheizung - Benutzerhandbuch, K. Verfondern and D. Müller, Internal Report, KFA-ISR-IB-2/91, Research Center Jülich (1991).

(26) Mehrphasendiffusion von Spaltprodukten in Graphit - Ein Beitragüber die Sicherheit von Hochtemperaturreaktoren, V. Dannert, Report Jül-2277, Research Center Jülich (1989).

(27) Spaltproduktttransport im Hochtemperaturreaktor : Theorie, programmtechnische Umsetzung und Überprüfung an Experimenten, L. Kranz, Report Jül-2463, Research Center Jülich (1991).

(28) Analytical Method of Fractional Release of Fission Products from Fuel Elements of HTR, Behaviour of GCR Fuel under Accident Conditions K. Sawa, et al.(Proc. IAEA Specialists' Meeting, Oak Ridge, 1990), IAEA. IWGGCR/25, 55-61, Vienna (1991).

(29) FRESCO-II, Programm zur Berechnung der Spaltprodukdreisetzun- aus einem HTR-Brennelement lm Normalbetrieb (Bestrahlungsexperiment) und Kemaufheizstörfall (Heizexperiment) - Benutzerhandbuch, K. Verfondern and D. Müller, Internal Report KFA-ISR-IIB-4/91, Research Center Jülich (1991).

(30) Possible Explanation for HFR-K3,13 IMGA Results, K. Verfondern, Report ORNL/M-2248, Oak Ridge National Laboratory (1991).

List of figures

1. Context and Objectives

HTR Fuel Coated particles designed in the 1960s and 1970s have been perfected for steam cycle applications in the 1980s and early 1990s enabling the design of small inherently safe modular HTRs with self-limiting temperatures of less than 1600°C.

Now, new applications are of interest :

- gas turbine directly in primary circuit (direct cycle),
- burning of civil and weapons grade plutonium,
- higher in-reactor burnup for ecological and economical reasons.

On one hand, to make the coated particle equally convincing for these applications, available results should be re-analyzed and re-investigated in the light of these applications.

On the other hand, new results and new computing tools have been developed and have to be used in these tasks regarding :

- Re-evaluation of ^{110m}Ag release data during normal operations for better source term data base in direct cycle applications.
- Determination of the influence of burnup greater than 10% FIMA on irradiation performance.
- Accident condition performance analysis at temperature greater than 1600°C for an improved coated particle model.

In order to achieve these goals, in the Work Package 3 (Modelling) in HTR-F (Fuel Technology) funded by the European Community, the participants intend, in order to understand and to predict the irradiation behaviour of HTR fuels, to model the different phenomenon occurring in the fuel in reactor.

A common code taking into account relevant existing models will be developed at the European level.

This document deals with fission products behaviour.

2. HTR Fuel Description

Generally, the TRISO HTR Fuel particles have a 500 µm diameter UO_2 kernel and a 200 µm thick coating, consisting of a porous buffer layer and two dense layers of pyrocarbon with a silicon carbide layer in between, named IPyC and OPyC for inner and outer pyrocarbon. While all these layers have important mechanical and chemical functions, it is the SiC that guarantees the highest degree of fission product retention.

In normal and transient operation, and in accidents not exceeding 1600-1700°C, it was demonstrated that all radiologically relevant fission products (iodine, caesium, strontium) are

completely retained inside the silicon carbide layer of intact fuel particles. The dominant source term of fission product release will, therefore, be the small number of particles with defective coatings [2, 3].

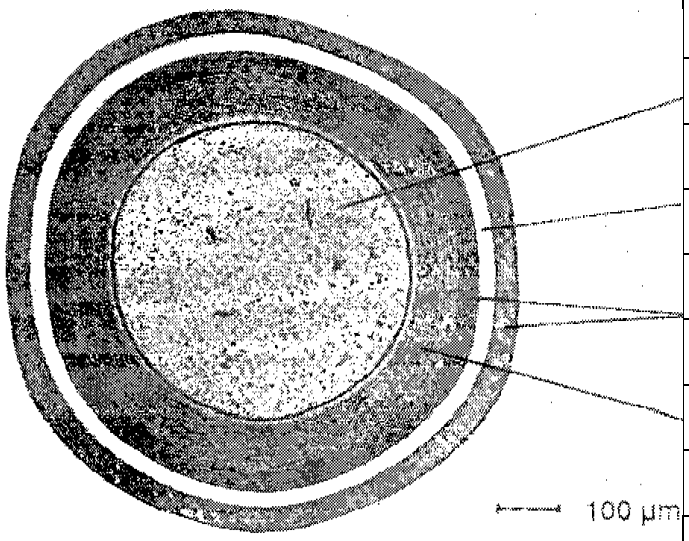

Cross-section through an LEU TRISO coated particle

3. Fission Products Diffusion

The equation that governs the fission products diffusion is the second Fickian equation using average diffusion coefficients for the fission product species in the different barriers of reactor materials. All the transport mechanisms are summarised in this simplified single transport law for the HTR fuel particle materials. The diffusion model is generally regarded to be valid both for normal operation and for accident conditions.
The equation is used, with a transient system and a spherical symmetry. The source term and radioactive disintegration must be added to complete the balance sheet :

$$\frac{\partial c^{(i)}}{\partial t} = \frac{1}{r^2}\frac{\partial}{\partial r}\left(r^2 D^{(i)}\frac{\partial c^{(i)}}{\partial r}\right) - \lambda c^{(i)} + \dot{s}$$

Where

- λ is the radioactive disintegration constant (s^{-1});
- $\dot{s}$ is the source term ($kg.m^{-3}.s^{-1}$),
- $D^{(i)}$ is the diffusion coefficient in the layer number i ($m^2.s^{-1}$): the 1st is the kernel, the 2nd is the buffer, the 3rd is the IPyC, the 4th is the SiC and the 5th is the OPyC,
- $c^{(i)}$ is the fission products concentration in the i^{th} layer ($kg.m^{-3}$),

Thus, the variation in fission product concentration is due to three terms:

- The Fickian diffusion, by the term $\frac{1}{r^2}\frac{\partial}{\partial r}\left(r^2 D^{(i)} \frac{\partial c^{(i)}}{\partial r}\right)$.
- The radioactive disappearance, by the term $-\lambda c^{(i)}$.
- The creation by fission reaction, by the term $\dot{s}$.

4. Source Term Input Data

The source term is the expression in the Fickian law that gives the creation of a fission product during the irradiation.

This input data term is noted $\dot{s}$ in the equation of diffusion.

The concentration of 90-Strontium, 137-caesium and 110m-Silver are concerned.

5. Diffusion Coefficients Data

The diffusion coefficients are usually given as an Arrhenius type equation as a function of temperature. Empirically found deviations from this behaviour could be overcome by assuming additional dependencies, for instance on fast neutron fluence or fission product concentration or burnup, or by combining diffusion processes with different activation energies in different temperature ranges :

$$D(T,\Gamma,c,...) = \sum_i D_{0,i}(\Gamma,c,...)\exp\left(-\frac{Q_i}{RT}\right)$$

where :

- $D_{0,i}$ is the pre-exponential term, in $m^2.s^{-1}$,
- Q_i is the activation energy, in J/mole,
- T is the temperature, in K,
- R=8.314 in mol/J/K,
- Γ is the fast fluence in 10^{25} m^{-2}, E>16fJ (different cut-off limit for the neutron energy E>0.1 MeV (16fJ), E>0.18 MeV (29 fJ), or EDN are found in the literature. The correct unit is explicitly mentioned wherever necessary.
- c is the fission product concentration in m^{-3}.

Diffusion coefficients have been adopted from the evaluation of numerous irradiation and heating experiments with complete spherical fuel elements, fuel compacts, single fuel particles, or graphite samples.

Recommendations of transport data have been collected over many years and were continuously revised. In a joint effort of KFA and German industries within the project "Hochtemperaturreactor-Brennstoffkreislauf" (HBK), a set of data to be used for predicting fission product transport during HTGR normal operation has been established [4]. Its purpose was to

summarise the data base for HTGR design calculations for licensing procedure. A comprehensive data collection was created in the 1970s by UKAEA/AERE Harwell. Transport data as applied to US HTGR designs have been published as part of the Fuel Design Data Manual by General Atomics.

A common assumption in most diffusion models is the neglect of any effects of sorption or trapping within a coating layer or of any preferential retention in a specific layer. The ratio of fission product concentrations at the surfaces of contiguous materials (partition coefficient) is assumed to be one. Consequently, the concentrations are equal at contiguous surfaces. Measurements of this ratio range from about 0.3 to 3 and may change with temperature and fast fluence. For lack of adequate measurements of the ratio under a sufficiently large range of conditions, the error associated with the assumed value of 1.0 has been accepted. The few experimental studies related to desorption from coating materials indicate some kind of discontinuity in concentration profiles at coating interfaces, for instance for caesium between buffer and inner pyrocarbon (IPyC) layer or the significant palladium peaks at the inner surface of the SiC layer [5] in microprobe profiles.

Experiments at KFA have been proposed in 1989 for investigation of the thermal chemical partition coefficients at material boundaries to better estimate the magnitude of this effect. The development of an alternative calculation model has even been proposed at KFA which considered the fission product transport to be dependent on the gradient of the chemical potential rather than of the concentration. This alternative is described in [6].

5.1 Fuel Kernel

Diffusion coefficients in UO_2 fissile particle kernels which were used in recent German safety analysis have been derived from irradiation and heating experiments with designed to fail UO_2 particles (kernel and buffer layer). According to an evaluation of the German irradiation and heating experiment FRJ2-P28, caesium and iodine release under accident conditions is considered at KFA to be best approximated by a two branch diffusion coefficient while those for strontium and silver were lowered by a factor of 20 and 10, respectively, compared to the recommendation of the last HBK data set. A different recommendation is given for iodine at lower temperatures(< 1000°C) which was derived from irradiation experiments in the R2 reactor at Studsvik.

In the US, most data were derivated from ThO_2, fertile kernels. A significant dependence of the reduced diffusion coefficient on temperature and burnup but no dependence on fast fluence was found. The diffusion data for metallic fission products [7] are also used for UO_2, with a separate set of constants used for UCO kernels which are slightly higher than those for UO_2. UC_2 fuel is assumed to retain no metallic fission products. However, for safety analysis calculations, the use of KFA data for the metallic fission products is recommended.

Japanese transport data for caesium were derived from in-pile fractional release measurements. The curve is below corresponding German and US data [8].

The Figure 1, from reference [1], gives the values of the diffusion coefficients of solid fission product (Ag, Cs and Sr) and gaseous fission products (I, Kr and Xe) in UO_2 used in different countries (FRG, USA and Japan) as function of temperature.

5.2 Buffer Layer

The carbonaceous buffer layer is assumed in the diffusion model to have no significant retention capability for fission products. In FRG calculations, a value of the diffusion coefficient of 10^{-8} $m^2.s^{-1}$ with no temperature dependence (activation energy equal to zero) is used. The US recommendation for the corresponding diffusion coefficient is 10^{-10} m^2/s. The difference is negligible since either one is significantly larger than the diffusion coefficient for the other coating materials.

5.3 Pyrocarbon Layers

Diffusion coefficients in pyrocarbon were mostly derived from early experimental data with LTI and HTI-PyC from BISO particles. Due to its comparably smaller retention capability, diffusion in PyC has not been investigated in that detail as it has been for the main barrier silicon carbide. At temperatures beyond 1900°C, it is recommended to assume rapid diffusive transport (similar to the buffer layer) for metallic fission products in LTI-PyC. For HTI-PyC, this critical temperature has been assumed in German safety analysis calculations for the THTR-300 to be as low as 1200°C, except caesium for which experimental evidence suggests much better retention than strontium or silver. The diffusion coefficient of krypton in PyC is based on an evaluation of GA heating data at 2050°C and ramp tests and of KFA 1600 °C tests [9]. No modification of KFA transport data is considered to take into account possible irradiation damage in PyC due to a high probability of irradiation damage annealing [9]. No change of KFA data has been made compared to the status report.

US recommendations for strontium and silver as well as for iodine and fission gases are identical to those at KFA. The data for caesium and strontium represent an average of the measurements of many authors. Early US studies [10] have also found the caesium transport data through isotropic pyrocarbon to be orders of magnitude lower than those for strontium, both being in the range of the later reported data.

In Japan, several studies have been made on caesium in different temperature ranges [8]

Diffusion data given by other authors ([10], [11]) are fairly close to each other despite their strong dependence on the pyrocarbon deposition conditions during manufacture and material characteristics. This dependence was reported to be the reason for the relatively large difference in JAERI and KFA activation energies for caesium [12].

The Figure 2, from reference [1], gives the values of the diffusion coefficients of solid fission product (Ag, Cs and Sr) and gaseous fission product Kr in LTI Pyrocarbon used in different countries (FRG, USA, Russia and Japan) as function of temperature.

5.4 Silicon Carbide Layer

The transport properties of fission products in silicon carbide, as the most efficient barrier of the coated particle, were the subject of many detailed studies in the past years. The experimental data gave impetus to either confirm and/or refine existing models or even to develop new ones.

The original way to describe the permeability of the SiC coating for fission products was a diffusion coefficient derived from numerous heating tests at KFA with single coated fuel particles. The radio nuclide caesium was investigated more than any other relevant metallic fission product

species. The Arrhenius relation for caesium proposed by Allelein entered the HBK data set as recommended data for use in HTGR core release predictions under normal operating conditions.

For irradiation experiments with modem HTGR fuel, the Allelein diffusion coefficient was found to overestimate in some cases the caesium release fraction from fuel particles. An evaluation of the experimental data by Christ has taken the fast neutron fluence as a parameter for the Arrhenius relation, thus influencing the amount of caesium penetrating the SiC layer during irradiation and the delay of the diffusive break-through at elevated temperatures. This new recommendation for the low-temperature branch of KFA data is -for zero fast fluence- lower compared to the Allelein data but will come close to it with increasing fast fluences.

The Figure 3, from reference [1], gives the values of the diffusion coefficients of solid fission product (Ag, Cs and Sr) and gaseous fission product Xe in SiC used in different countries (FRG, USA, Russia and Japan) as function of temperature.

A theoretical evaluation of several researchers' experimental caesium release data from coated particles was made by Myers in the early 1980s. The result was a diffusion coefficient subdivided into, a low temperature branch and a high temperature branch dominant at greater than 1600°C. The Figure 4, from reference [1], gives the values of the diffusion coefficients of Cs as function of temperature and fast fluence dependence.

The upper curve was chosen in 1986 as the reference data for accident temperature conditions with the goal of being at least conservative in German safety analyses calculations.

A evaluation of data from all heating experiments conducted in the KüFA furnace -a total of 44 tests with respect to caesium- using the diffusion code FRESCO-II has led to a new KFA recommendation for a diffusion coefficient in silicon carbide which is very similar to the lower Myers curve.

An analogous evaluation has been made for strontium on the basis of 11 KüFA heating tests with modem HTGR fuel in the temperature range between 1600 and 1800°C. The new diffusion coefficient shown in Figure 3 has a higher activation energy resulting in a diffusion coefficient lower by a factor of about 20 at 1600°C compared to the old recommendation. Unfortunately, the combination of this new high-temperature Arrhenius relation with the old HBK relation for normal operation temperatures into a single two branch diffusion coefficient significantly underestimates the experimental retention quality of SiC for strontium at 1600°C.

KFA silver transport data have been taken from the HBK data set. No evaluation of available silver release data from KüFA heating tests has been made because no consistent release behaviour was observed and is in many cases not reproducible by any existing model. A possible explanation as proposed by Myers could be the silver to be trapped at neutron induced defects in the silicon carbide structure at normal operation temperatures resulting in a burst release of the trapped silver at elevated temperatures.

According, to the definition of the "Integrated Failure and Release Mode for Standard Particles" which represents the US reference model, no diffusion of caesium and strontium through silicon carbide is assumed to occur. There are, however, US diffusion data available which were published before the statistical model was created. Ongoing work by Martin, [13], suggests that a fast fluence dependent diffusion coefficient similar to that of Christ represents an improvement over the reference model.

No big difference between Japanese and KFA data was found for caesium and silver. For strontium, the same data as KFA for the low-temperature branch are used.

The uncertainty range for transport data in silicon carbide is a result of the very low release level for high quality fuel at temperatures less than 1600°C which sometimes only allows the indication of an upper limit. When considering heating tests with complete fuel elements, other parameters such as heavy metal contamination fraction in the graphite grain are of importance.

The approach in the JAERI code FORNAX uses a third type of particle with a degraded SiC layer simulated by larger values for the diffusion coefficient. No specific transport data have been published.

Röllig has provided an interesting analysis of the Cs137 release data for FRG sphere R2-K13/1 heated to 1600°C for 1000 hours [14]. Nearly 2000 particles were gamma counted, and 7% had released over 10% of their Cs137 inventory, with a small number of particles releasing 50 to 90%. Röllig applied a diffusion model to the release data, but rather than a single diffusion coefficient lie assumed a log-normal distribution of values around the average diffusion coefficient. He obtained reasonable agreement with the data for particle release as a function of position within the sphere. This method of assuming a distribution of diffusion coefficients is a promising approach to account for the inherent microstructural variation in SiC and its effect on particle-to-particle release comparisons.

5.5 Graphite

The uncertainty for the given transport data in graphitic materials is considered to be fairly high. The metallic radionuclide transport in graphite is strongly dependent on graphite type and nature, structure, temperature, fission product concentration, state of oxidation, irradiation damage, coolant gas pressure, and interference with other fission product species.

The trapping mechanism is not considered, which is known to better approximate the real transport process in graphite. The overall uncertainty range is estimated to be at least one order of magnitude, for silver as high as three orders of magnitude. For safety analysis purposes, however, transport data for the oversimplifying Fickian diffusion model in graphite can be used to obtain realistic, or at least conservative radionuclide release data.

5.5.1 Matrix Graphite

Effective diffusion data are relatively well known for caesium and silver [15] and strontium [16] in German A3-3 matrix graphite in the Henrian concentration regime as well as the influence of irradiation and corrosion on the diffusive process. The matrix graphite type A3-3 was used for the THTR-300 spherical fuel elements and was chosen to be the reference fuel element graphite for future German HTGRs. In contrast, all of the last German fuel elements which were used in irradiation and post irradiation experiments consisted of the matrix graphite type A3-27. Comparative measurements of Hoinkis showed diffusion coefficients for caesium and silver in as-received A3-27 lower by a factor of 20 and 7, respectively, at 1000°C compared to as-received A3-3 [15]. A Hoinkis report presents the diffusion coefficients of silver in as-received A3-3, as-received A3-27, and irradiated A3-3 in the temperature range of 800 - 1300°C [17] confirming, the above single measurement.

The Figure 5 gives the values of the diffusion coefficients of solid fission product (Ag, Cs and Sr) and gaseous fission product I and Kr in matrix graphite used in different countries (FRG, United Kingdom, Russia and Japan) as function of temperature.

According to the experience from measurements, caesium and strontium diffusion through graphite has been assumed in German safety analyses to proceed rapidly at temperatures beyond 2000°C, for silver already at temperatures less than 1000°C.

The evaluation of caesium inventory measurements in the matrix of heated fuel elements with the KFA code FRESCO-II have also demonstrated the diffusion coefficient in A3-27 to be at least one order of magnitude lower compared to A3-3 in the accident temperature range of 1600 to 1800°C. But the fitted diffusion coefficients for A3-27 cannot consistently be described in a new Arrhenius relation on a lower level [18]. The choice of heavy metal contamination fraction in the matrix which is used as input data for the model calculations has a major effect on the release level from the fuel element, especially at lower heating temperatures less than 1600°C (when the release from the coated particles is comparably small) and especially for strontium which is more strongly bound in graphite than is caesium. An adequate recommendation for caesium and strontium transport in A3-27 matrix graphite may be the reduction of the Hoinkis diffusion coefficient curves (for A3-3) by one order of magnitude which would still envelope the calculated results [18].

US diffusion data on fuel compact matrix material are not given due to the assumption of a rapid transport of the metallic and gaseous fission products through this porous material zone.

Japanese data have been published for strontium in graphite matrix for the VHTR design [19] which is one to two orders of magnitude above German reference data. The Japanese data are, however, somewhat smaller compared to early KFA measurements conducted for strontium and caesium in irradiated A3 matrix of AVR fuel elements.

Fission gases released from the coated particles are assumed in US modeling to be transported through the fuel compact matrix material without any time delay both under normal operating and accident conditions. This assumption has the same result as the German approach which uses a large diffusion coefficient for xenon in helium to simulate fission as and iodine transport in the graphite pores (= grain boundaries). The US modeling of radionuclide transport in graphite has been recently refined by introducing the effect of graphite oxidation into the diffusion coefficient by making the pre-exponential factor a function of weight percent burnoff.

The transport behaviour of iodine in graphite under accident conditions is considered in German model calculations to be similar to that of the noble gases krypton and xenon. Rather than simulating an effective, one-phase diffusion, the iodine transport is conservatively treated in the KFA reference modeling to consist of a slow diffusion phase out of the graphite grain proposed by Müller at temperatures less than 1250°C and of rapid diffusion phase via the pores and the graphite grain boundaries. The iodine from the heavy metal contamination is assumed to be buried deep inside the grains. In contrast, iodine released from defective particles into the graphite is assumed to be immediately transported in the graphite pores. The quick phase transport is independent of temperature and corresponds to the diffusive behaviour for Xenon in helium, and does not allow for any realistic retention in the graphite.

The transport of iodine and fission gases in graphite has been recently the subject of a special series of KFA experiments [20]. Spherical fuel elements with low burnup were heated to investigate the release behaviour of short-lived isotopes originating from the heavy metal contamination. Iodine release curves were found to be akin to those for xenon, with both supporting the interpretation of a release from traps in the matrix graphite. Diffusion coefficients derived from these experimental data using the FRESCO model [18] revealed that the reference diffusion coefficient as explained in the above paragraph was too small at lower temperatures and too large at higher temperatures less than 1250°C. But from the arrangement of the fitted data, an activation energy could be recognised which is similar to that for an effective diffusion coefficient for xenon transport in irradiated AUF graphite which was impregnated with uranium carbide. This

Canadian investigation had shown that relatively high fractions of xenon were retained in the graphite even at temperatures up to 2000°C.

The above mentioned evaluation of the KFA heating experiments with the FRESCO-II code was repeated, but now using for the contamination fraction in the spheres a single value (1.10^{-7}) rather than the release value measured at the end of each series. The last calculation results shown are up to two orders of magnitude lower than the earlier results, and the low temperature data fall close to the Müller slow phase diffusion coefficient. However, all things considered, these calculation results do not seem to represent a good basis for recommending a new diffusivity. The old one remains sufficiently conservative for safety analyses, although an approach using a trapping mechanism will be the more accurate one.

The objectives of tests conducted in the Russian Federation on iodine and fission gas release from HTGR fuel element graphite were to obtain the temperature dependence of the release and to study the correlation of gaseous and aerosol fission product release. The objects used for the investigations were standard spherical fuel elements, fuel element "failure" imitators, i.e., graphite spheres containing uncoated kernels instead of coated particles, coated particles with a different number of protective coatings, a mix of coated particles with kernels (in bulk), as well as "contamination" imitators, i.e., either 35 mm diameter spheres manufactured from a mix of graphite with uranium or 60 mm diameter spherical graphite models without fuel particles.

The investigations were conducted using the technique of "weak" irradiation. The fractional release of the iodine isotopes during isothermal heating was determined on the basis of a measurement of the activities of the daughter isotopes (Xe135, Xe133) built-in in the facility test section after its cooling down. The temperature dependence of the iodine release was obtained by cyclic heating of the investigated samples. The experimental results were analysed by means of the activation model.

The temperature dependence of the iodine and xenon isotopes has been obtained within the temperature range 200 - 1100°C. It has been observed that an increase of the graphite quantity in the sample results in a relative reduction of the iodine release, an effect which is apparently connected with iodine absorption especially at low concentrations. It has also been shown that a heat treatment of the imitator samples leads to an enhanced radionuclide release and also changes the character of the temperature dependence ; this influence can be explained by a probable uranium carbidization at high temperatures and, consequently, a decrease of the kernels' retention capability. It should be noted that an estimation of the primary circuit activity using Xenon135 benchmark nuclide release data can lead to overestimated values of iodine release (for release values < 10^{-2}).

5.5.2 Structural Graphite

No diffusion data are available for the German reference reflector graphite ASR-1RS. The US data for H-451 graphite grade have been used instead in model calculations. The transport of iodine and fission gases in structural graphite is only considered via the rapid diffusive phase since they have penetrated the graphite from the coolant side, thus being transported using the pores rather than entering the grains.

US data for caesium and strontium which approximate various authors' measurements and are recommended to be used in HTGR core (graphite type H-451) release predictions are presented in Figure 6 to also represent KFA transport data for structural graphite. The silver transport in H-451 measured at temperatures up to 800°C was supposed in [21] to consist of a slow phase with high concentrations near the surface and of a fast phase with low concentrations away from the surface.

JAERI studies of IG-110 structural graphite in in-pile experiments have revealed significant differences in caesium and silver diffusion data relative to German and US data [22]. In particular. silver released from the fuel compact was found to be effectively retained in the graphite sleeve for low burnups < 2% FIMA. Diffusion coefficients for caesium obtained from experiments with Cs impregnated IG-110 graphite specimens were found to be larger by 3-4 orders of magnitude and with a lower activation energy compared to those data obtained from the in-pile experiments. An explanation is proposed by assuming an additional trapping effect by irradiation induced surface defects with stronger binding energies than those of existing traps [23].

The Figure 6 gives the values of the diffusion coefficients of solid fission product (Ag, Cs and Sr) in structural graphite used in different countries (FRG, US, United Kingdom and Japan) as function of temperature.

British diffusion data shown in Figure 6 refer to fuel tube graphite AGL-9.

5.5.3 Concentration Dependence of the Diffusion Coefficient

Experimental data on the concentration dependence of transport data have been collected by several authors. A significant effect was found for strontium where a tremendous increase of diffusivity by several orders of magnitude occurred as soon as a certain concentration was exceeded. Only small effects were found for silver and caesium. The concentration dependence of strontium diffusion is expressed in the empirical equation

$$\log D(T, c_{gr}) = 4.51 - 2.58 \log c_{gr} - (29300 - 7000 \log c_{gr})/T$$

Where c_{gr} is the concentration in the range of 60- 2000 µg Sr/g of C

The following, empirical strontium diffusion coefficient dependent on temperature and concentration was found to be in good agreement with experimental data and recommended for US safety studies :

$$D(T, c_{gr}) = 3.47 * 10^{-13} {c_{gr}}^2 \exp\left[-\frac{64000\chi}{R}\left(\frac{1}{T} - \frac{1}{1273}\right)\right]$$

Where :

$$\chi = 0.422 + \frac{0.5805}{1 + {c_{gr}}^3 / 80}$$

and c_{gr} is the concentration in the range of 0.7- 50 µg Sr/g of C

The Figure 7 gives the concentration dependence of diffusion coefficients of solid fission product Sr in graphite as function of temperature.

A modeling refinement for diffusive transport of caesium and strontium in graphite which simulates this effect uses the British experimental data obtained for strontium [24]. In the FRESCO model, corresponding sorption data for strontium and caesium are taken to introduce a factor consisting of the ratio of the partition coefficient based on Freundlich sorption isotherms over that based on Henry sorption isotherms.

The partition coefficient $\alpha = \alpha(T)$ is defined by the equation :

$$c_{gas} = \alpha . c_{gr}$$

where c_{gas} is the concentration in coolant (atoms.m^{-3})

c_{gr} is the concentration in graphite surface layer (atoms.m^{-3})

The concentration dependence is given by modifying the pre exponential term of the diffusion coefficient in graphite by a factor ,which is equal to 1 for the Henrian concentration regime and greater than 1 for the Freundlich concentration regime :

$$D_0^x(c_{gr}) = D_0 \frac{\alpha_{Freundlich}}{\alpha_{Henry}}$$

with the above definition of α.

This type of concentration dependence is presented in Figure 7 for strontium reproducing the results of [24], and in Figure 8 for caesium. This procedure is also applied to the structural graphite of the reflectors in the 'core' version of FRESCO [25].

Another approach has been proposed in [26] which is employed in the SPTRAN code. The pre-exponential factor of the diffusion coefficient is additionally dependent on temperature

$$D_0^x(T, c_{gr}) = D_0 \left[1 + (\frac{c_{gr}}{c_t})^{\tau E_F / T} \right]$$

where :

c_t is the transition concentration between Henry and Freundlich regime,

τ is an empirical parameter,

E_F is a parameter of the Freundlich sorption isotherm.

A value of 0.25 for the parameter τ was fitted to best approximate caesium experimental data [26]. The diffusion coefficient according to equation above is shown in Figure 8 (dashed curves).

6. Temperature

The temperature is naturally used in the formulation of the Arrhenius' law and this input data has a highly important impact on results.

Temperature gradients have to be calculated in the particle and in the core.

7. Conceptual Models for Particle Failure

The principal potential mechanisms of coating failure at high temperatures are :

Pressure vessel failure whereby the internal gas pressure induces a stress in the SiC layer in excess of the SiC tensile strength. In addition to basic design and material properties, critical data are required about a possible decrease of SiC strength during irradiation and annealing.

Kernel migration –or amoeba effect– at high temperatures and under temperature gradients. It can lead to destruction of coating layers.

Interactions of fission products with silicon carbide that can lead to a thinning and weakening of the SiC layer (corrosion), thereby reducing strength and impermeability to fission products.

Finally, at very high temperatures, silicon carbide thermal decomposition that leaves only a disordered carbon structure in the place of the SiC layer.

Corrosion of the SiC Layer

Some corrosion or refinement of the SiC can lead to the fracture of this layer, or can create some micro-fissures that release the fission products.

At less temperatures than 2000°C, the interaction of fission products with the silicon carbide (corrosion) is the dominant failure mechanism. A linear dependence of the corrosion rate on the time has been determined with an activation energy of 252kJ/mol.

Some tests have shown that this corrosion rate, k, depends on irradiation parameters and fuel type: $k=k_0.\exp(-Q_i/RT)$ where :

R is the gas constant 8.3143 $J.mol^{-1}.K^{-1}$

T is the heating temperature

Q_i is the activation energy

$\log(k_0)=-36,53+3.\log(T_{irradiation})+\log(f_{SiC})$ (k_0 in s^{-1})

$T_{irradiation}$ irradiation temperature (K),

f_{SiC} density of fission (m^{-3}).

Qi are given for different countries in reference [1].

Some TRISO particles with a UO_2 kernel and containing palladium have shown 3 different possible interactions that are :

- Localised attacks characterised by the penetration of the palladium in the silicon carbide layer, constructions of palladium at the IPyC/SiC interface, and anisotropy of the environment.
- Emergence of little bright grains of palladium in the silicon carbide thickness.
- Metallic impacts distributed on the inner surface of the silicon carbide.

Decomposition of the SiC Layer

Thermal decomposition of SiC was confirmed to be the main failure mechanism at higher temperatures than 2000°C. An intact outer pyrocarbon layer leads to a retardation that is dependant on irradiation conditions. The 137-caesium release indicates the weight loss.

The decomposition rate is given by : $k=k_0.\exp(-Q_j/RT)$ where :

R is the gas constant 8.3143 $J.mol^{-1}.K^{-1}$

T is the heating temperature

Q_j is the activation enegy

$\log(k_0)=-1,58+2,67.\log(T_{irradiation})+0,61.\log(\Gamma)$ (k_0 in s^{-1}) where Γ is the fast fluence ($10^{25}m^{-2}$).

Qj are given for different countries in reference [1].

The chemical reaction involved in the thermal decomposition is: $SiC_{(s)} \rightarrow Si_{(g)}+C_{(s)}$.

The different countries working on the HTR field have determined some specifications from experiences and evaluations, which are given in the following table [1] :

	FRG	**USA**	**JAPAN**	**USSR**	**CHINA**
As-manufactured free uranium					
Heavy metal contamination	10^{-7}	10^{-5}	10^{-5}	4.10^{-6}	4.10^{-6}
Defective coating (exposed kernel)	3.10^{-5}	-	10^{-5}	$<5.10^{-5}$	
Failed-SiC	-	5.10^{-5}	5.10^{-4}	$<10^{-4}$	
TOTAL (expected value)	3.10^{-5}	6.10^{-5}	5.10^{-4}		
TOTAL (design value)	6.10^{-5}	$1,2.10^{-4}$	2.10^{-3}	10^{-4}	$\leq 3.10^{-4}$
Irradiation-induced failures					
Expected value	2.10^{-5}	5.10^{-5}	0		
Design value	2.10^{-4}	2.10^{-4}	8.10^{-3}	$<10^{-4}$	5.10^{-4}

The assumption of a defective or failed particle in the diffusion code FRESCO-II is equivalent to simulating, an exposed particle kernel. This means that fission products released from the particle kernel by diffusive transport are immediately released to the surrounding graphite structure. The failure of a particle coating, however, is not necessarily equivalent to a non-existing coating ; such an assumption is a conservative approach. There is experimental evidence for a better retention of fission products in particles with a broken coating compared to exposed kernels. The simulation of a partly existing coating as a kind of a third type of particle (besides intact particles and exposed kernels) has been proposed by JAERI [28]. Another possibility of modeling a broken but still existent coating is the choice of a smaller diffusion coefficient in the kernel as an simulative diffusion coefficient for this 3rd type of particle as has been done in the FRESCO-II code [29]. A post calculation of the 1800 °C isothermal heating, test HFR-K3/3 has shown that the reduction of the kernel diffusion coefficient by two orders of magnitude simulates a failed but still

existing coating, and reproduces the high release peak of the observed IMGA bimodal distribution of single particle inventories [30].

To be modelled, the particles have to be separated in three categories such as described in the international experience :

1°) Intact Coated Particles

Intact particles will be modelled in one dimension. The important parameters are the diffusion coefficients of the fission products in the different layers. All those layers are intact and the retention of the fission products is high.

The Figure 9 gives the structure of an intact particle built and proposed.

2°) 'Failed-SiC' Coated Particles

For this second kind of particles is the 'failed-SiC', the FORNAX code considers that the diffusion coefficient in the silicon carbide is the same as in the pyrocarbon, but the results do not suit the experience. To solve this problem, this code adapts the diffusion coefficient to the experimental results and considers that the coefficient in silicon carbide is 100 times higher than the normal one.

A fissure, all around the particle, going through the SiC layer, will model this kind of defective layer. The parameter will be the thickness of the fissure.

The Figure 10 gives the structure of a failed-SiC particle built and proposed.

3°) Exposed Kernels

The three layers, IPyC, SiC and OPyC, of this last kind of particles are cracked. The kernel is directly exposed to the outside.

The Figure 11 gives the structure of an exposed kernel built and proposed.

8. Conclusion

This document describes the methodology and the currently data used for fission products behaviour in order to predict and to understand the irradiation behaviour of HTR Fuels and to model the different phenomenon occurring in the fuel in reactor.

This document is the FRAMATOME-ANP contribution in the Work Package 3 (Modelling) in HTR-F (Fuel Technology) funded by the European Community.

Figure 1

Diffusion coefficients of Ag, Cs, Sr, I, Kr and Xe in UO_2

The Figure 1 gives the values of the diffusion coefficients of solid fission product (Ag, Cs and Sr) and gaseous fission products (I, Kr and Xe) in UO_2 used in different countries (FRG, USA and Japan).

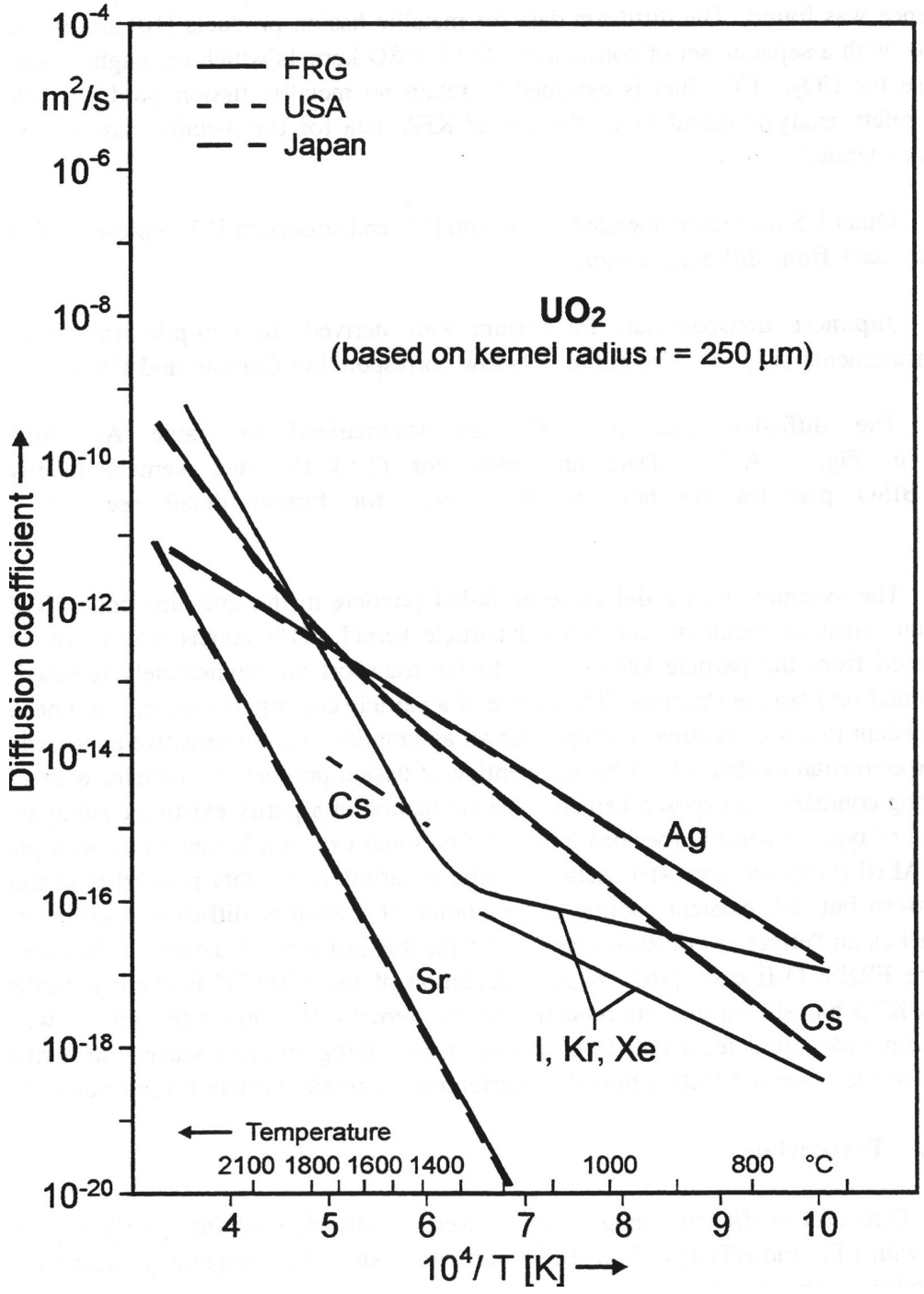

Figure 2

Diffusion coefficients of Ag, Cs, Sr and Kr in LTI Pyrocarbon

The Figure 2 gives the values of the diffusion coefficients of solid fission product (Ag, Cs and Sr) and gaseous fission product Kr in LTI Pyrocarbon used in different countries (FRG, USA, Russia and Japan) as function of temperature.

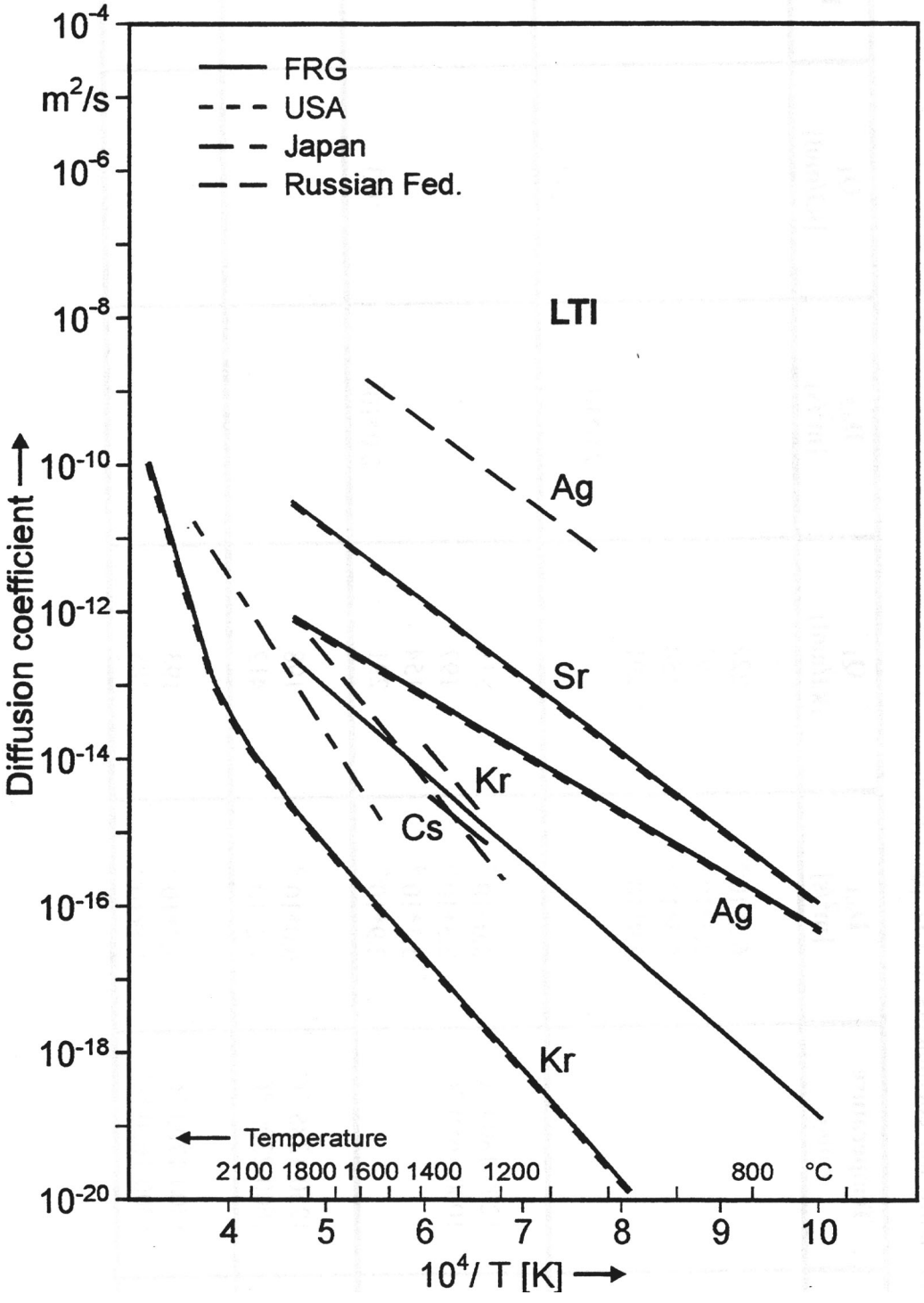

Figure 3

Diffusion coefficients of Ag, Cs, Sr and Xe in SiC

The Figure 3 gives the values of the diffusion coefficients of solid fission product (Ag, Cs and Sr) and gaseous fission product Xe in SiC used in different countries (FRG, USA, Russia and Japan) as function of temperature.

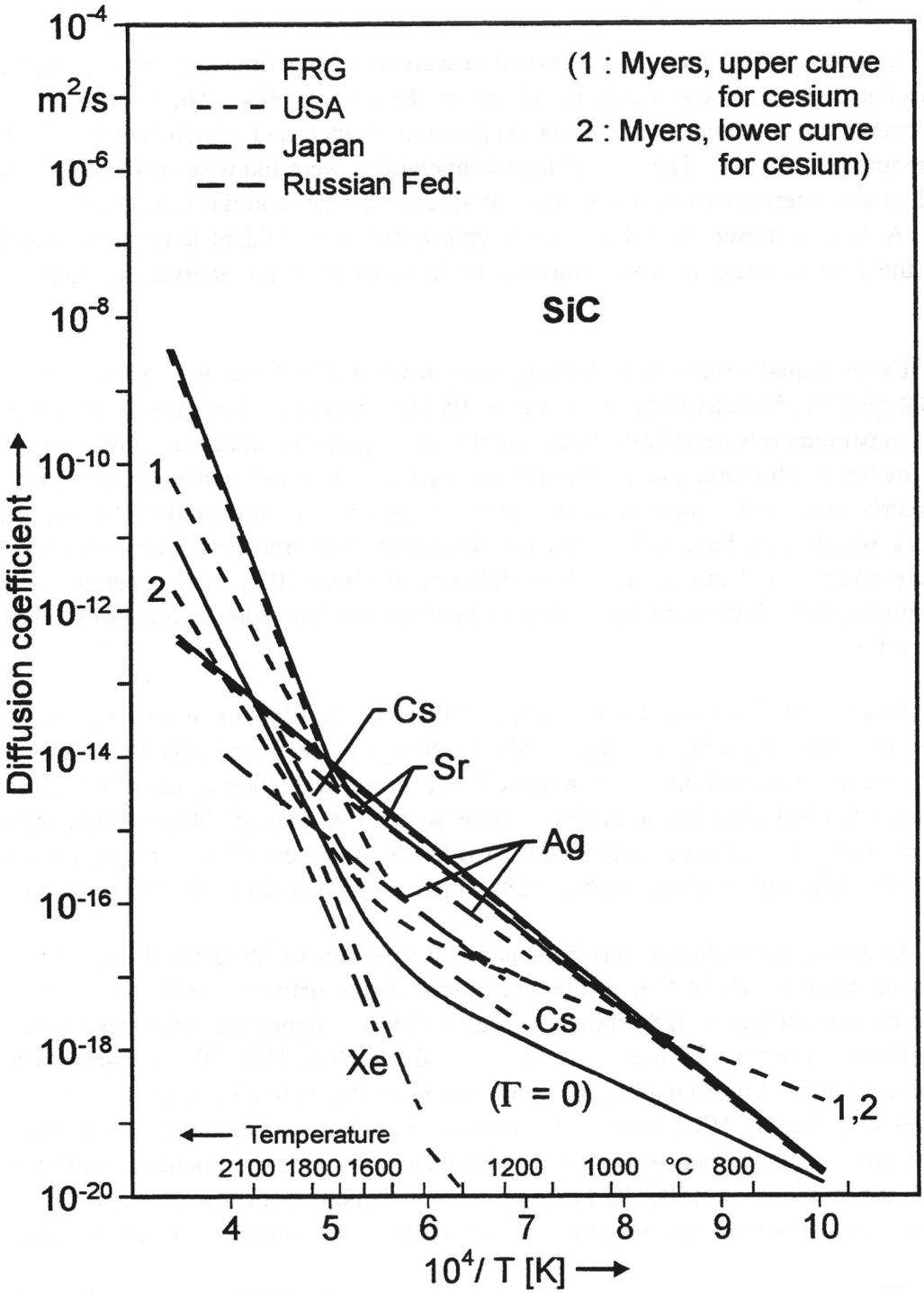

Figure 4

Diffusion coefficients of Cs with fast fluence dependence

The Figure 4 gives the values of the diffusion coefficients of Cs as function of temperature and fast fluence dependence.

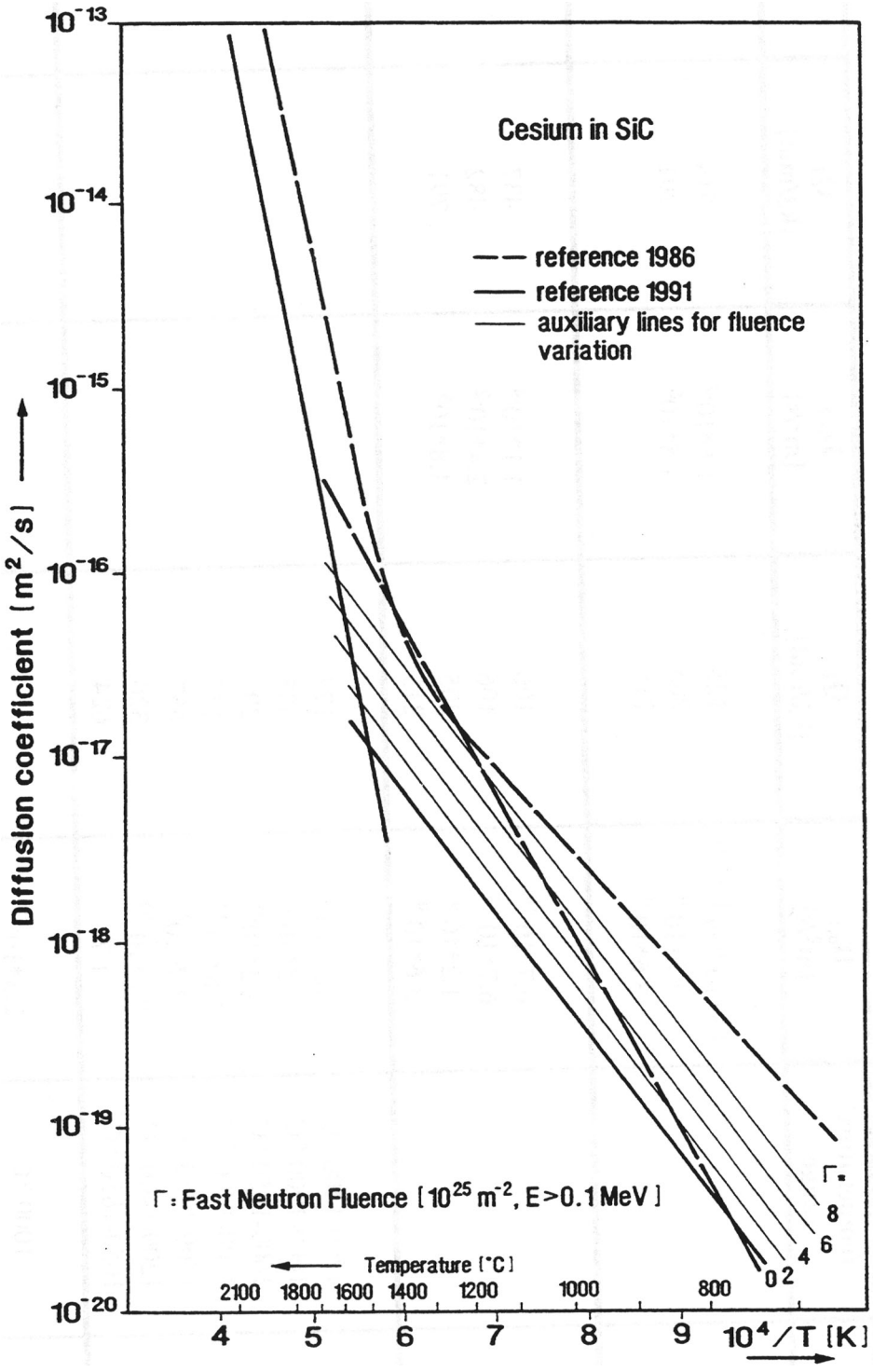

Figure 5

Diffusion coefficients of Ag, Cs, Sr, I and Kr in matrix graphite

The Figure 5 gives the values of the diffusion coefficients of solid fission product (Ag, Cs and Sr) and gaseous fission product I and Kr in matrix graphite used in different countries (FRG, United Kingdom, Russia and Japan) as function of temperature.

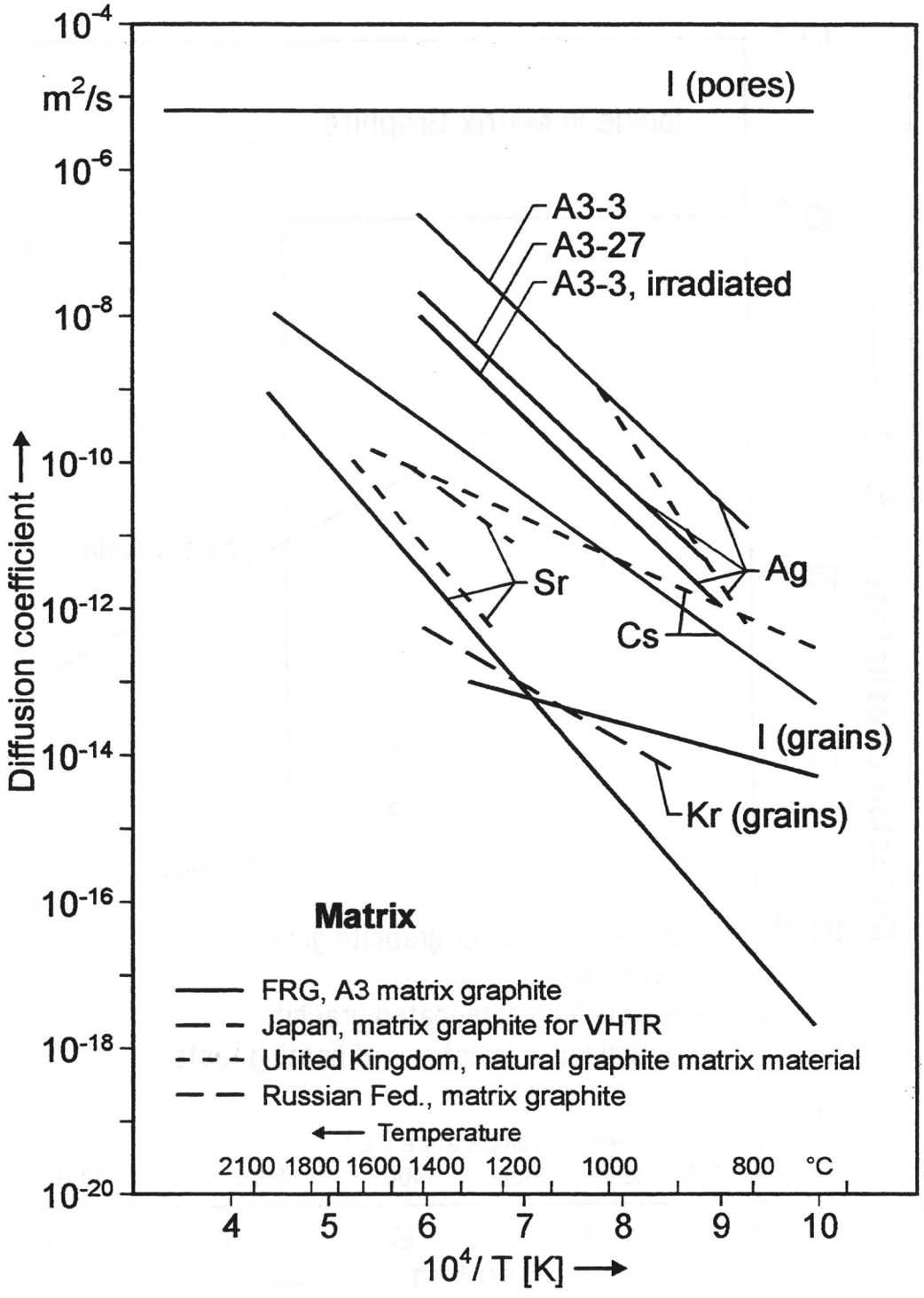

Figure 6

Diffusion coefficients of Cs and Ag in structural graphite

The Figure 6 gives the values of the diffusion coefficients of solid fission product (Cs and Ag) in structural graphite used in different countries (FRG, US, United Kingdom, and Japan) as function of temperature.

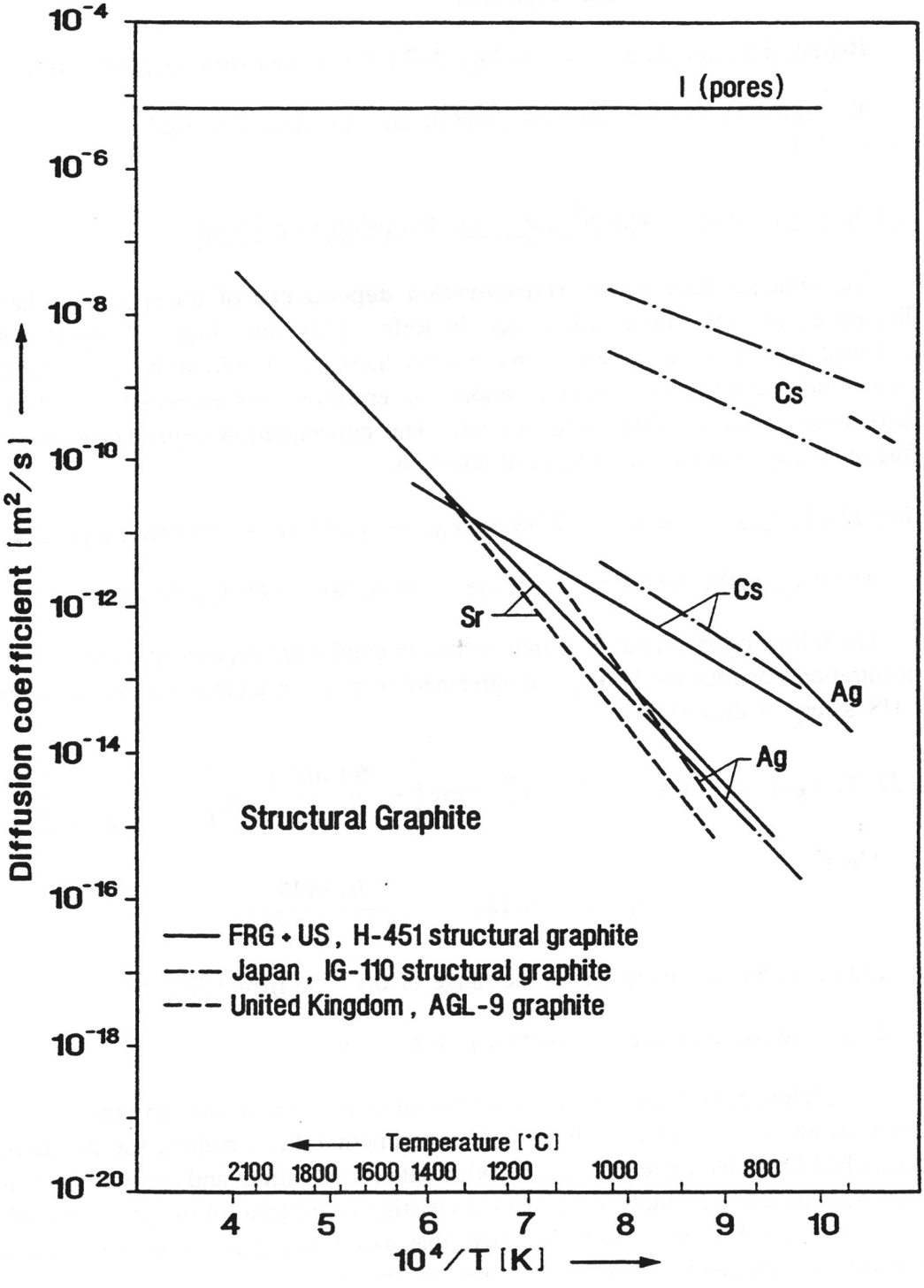

Figure 7

Concentration dependence of diffusion coefficient of Sr in graphite

The Figure 7 gives the concentration dependence of diffusion coefficients of solid fission product Sr in graphite as function of temperature.

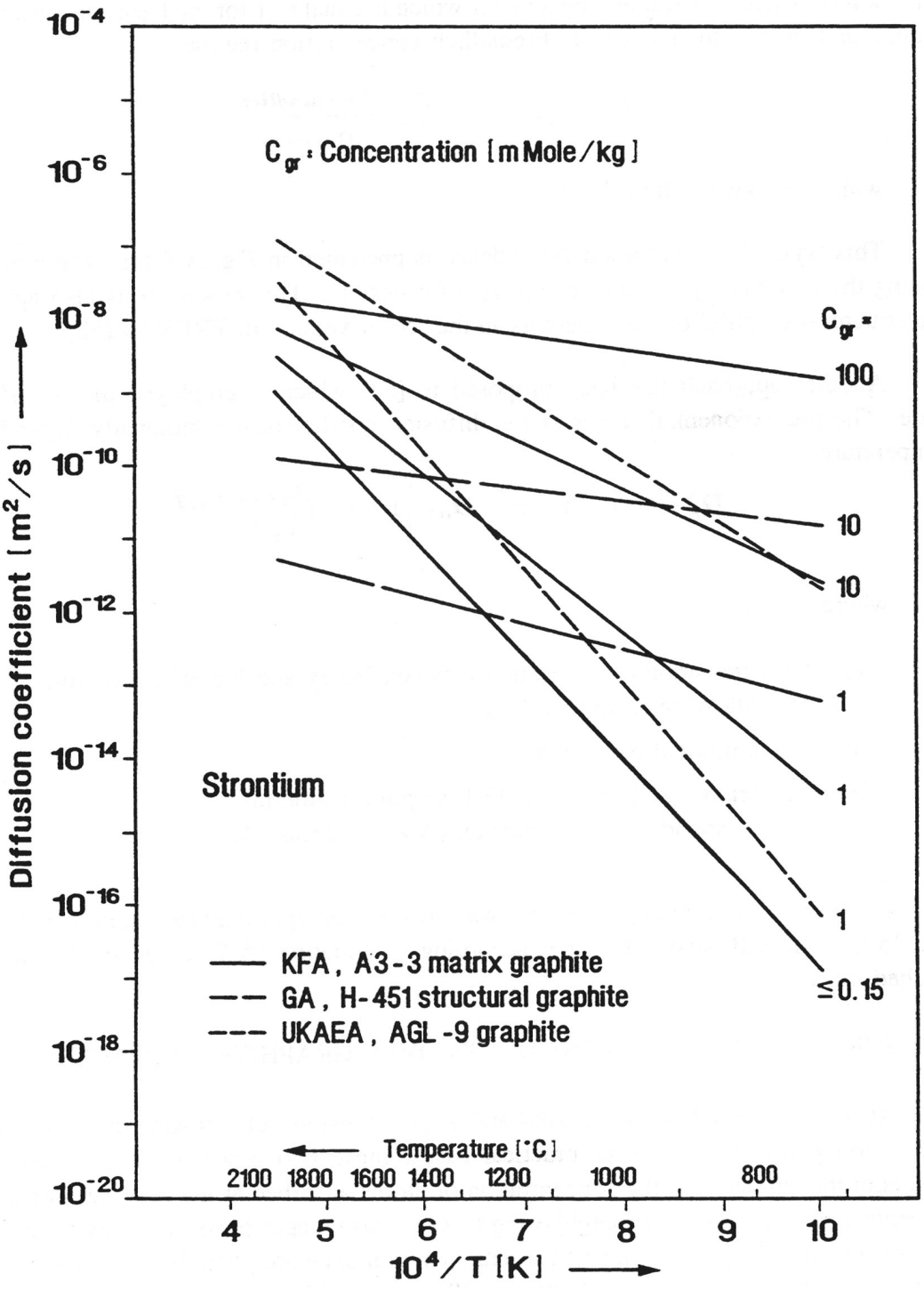

Figure 8

Concentration dependence of diffusion coefficient of Cs in graphite

The Figure 8 gives the concentration dependence of diffusion coefficients of solid fission product Cs in graphite as function of temperature.

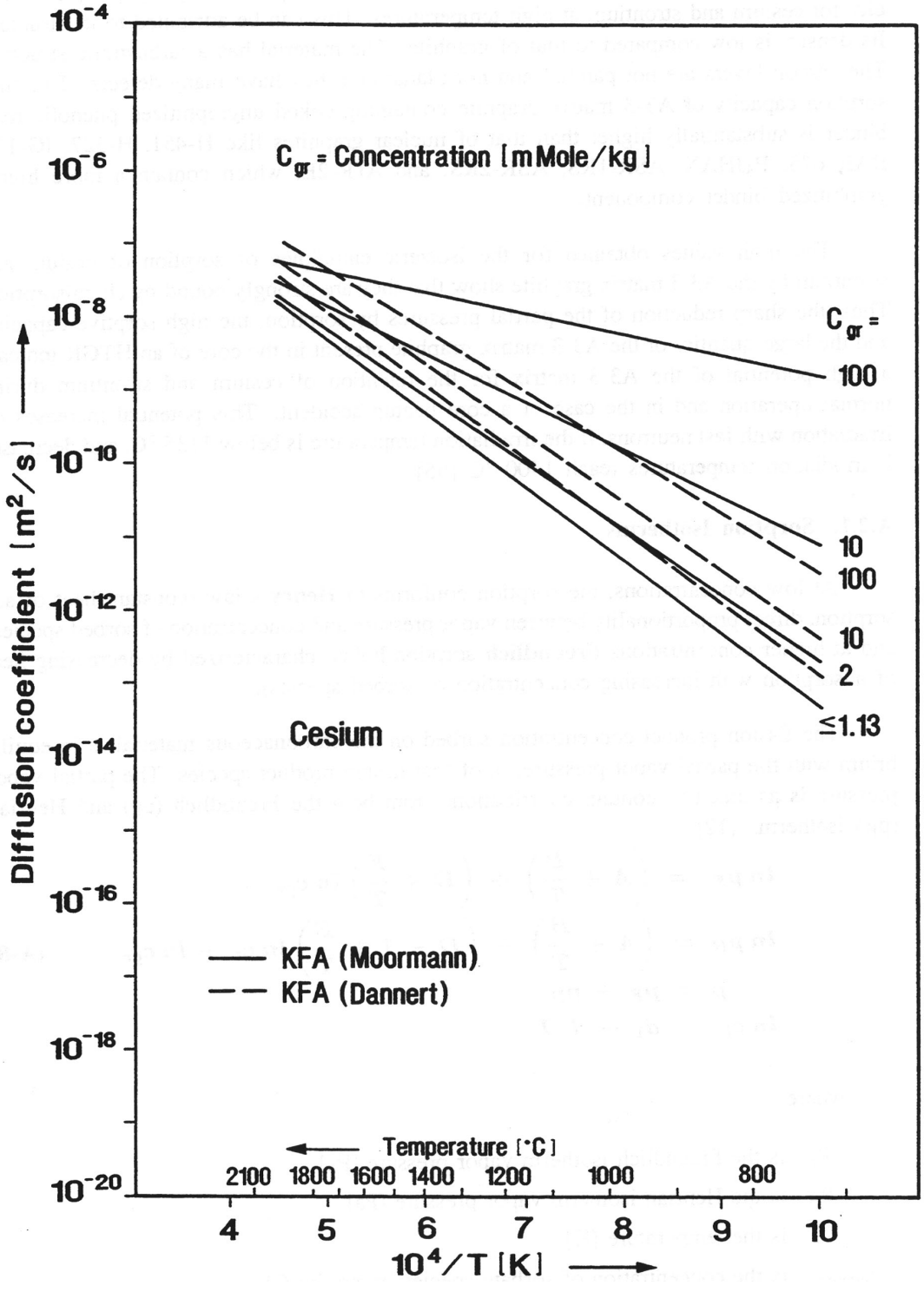

Figure 9

Structure of an intact particle built and proposed

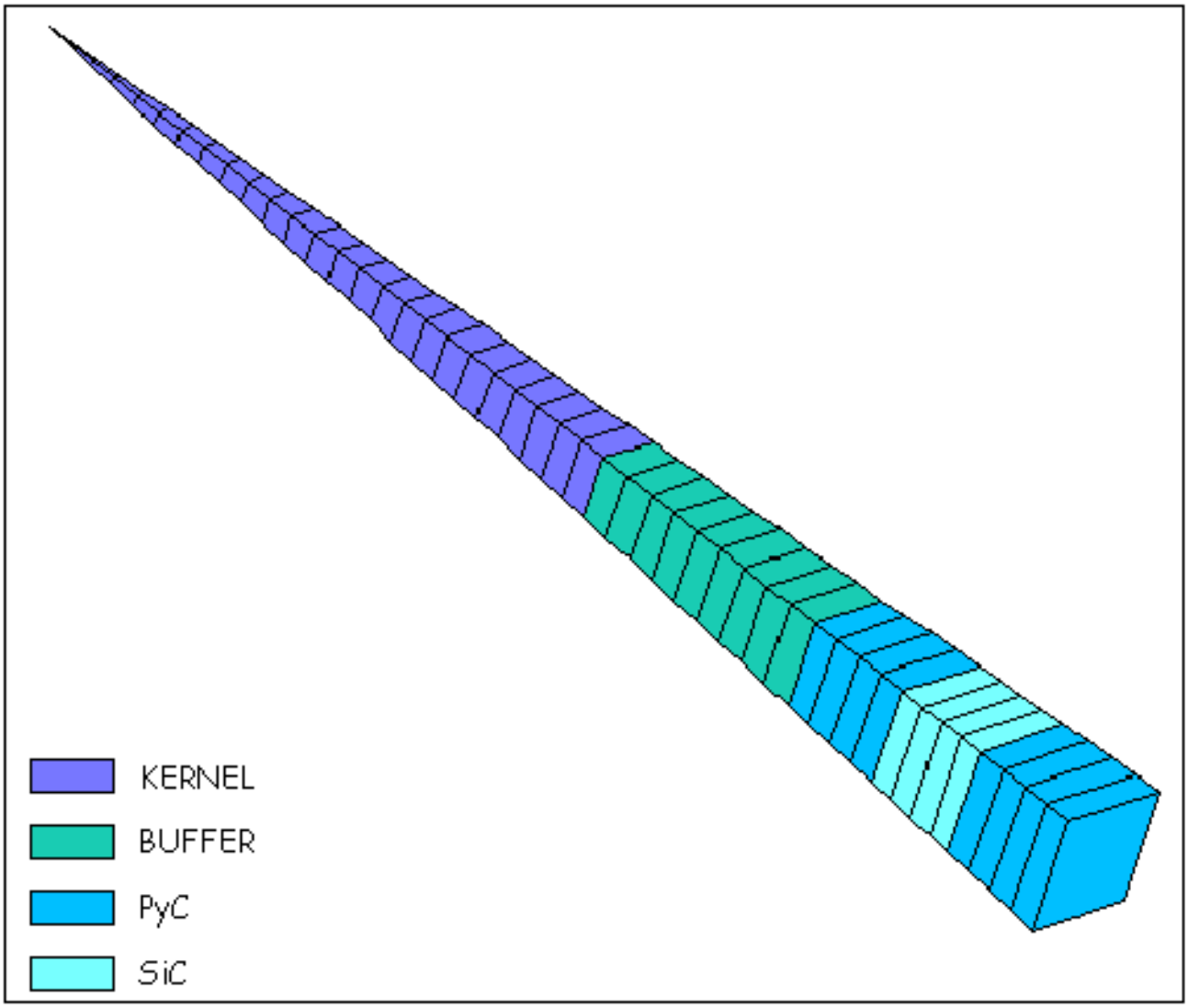

Figure 10

Structure of a failed-SiC particle built and proposed

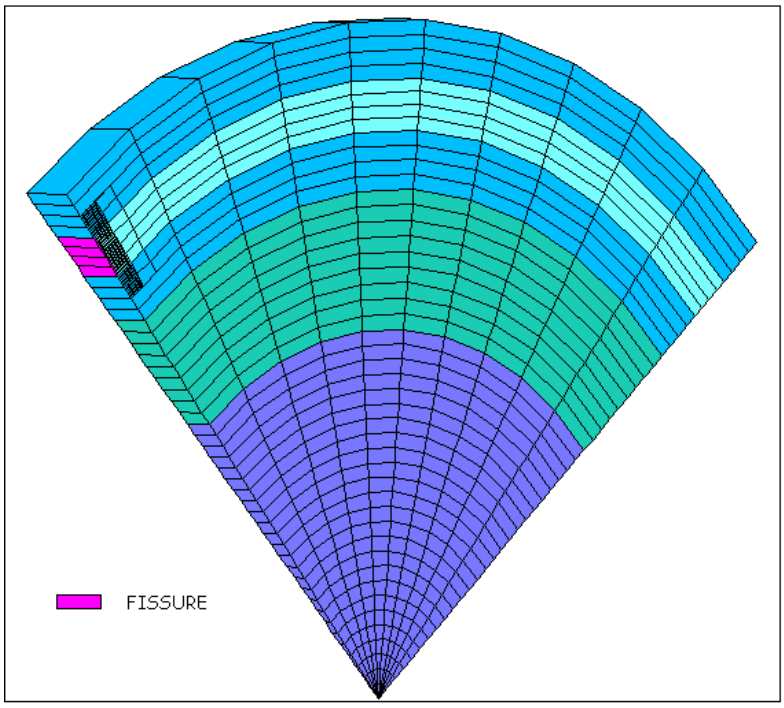

Zoom near the fissure

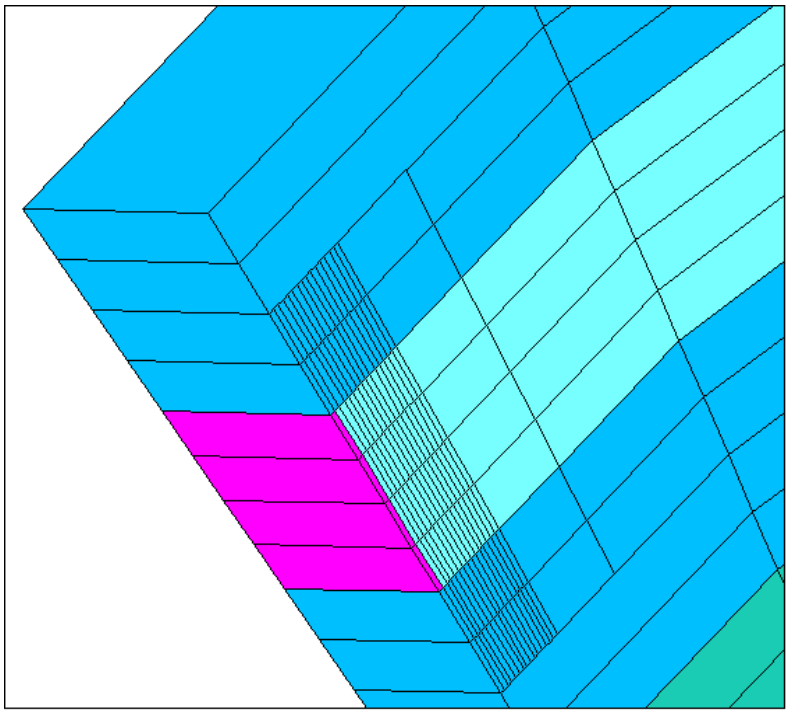

Figure 11

Structure of an exposed kernel particle built and proposed

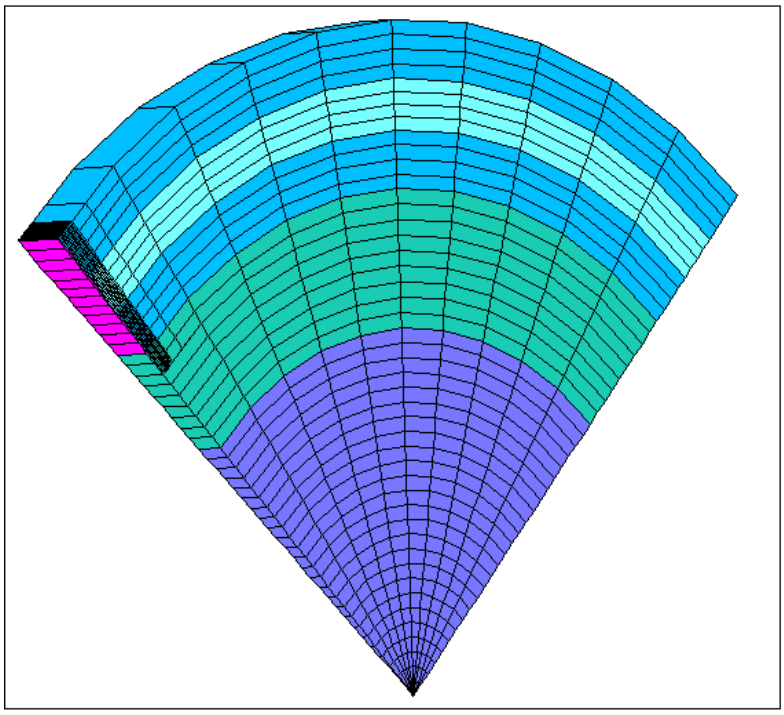

Zoom near the fissure

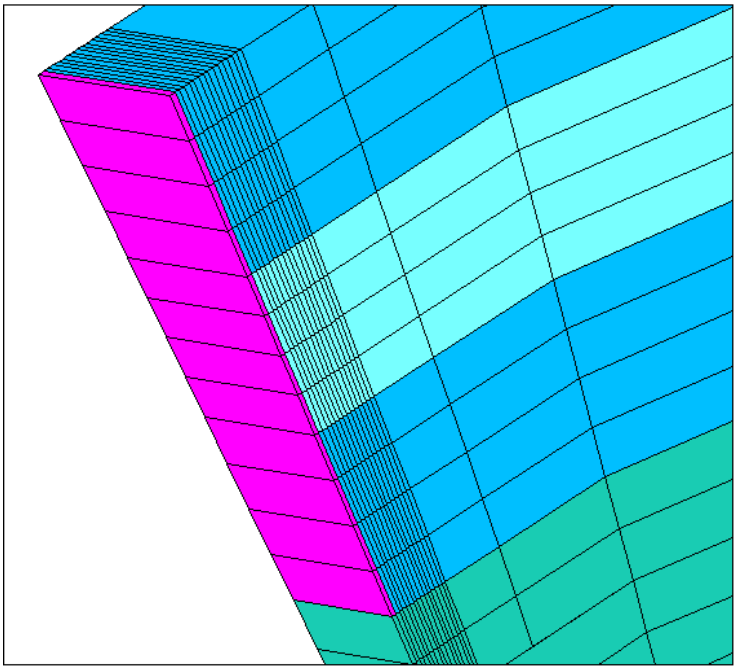

DIRECTION DE L'ENERGIE NUCLÉAIRE

DIRECTION DU CEA/CADARACHE

DÉPARTEMENT D'ETUDES DES COMBUSTIBLES

SERVICE D'ETUDES ET DE SIMULATION DU COMPORTEMENT DES COMBUSTIBLES

LABORATOIRE D'ÉTUDES ET DE SIMULATION DU COMPORTEMENT DES COMBUSTIBLES

HTR-F PROJECT: COLLECT OF THE CURRENT KNOWLEDGE ON EXISTING PROPERTIES AND MODELS FOR THE COATED PARTICLE

- PyC AND SiC -

M. PELLETIER, H. NABIELEK (FZJ) AND T. ABRAM (BNFL)

Report SESC/LSC 02-037 **First Issue 0** **November 2002**

CEA/CADARACHE - BÂTIMENT N°315 - DEN/CAD/DEC/SESC/LSC – 13108 – SAINT PAUL LEZ DURANCE CEDEX

04 42 25 38 62 - 04 42 25 29 49 - sesclsc@drncad.cea.fr

DIRECTION DE L'ENERGIE NUCLÉAIRE

DIRECTION DU CEA/CADARACHE
DÉPARTEMENT D'ETUDES DES COMBUSTIBLES
SERVICE D'ETUDES ET DE SIMULATION DU COMPORTEMENT DES COMBUSTIBLES
LABORATOIRE D'ÉTUDES ET DE SIMULATION DU COMPORTEMENT DES COMBUSTIBLES

Title : HTR-F PROJECT: COLLECT OF THE CURRENT KNOWLEDGE ON EXISTING PROPERTIES AND MODELS FOR THE COATED PARTICLE - PYC AND SIC -

Authors : M. PELLETIER, H. NABIELEK (FZJ) AND T. ABRAM (BNFL)

Summary:

The Work Package 3 of the HTR-F program is dedicated to the modelling of the different phenomena which occur into the fuel particle during irradiation and to develop at the European level a common code. This tool has to main mission to predict the time-to-failure taking into account several mechanisms such pressure vessel, SiC layer corrosion, coating debonding or kernel migration.

The first task of the WP3 consists to gather the knowledge on particle component properties and fundamental models for describing the behaviour of the coated particle under irradiation in order to reach the best accuracy. This collection of the current knowledge on physical processes and relevant existing models is the first "Deliverable" of the HTR-F WP3 and must be supplied by the end of October 2002.

The present document builds up the FZJ and BNFL contributions for this task which is mainly focused on the coating properties and their behaviour under irradiation.

The chapter 2 is devoted to physical and mechanical properties of porous and dense pyrolytic carbons (PyC) and the chapter 3 to the silicon carbide (SiC) ones.

Key Words	HTR, COATING, PYROCARBON, SILICON CARBIDE, PHYSICAL PROPERTIES, BEHAVIOUR, MODELLING

EOTP	A-FIHTR-03-01

	Name	Signature	Date	Classification				
Quality Assurance	***G. ARÈNE***			Open	DR	CC	CD	SD
Head of Unit	***P. OBRY***							
Checked by	***M. PHELIP***			Framework				
Written by	***M. PELLETIER***			*DDIN/SYST. DU FUTUR : FILIÈRE HTR*				

REVISIONS

DATE	PURPOSE OF THE REVISIONS	ISSUE
déc. 2002	Initial distribution.	0

CONTENTS

1. INTRODUCTION

In order to develop HTR reactor in Europe, a program devoted to fuel technology development (HTR-F) was launched in 2000 in the framework of the European Project HTR-TN. Around the world, the HTR fuel is based on spherical coated particles inserted in graphite blocks or pebble type elements. Their kernel generally consists of enriched uranium dioxide and the coatings are made of ceramic layers ensuring leak tightness to the fission products during normal and accidental situations.

One of the four Work Package of the HTR-F program (WP3) is dedicated to the modelling of the different phenomena which occur into the fuel particle during irradiation and to develop at the European level a common code. This tool has to main mission to predict the time-to-failure taking into account several mechanisms such pressure vessel, SiC layer corrosion, coating debonding or kernel migration.

Among the tasks of the WP3, the first one consists to gather the knowledge on particle component properties and fundamental models for describing the behaviour of the coated particle under irradiation in order to reach the best accuracy. This collection of the current knowledge on physical processes and relevant existing models is the first "Deliverable" of the HTR-F WP3 and must be supplied by the end of October 2002.

The present document builds up the FZJ and BNFL contributions for this task which is mainly focused on the coating properties and behaviour under irradiation. The chapter 2 is devoted to physical and mechanical properties of porous and dense pyrolytic carbons (PyC) and the chapter 3 to the silicon carbide (SiC) ones.

WARNING: All fast neutron flux ($\frac{dD}{dt}$) and fluence (D) in this document are in units: n/m^2 for E > 0.1 MeV or 16 fJ. The conversion to other used units such as: Dido Nickel Equivalent (DNE) or E > 0.18 Mev or 29 fJ are as follows:

n/m^2 (E > 0.1 MeV or 16 fJ)	n/m^2 (E > 0.18 MeV or 29 fJ)	n/m^2 (DNE)
1.67	1.52	1

2. PYROLYTIC CARBONS

Pyrolytic carbons (PyC) are key protective materials in the design of the classical HTR fuel coated particles (CP).

PyC are basically used for the constitution of the first porous coating (50%) named "buffer" layer and for the two "dense" layers: the inner pyrolytic carbon (IPyC) and the outer pyrolytic carbon (OpyC) which enclose the usual silicon carbide layer (SiC) of the TRISO particle.

According to both the temperature of the pyrolysis process and the nature of the hydrocarbon, one commonly consider two classes of "dense" PyC materials: the high-temperature isotropic (HTI) PyC (θ > 1800 °C and CH_4 - Ar mixture) and the low-temperature isotropic (LTI) PyC (θ < 1500 °C and generally C_3H_6 - Ar mixture). Many available data come from the first class (HTI), because the greatest amount of tests was performed during the 60 and 70ties on this category of materials.

In this chapter, we provide the properties for the porous and dense PyC which are needed for the calculation of the behaviour and the prediction of failure during irradiation and heating of coated particles.

These properties are mainly from proposals of BNFL *[1] [2]*and FZJ *[3]* organisations which provide the data in the framework of the WP3 of the HTR-F European programme.

2.1. DENSITY

The theoretical density of graphite material is 2.27 g/cm^3. The value supplied by FZJ and BNFL for a 100 % dense PyC is a little lower than this value:

	FZJ	BNFL
Theoretical density (g/cm^3)	2.2	
fabricated density for:		
"buffer" layer (g/cm^3)	~ 1 (P > 50%)	
dense PyC layers (g/cm^3)	1.6 < ρ < 2	

2.2. COEFFICIENT OF THERMAL EXPANSION

Very often, the data reported in the literature is not the true linear thermal expansion coefficient (α) but the mean value ($\overline{\alpha}$) given between two temperatures T_1 and T_2.

	FZJ	BNFL
"buffer" layer α (10^{-6} K^{-1})	$\alpha = 3.5$	
dense isotropic PyC layers α (10^{-6} K^{-1})	$\alpha = 5.5$	*For 300 < T < 750 K:* $\alpha = 2.5523 + 8.22\ 10^{-3}\ T - 5.509\ 10^{-6} T^2$ *For T > 750 K:* $\alpha = 5.62$

SPECIFIC HEAT

	FZJ [1]	BNFL
For graphite materials: c_p (cal mol^{-1} K^{-1})	*For 298 < T < 1100 K:* $c_p = 0.026 + 9.307\ 10^{-3}\ T - 0.354\ 10^{5}\ T^{-2} - 4.155\ 10^{-6}\ T^2$ *For 1100 < T < 4073 K:* $c_p = 5.841 + 0.104\ 10^{-3}\ T - 7.559\ 10^{5}\ T^{-2}$	No recommendation

NB : The conversion factor is 1 cal = 4.1868 J

[1] Data according to Ihsan Barin and Ottmar Knacke (1973)

2.3. THERMAL CONDUCTIVITY

The thermal conductivity depends on the porosity and, consequently on the made-up density.

	FZJ	BNFL
"buffer" layer λ (W m^{-1} K^{-1})	$\lambda = 0.5$	No recommendation
dense isotropic PyC layers λ (W m^{-1} K^{-1})	$\lambda = 4$	After Bockros' data (1966) : *density* / *BAF* * / λ: *1.55* / *1* / 9.61 *1.82* / *1.05* / 12.54 *2* / *1.3* / 7.52

* The BAF (Bacon Anisotropy Factor) is determined by the variation in intensity of the {0002} X ray Debye-Scherrer diffraction ring. The value 1 corresponds to a perfect isotropic material.

2.4. YOUNG'S MODULUS

	FZJ [1]	BNFL [2]
"buffer" layer E (MPa) D (10^{25} n/m² >0,1MeV)	*For 0 < D < 0.5* E = 7000 + 6000 D *For D > 0.5* E = 10000	*For D < 1.35* E = -5000 D^2 + 13500 D + 7000 *For D > 1.35* E = 16115
dense isotropic PyC layers E (MPa) D (10^{25} n/m² >0,1MeV)	E = 29000	*For D < 1.4* E = - 9554 D^2 + 26750 D + 13820 *For D > 1.4* E = 32545

[1] Polynomial adjustment according to the Figure 1 (FZJ contribution).

[2] Polynomial adjustment according to the constants of compliance used in the code STRESS 3 (Table 1). The Young's modulus is deduced from the constants by the relation: $E = 1/E_{11}$

2.5. POISSON RATIO

	FZJ	BNFL [1]
"buffer" layer ν (/)	ν = 0.3	ν = 0.33
dense isotropic PyC layers ν (/)	ν = 0.3	ν = 0.33

[1] The Poisson's ratio is deduced from the constants of compliance currently used in the code STRESS 3 (Table 1) by the relation: $\nu = - E_{12}/E_{11}$

2.6. ULTIMATE TENSILE STRENGTH

Pyrolytic carbons are generally treated as brittle materials. The scatter in the fracture strength (UTS) is often rather large because failure starts from the defects existing inside and at the surface of the material. The distribution density of failure "f" is given by a statistical distribution expressed in terms of a Weibull equation:

$$f = 1 - \exp\left\{ - \ln 2 \left(\frac{\sigma}{\sigma_{med}} \right)^{m} \right\}$$

where σ_{med} and m are constants whose values are determined from experiments.

	FZJ	BNFL [1]
"buffer" layer	No recommendation	No recommendation
dense isotropic PyC layers σ_{med} (MPa) m (/) P (/)	No recommendation	$\sigma_{med} = 3518\ P^2 - 3277\ P + 985$ $m = -7{,}375\ P + 7$

[1] Polynomial adjustment versus the porosity according to the data from Bongartz *et al* (1976) on results obtained from propylene derived PyC deposits on flat discs.

2.7. IRRADIATION INDUCED CREEP

The irradiation induced creep rate is given by the following expression:

$$\dot{\varepsilon}_1 = K \left[\sigma_1 - \nu_c (\sigma_2 + \sigma_3) \right] \frac{dD}{dt}$$

where

K:	creep constant
σ_1, σ_2 and σ_3	components of the stress tensor
ν_c	Poisson's coefficient for creep
$\frac{dD}{dt}$	fast neutron flux

Values of the creep constant K present a wide scatter of magnitude according to the different sources (see Table 2).

The recommendations of FZJ and BNFL are the following:

	FZJ	BNFL [1]
"buffer" layer K [MPa n m^{-2}(E> 0.1 MeV)]$^{-1}$ ν_c (/)	$K = 9.6\ 10^{-30}$ $\nu_c = 0.5$	$K = 4.4\ 10^{-29}$ $\nu_c = 0.4$

	FZJ	BNFL [1]
dense isotropic PyC layers K [MPa n m^{-2}(E> 0.1 MeV)]$^{-1}$ ν_c (/)	K = 1.4 10^{-29} ν_c = 0.5	K = 4.4 10^{-29} ν_c = 0.4

[1] data from Buckley et al (1975)

2.8. IRRADIATION INDUCED DIMENSIONAL CHANGE RATE

Under irradiation, the buffer and the dense PyC are submitted to a fast neutron flux which brings about an irradiation induced dimensional change. According to the density of fabrication and the initial anisotropy of the material, the dimensional change rate can vary considerably.

A considerable number of measurements of dimensional change in unrestrained PyC has been reported in the open literature.

Data recommended by both FZJ and BNFL (see Table 3 and Table 4) are summarized in the following table:

	FZJ [1]	BNFL [2]
"buffer" layer $\dot{\varepsilon}_r$ $\dot{\varepsilon}_\theta$ [10^{25} n m^{-2} (>0,1MeV)]$^{-1}$	$\dot{\varepsilon}_r = \dot{\varepsilon}_\theta = -0.176 \exp(-1.75\,D)$	$\dot{\varepsilon}_r = \dot{\varepsilon}_\theta = -0.241 \exp(-2.2\,D^{1.05})$
dense isotropic PyC layers $\dot{\varepsilon}_r$ $\dot{\varepsilon}_\theta$ [10^{25} n m^{-2} (>0,1MeV)]$^{-1}$	$\dot{\varepsilon}_r = -0.077 \exp(-D) + 0.031$ $\dot{\varepsilon}_\theta = -0.036 \exp(-2.1\,D) - 0.01$	$\dot{\varepsilon}_r = -0.1335 \exp(-1.5\,D^{0.8}) - 1.12\,10^{-3} D^2 + 1.85\,10^{-2} D$ $\dot{\varepsilon}_\theta = -0.0225 \exp(-0.7\,D) - 2.1\,10^{-3} D - 8\,10^{-3}$

[1] Adjustment according to the Figure 2 and Figure 3 (FZJ contribution)

[2] Adjustment from the data used in the code STRESS 3 and given in the "Tableau" 3

3. SILICON CARBIDE

As the PyC layers, the silicon carbide (SiC) layer of the CP is set down from a mix of gases ; the more often used is the methyltrichlorosilane (MTS) with argon. The microstructure of pyrolytic SiC depends on temperature and rate of deposition of MTS.

The β (cubic) structure dominates but α phase and free silicon may be present at low (<1250 °C) deposition temperature.

Material property considerations are generally less of a problem for the SiC compared with the PyC materials. However, this layer plays a fundamental role for the mechanical and diffusion resistance of the CP ; consequently, a good knowledge of the UTS of the SiC layer which can be enhanced by reducing the flaws, is very important for achieving high burn-up.

In this chapter, we provide the properties and for pyrolytic SiC which are needed for the calculation of the behaviour and the prediction of failure during irradiation and heating of coated particles.

These properties are mainly from proposals of BNFL ***[1] [2]*** and FZJ ***[3]*** organizations which provide the data in the framework of the WP3 of the HTR-F European programme.

3.1. DENSITY

	FZJ	BNFL
Theoretical density (g/cm^3)	3.216	
fabricated density (%TD)	99	

3.2. COEFFICIENT OF THERMAL EXPANSION

Very often, the data reported in the literature is not the true linear thermal expansion coefficient (α) but the mean value ($\overline{\alpha}$) given between two temperatures T_1 and T_2.

	FZJ	BNFL
α (10^{-6} K^{-1})	α = 5	

3.3. SPECIFIC HEAT

	FZJ [1]	BNFL
c_p (cal mol^{-1} K^{-1})	*For 298 < T < 3259 K:* $c_p = 12.139 + 0.466\ 10^{-3}\ T$ $- 11.76\ 10^{5}\ T^{-2} + 1.961\ 10^{-6}\ T^{2}$	No recommendation

NB : The conversion factor is 1 cal = 4.1868 J

[1] Data according to Ihsan Barin and Ottmar Knacke (1973)

3.4. THERMAL CONDUCTIVITY

	FZJ	BNFL
λ (W m^{-1} K^{-1})	$\lambda = 16$	No recommendation

3.5. YOUNG'S MODULUS

	FZJ [1]	BNFL [2]
E (MPa)	*For 298 < T < 573 K:* E = 386000 *For 573 < T < 1873 K:* $E(T)/E(298\ K) = -2.12\ 10^{-7}\ T^2$ $+ 2.52\ 10^{-4}\ T + 0{,}9252$	E = 421000

[1] The fractional variation of the Young's modulus : E(T)/E(298 K) with temperature is according to the of the FZJ contribution.

[2] The Young's modulus is deduced from the constants of compliance used in the code STRESS 3 (Table 1) by the relation: $E = 1/E_{11}$

3.6. POISSON RATIO

	FZJ	BNFL [1]
dense isotropic PyC layers ν (/)	$\nu = 0.3$	$\nu = 0.33$

[1] The Poisson's ratio is deduced from the constants of compliance currently used in the code STRESS 3 (Table 1) by the relation: $\nu = - E_{12}/E_{11}$

3.7. ULTIMATE TENSILE STRENGTH

The disparities of nature, size, geometry, localization and orientation of the defects, as well as the differences of state of surface of the nominally identical test samples explain the big variations of the ultimate tensile strength (UTS) frequently observed. The distribution density of failure "f" is given by a statistical distribution expressed in terms of a Weibull equation:

$$f = 1 - \exp\left\{ - \ln 2 \left(\frac{\sigma}{\sigma_{med}} \right)^m \right\}$$

where σ_{med} and m are constants whose values are determined from experiments.

	FZJ [1]	BNFL
σ_{med} (MPa) m (/) T (K) D (10^{25} n/m^2)	$\sigma_{med} = \sigma_{med0}\left(1 - \frac{D}{D_\sigma}\right)$, $\sigma_{med\,min} = 196$ $\log D_\sigma = 0.556 + \frac{650}{T}$ $\sigma_{med0} = 834$ $m = m_0\left(1 - \frac{D}{D_m}\right)$, $m_{min} = 2$ $\log D_m = 0.394 + \frac{650}{T}$ $m_0 = 8.02$	UTS = 400

[1] The relationship of the UTS comes from Allelein (1983) who proposes a decreasing of σ_{med} and m under irradiation. Data for σ_{med0} and m_0 in the previous table come from measurements performed on German particle variety : EO 1607 (Figure 5).

3.8. IRRADIATION INDUCED CREEP

The irradiation induced creep rate for the SiC is given by the following expression:

$$\dot{\varepsilon}_{eq} = K\,\sigma_{eq}\,\frac{dD}{dt}$$

where

K:	creep constant
σ_{eq}	equivalent stress
$\frac{dD}{dt}$	fast neutron flux

	FZJ	BNFL
K [MPa n m^{-2}(E> 0.1 MeV)]$^{-1}$	$K = 8.4\ 10^{-32}$	$K = 1.68\ 10^{-29}$

One notes a very large divergence between the creep constants proposed by both organization.

3.9. IRRADIATION INDUCED DIMENSIONAL CHANGE RATE

	FZJ [1]	BNFL [2]
$\dot{\varepsilon}_r\ \dot{\varepsilon}_\theta$ [10^{25} n m^{-2} (>0,1MeV)]$^{-1}$	$\dot{\varepsilon}_r = \dot{\varepsilon}_\theta = 3.65\ 10^{-3}\ \exp(-14\ D)$	$\dot{\varepsilon}_r = \dot{\varepsilon}_\theta = 6.6\ 10^{-4}$

[1] Adjustment according to the Figure 4 (FZJ contribution)

[2] Adjustment from the data used in the code STRESS 3 and given in the "Tableau" 3

3.10. CORROSION RATE

Corrosion of the SiC layer by diffusion of metallic fission products leads to strength loss which is assumed by a spread of the Weibull distribution as a function of time and temperature:

	FZJ	BNFL
$\dot{\eta}$ (1/s) T (K) R = 4.186 m t (s)	grain boundary corrosion rate : $\dot{\eta} = 0.565 \exp\left(-\frac{1.874\ 10^5}{R\ T}\right)$ Evolution of Weibull modulus: $m = m_0\ [0.44 + 0.56 \exp(-\dot{\eta}\ t)]$	No recommendation

REFERENCES

[1] « Physical and mechanical properties of the constituents of coated fuel particles and the effect of irradiation"
D.G. Martin (Nuclear Fuels Consultant)
HTR-F WP3 Meeting Lyon 18 October 2001

[2] "Pyrocarbon in high temperature nuclear reactors" Chapter 7 of "Irradiation damage in graphite due to fast neutrons in fission and fusion systems"
IAEA-TECDOC-1154 September 2000

[3] « Coating properties of HTR particles »
FZJ contribution to HTR-F Work Package 3: Modelling
H. Nabielek, K. Verfondern and H. Werner
Draft document from 1 August 2002

LIST OF TABLES

TABLE 1 : COMPLIANCE CONSTANTS USED IN STRESS 3

Compliance Constants $[kgf.cm^{-2}]^{-1}$				Dose $\times 10^{24}$ n.m-2 DNE
E_{11}	E_{12}	E_{13}	E_{33}	
Kernel				
0.500E-06	-0.150E-06	-0.150E-06	0.500E-06	0.00
Buffer				
0.140E-04	-0.460E-05	-0.460E-05	0.140E-04	0.00
0.120E-04	-0.400E-05	-0.400E-05	0.120E-04	0.50
0.100E-04	-0.330E-05	-0.330E-05	0.100E-04	1.00
0.900E-05	-0.300E-05	-0.300E-05	0.900E-05	2.00
0.800E-05	-0.260E-05	-0.260E-05	0.800E-05	3.00
0.660E-05	-0.220E-05	-0.220E-05	0.660E-05	5.00
0.620E-05	-0.204E-05	-0.204E-05	0.620E-05	8.00
0.600E-05	-0.198E-05	-0.198E-05	0.600E-05	15.00
PyC				
0.710E-05	-0.230E-05	-0.230E-05	0.710E-05	0.00
0.600E-05	-0.200E-05	-0.200E-05	0.600E-05	0.50
0.530E-05	-0.180E-05	-0.180E-05	0.530E-05	1.00
0.450E-05	-0.150E-05	-0.150E-05	0.450E-05	2.00
0.400E-05	-0.130E-05	-0.130E-05	0.400E-05	3.00
0.330E-05	-0.110E-05	-0.110E-05	0.330E-05	5.00
0.310E-05	-0.103E-05	-0.103E-05	0.310E-05	8.00
0.300E-05	-0.100E-05	-0.100E-05	0.300E-05	15.00
SiC				
0.233E-06	-0.770E-07	-0.770E-07	0.233E-06	0.00

TABLE 2 : SOME PUBLISHED VALUES OF THE IRRADIATION CREEP CONSTANT OF PyC

Authors	Creep Constant $\times 10^{-29}$[MPa. n.m^{-2}(DNE*)]$^{-1}$	Notes
Kaae *et al.* [6]	1.5	Estimated from fracture of coatings
Price and Bokros [7]	2.0	Estimated from fracture of discs
Buckley *et al.* [8]	7.4 (>5)	Estimated from fracture of coatings
Buckley *et al.* [8]	6	Measured following electron irradiation
Brocklehurst and Gilchrist [9]	5.0 2.5	Initial Density = 1.64 Mg.m^{-3} Initial Density = 1.95 Mg.m^{-3} Measured following neutron irradiation
Morgand [10]	20	Measured following neutron irradiation

TABLE 3 : PyC DIMENSIONAL CHANGE RATES USED IN STRESS 3

Dimensional Change Rates

tangential	radial	dose
Buffer		
-0.402E-01	-0.402E-01	0.00
-0.220E-01	-0.220E-01	1.00
-0.110E-01	-0.110E-01	3.00
-0.250E-02	-0.250E-02	9.00
0.000E+00	0.000E+00	15.00
PyC		
-0.510E-02	-0.223E-01	0.00
-0.438E-02	-0.110E-01	2.00
-0.400E-02	-0.510E-02	4.00
-0.386E-02	-0.210E-02	6.00
-0.376E-02	0.000E+00	8.00
-0.369E-02	0.140E-02	10.00
-0.359E-02	0.260E-02	12.00
-0.345E-02	0.370E-02	14.00
-0.325E-02	0.460E-02	16.00
-0.293E-02	0.550E-02	18.00
-0.286E-02	0.650E-02	20.00
-0.299E-02	0.760E-02	22.00
-0.312E-02	0.910E-02	24.00
-0.325E-02	0.109E-01	26.00
-0.337E-02	0.125E-01	28.00
-0.349E-02	0.135E-01	30.00
-0.360E-02	0.141E-01	32.00
-0.368E-02	0.144E-01	34.00
-0.374E-02	0.145E-01	36.00
-0.377E-02	0.145E-01	38.00
-0.379E-02	0.145E-01	40.00
SiC		
0.110E-03	0.110E-03	0.00

TABLE 4 : OTHER DIMENSIONAL CHANGE RATE DATA RELATING TO PYROCARBONS

Williams and Shipp Data

1.6 g/cc

-0.124E-01	-0.136E-01	0.00
-0.920E-02	-0.990E-02	2.00
-0.662E-02	-0.700E-02	4.00
-0.463E-02	-0.460E-02	6.00
-0.312E-02	-0.284E-02	8.00
-0.214E-02	-0.175E-02	10.00
-0.158E-02	-0.100E-02	12.00
-0.109E-02	-0.750E-03	14.00
-0.710E-03	-0.580E-03	16.00
-0.440E-03	-0.450E-03	18.00
-0.250E-03	-0.350E-03	20.00
-0.130E-03	-0.270E-03	22.00
-0.600E-04	-0.200E-03	24.00
-0.200E-04	-0.140E-03	26.00
0.000E+00	-0.100E-03	28.00
0.000E+00	-0.600E-04	30.00
0.000E+00	-0.300E-04	32.00
0.000E+00	-0.100E-04	34.00
0.000E+00	0.000E+00	36.00

Manzel Data. 1.6 g/cc

-0.103E-01	-0.170E-01	0.00
-0.957E-02	-0.138E-01	2.00
-0.833E-02	-0.755E-02	4.00
-0.687E-02	-0.180E-02	6.00
-0.543E-02	-0.200E-02	8.00
-0.430E-02	-0.130E-02	10.00
-0.225E-02	0.000E+00	12.00
-0.750E-03	0.210E-03	16.00
0.000E+00	0.560E-03	20.00
0.600E-04	0.910E-03	24.00
0.600E-04	0.127E-02	28.00
0.000E+00	0.137E-02	32.00
0.000E+00	0.141E-02	36.00
0.300E-04	0.146E-04	40.00
0.500E-04	0.138E-04	44.00
0.305E-03	0.136E-02	48.00

Manzell Data. 1.7 g/cc

-0.937E-02	-0.175E-01	0.00
-0.762E-02	-0.125E-01	2.00
-0.625E-02	-0.737E-02	4.00
-0.550E-02	-0.238E-02	6.00
-0.500E-02	0.800E-03	8.00
-0.437E-02	0.230E-02	10.00
-0.275E-02	0.322E-02	12.00
-0.162E-02	0.341E-02	16.00
-0.106E-02	0.337E-02	20.00
-0.100E-02	0.337E-02	24.00
-0.100E-02	0.356E-02	28.00
-0.100E-02	0.356E-02	32.00
-0.937E-03	0.363E-02	36.00
-0.875E-03	0.356E-02	40.00
-0.937E-03	0.331E-02	44.00
-0.106E-02	0.319E-02	48.00

Manzell Data 1.8g/cc

-0.562E-02	-0.135E-01	0.00
-0.537E-02	-0.100E-01	2.00
-0.512E-02	-0.630E-02	4.00
-0.500E-02	-0.175E-02	6.00
-0.450E-02	0.192E-02	8.00
-0.387E-02	0.367E-02	10.00
-0.308E-02	0.492E-02	12.00
-0.240E-02	0.554E-02	16.00
-0.206E-02	0.587E-02	20.00
-0.204E-02	0.587E-02	24.00
-0.196E-02	0.584E-02	28.00
-0.194E-02	0.587E-02	32.00
-0.201E-02	0.585E-02	36.00
-0.200E-02	0.575E-02	40.00
-0.196E-02	0.575E-02	44.00
-0.204E-02	0.575E-02	48.00

LTI Data 1.8 g/cc

-0.700E-02	-0.757E-02	0.00
-0.610E-02	-0.592E-02	2.00
-0.530E-02	-0.443E-02	4.00
-0.460E-02	-0.310E-02	6.00
-0.390E-02	-0.183E-02	8.00
-0.320E-02	-0.600E-03	10.00
-0.217E-02	0.105E-02	12.00
-0.152E-02	0.247E-02	16.00
-0.103E-02	0.407E-02	20.00
-0.712E-03	0.489E-02	24.00
-0.512E-03	0.500E-02	28.00
-0.363E-03	0.501E-02	32.00
-0.250E-03	0.505E-02	36.00
-0.150E-03	0.511E-02	40.00
-0.500E-04	0.515E-02	44.00
-0.500E-04	0.515E-02	48.00

LIST OF FIGURES

FIGURE 1 : YOUNG'S MODULUS OF BUFFER LAYER AS FUNCTION OF FAST NEUTRON FLUENCE

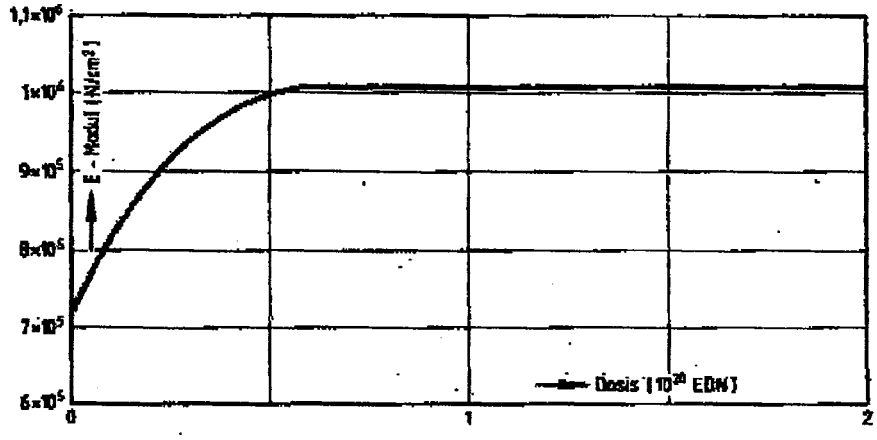

FIGURE 2 : BUFFER LAYER IRRADIATION INDUCED SHRINKAGE RATE AS A FUNCTION OF FAST NEUTRON FLUENCE

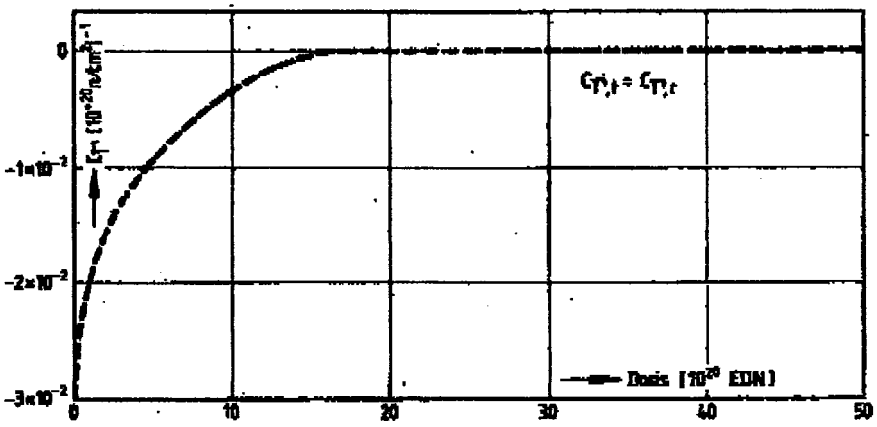

FIGURE 3 : PYC LAYERS IRRADIATION INDUCED SHRINKAGE RATE AS A FUNCTION OF FAST NEUTRON FLUENCE

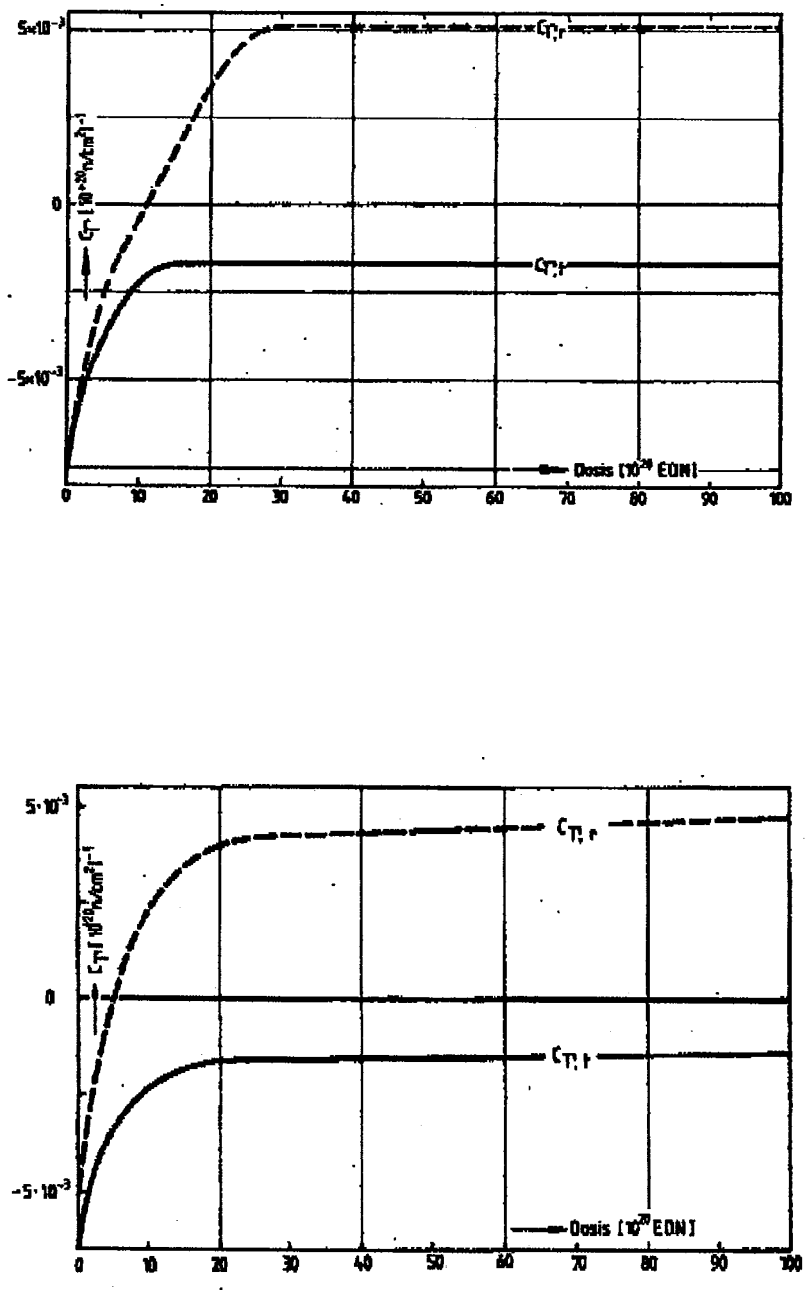

FIGURE 4 : SIC LAYER IRRADIATION INDUCED SHRINKAGE RATE AS A FUNCTION OF FAST NEUTRON FLUENCE

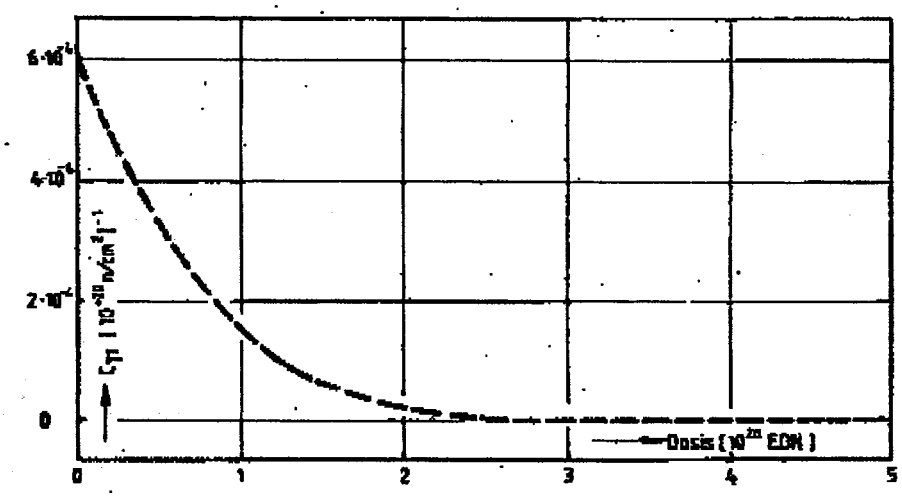

FIGURE 5 : FRACTIONAL CHANGE IN SIC YOUNG'S MODULUS : E(T)/E(298K)

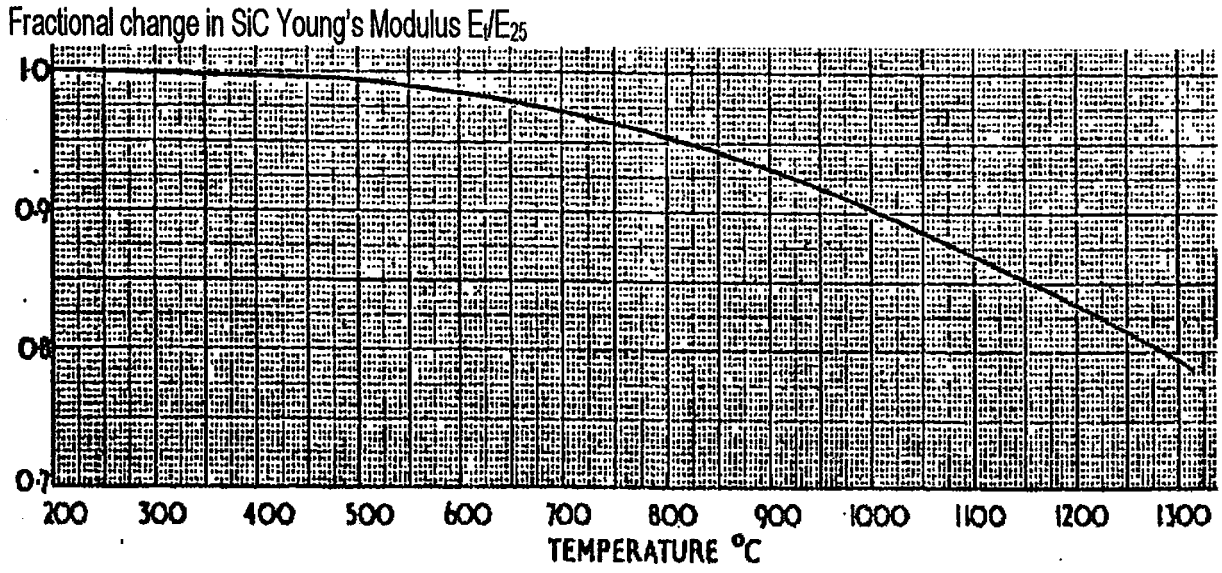

FIGURE 6 : MEASURED LOSS OF STRENGTH ON THE PARTICLE VARIETY EO 1607

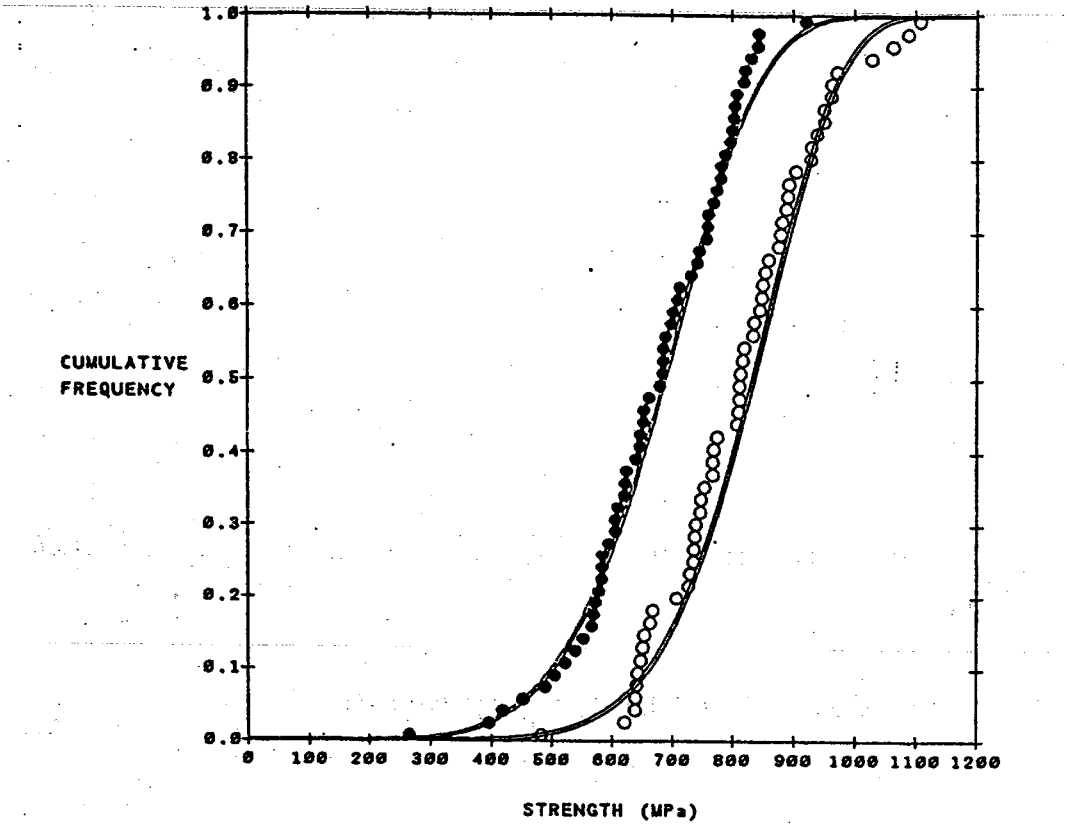

Fig. 5: Measurement of SiC Tensile Strength Distribution on Irradiated and Unirradiated Specimens of the Particle Variety EO 1607

o Unirradiated $1 - e^{-\ln 2 * (\sigma_t/834)^{8.02}}$

• Irradiated $1 - e^{-\ln 2 * (\sigma_t/687)^{5.98}}$